INJURY-INDUCED INHIBITION OF BYSTANDER NEURONS REQUIRES DSARM AND SIGNALING FROM GLIA

By

Jiun-Min Hsu

A THESIS/DISSERTATION

Presented to the Neuroscience Graduate Program and the Oregon Health & Science University, Portland School of Medicine in partial fulfillment of the requirements for the degree of

DOCTOR OF PHILOSOPHY

June 2020

CERTIFICATE OF APPROVAL

This is to certify that the PhD Dissertation of

Jiun-Min Hsu

"Injury-induced inhibition of bystander neurons requires dSarm and signaling from glia"

has been approved

_____
Mentor/Advisor – Marc Freeman, PhD

_____
Committee Member – Kelly Monk, PhD

_____
Committee Member – Richard Goodman, MD, PhD

_____
Committee Member – Gary Westbrook, MD

_____
Committee Member – Michael Cohen, PhD

_____
Outside Reader – Mary Logan, PhD

TABLE OF CONTENTS

LIST OF FIGURES

LIST OF ABBREVIATIONS

- ARM – armadillo/HEAT domain
- ADP – adenosine diphosphate
- ADPR – adenosine diphosphate ribose
- ATP – adenosine triphosphate
- APEX – ascorbic acid peroxidase
- APF – after puparium formation
- BAC – bacterial artificial chromosome
- BACK – BTB and carboxyterminal kelch
- BBB – blood brain barrier
- BTB – bric-a-brac, tramtrack and broad complex
- BTBD – BTB/POZ domain-containing protein
- BSA – bovin serum albumin
- Bsk – Basket
- Ca^{2+} – calcium ion/s
- Cac – cacophony
- CaMKII – calcium/calmodulin-dependent protein kinase II
- CB – cell body
- CIPN – chemotherapy-induced peripheral neuropathy

- CNS – central nervous system
- Cul – cullin
- DAI – diffused axonal injury
- DAPI – 4′,6-diamidino-2-phenylindole
- DMEM – Dulbecco's Modified Eagle Medium
- DNA – Deoxyribonucleic acid
- cDNA – complementary DNA
- Dox – doxycycline
- Dpa – day post axotomy
- Dpe – day post eclosion
- Drpr – Draper
- DRG – dorsal root ganglia
- EMS – ethyl methane sulfonate
- FBS – Fetal Bovine Serum
- FLP – flippase
- FRT – flippase recognition target
- GFP – green fluorescent protein
- GOF – gain-of-function
- HE – head eversion
- HEK – human embryonic kidney cell

- Hiw - highwire
- hpa – hours post axotomy
- HPLC – high-performance liquid chromatography
- hs – heat shock
- hsp – heat shock protein
- ITAM – immunoreceptor tyrosine-based activation motif
- ITIM – immunoreceptor tyrosine-based inhibition motif
- JNK – c-Jun NH_2-terminal kinase
- MAPK – mitogen-activated protein kinase
- MARCM – mosaic analysis with a repressible cell marker
- Mito – mitochondria
- MKK – mitogen-activated protein kinase kinase
- MMP – matrix metalloprotease
- NAM – nicotinamide
- NAD^+ – nicotinamide adenine dinucleotide
- NaMN – Nicotinate mononucleotide
- NAMPT – nicotinamide phosphoribosyltransferase
- NMN – nicotinamide mononucleotide
- NMNd – nicotinamide mononucleotide deamidase
- Nmnat – nicotinamide mononucleotide adenylytransferase

- NR – nicotinamide riboside
- NRK – nicotinamide riboside kinase
- PAM – protein associated with myc
- PARP – poly(ADP ribose) polymerase
- PBS – phosphate buffered saline
- PBST – phosphate buffered saline with Tween-20
- PHR – PAM Hiw RPM-1
- PNS – peripheral nervous system
- RNA – ribonucleic acid
- RNAi – ribonucleic acid interference
- ROI – region of interest
- SAM – sterile alpha motif
- Sarm – sterile alpha and armadillo motif
- SCG – superior cervical ganglion
- Syt – synaptotagamin
- TBI – traumatic brain injury
- TIR – toll/interlukin-1 receptor homology domain
- UAS – upstream activating sequence
- UPS – ubiquitin-proteasome system
- VGCC – voltage gated calcium channel

- WD – Wallerian degeneration
- Wld^s – Wallerian degeneration slow
- wL3 – wandering 3rd instar larval stage
- WT – wildtype

ACKNOWLEDGEMENT

It is really a chaos now in 2020. I am glad that I can still complete my thesis defense and this dissertation during this pandemic. Look back these five years of my graduate school, I can clearly recall the moment when I first met my mentor, Marc Freeman in UMass medical school. I knocked the door, walk into his office, saw him sit on his couch. You gave me a bright smell, with your sharp eyes, and came to me. We had a brief handshake, took a sit, and started our first meeting. The first question he asked me was "Could you tell me what you have done in the past?" That was the time I first came to the school in the US, and introduce myself in English. Surprisingly, I did not feel that nervous, probably because your reactions made me calm. In fact, this is truly the reason. After I joined the lab, such emotion always come to me at every one-on-one lab meeting. You let me feel my data is meaningful even I thought it is nonsense. You let me know how to look data on different angles, all data has its meaning. I am really appreciated that having mentor like a friend, you could help me find the new direction of my project and guide me on the right track, instead of yelling on my negative data and kick me out… I am also appreciated you were willing to bring me across the States to OHSU, I hope I fulfilled your expectations. With your instruction, I can see my growth and maturation as a scientist, and I am dare to take higher challenges in this

field, to solve harder questions, and pursue my dream – contribute to this world and make it better. For example, save the lives from this pandemic… You not only care my work but also my life. I am really thankful that you could hire my wife, Ya-Chen, to the lab and work with me.

I also want to thank all the people in Freeman lab, presence and past. Sukhee Cho and Tom Burdett helped me on my rotation projects; Excellent postdocs including Megan, Jaeda, Lukas, Zhiguo, Tobi, Jiakun, Yunsik, Owen, Gaynor, Adel, Ernesto, Taylor, Leire, and Matt on their helped in the lab, and even outside of the lab. They are really good role models I can look up to; My graduate student peers including Leo, Alex, Jon, Danielle, and Katy, we can fight together to complete our graduate school works. I also have to thank our great lab manager Amy, I cannot image the lab life without her. Other lab members including Paul, Amanda, Scott, Kevin, and Rachel, I feel I am so lucky to have these good guys around me.

I would like to thank my family in Taiwan, my parents and my in-laws, and my brothers. You are willing to support me leave my hometown, fly through half of the earth to the US to pursue a higher goal of my life, and believe me that what I am doing could one day save lives of our society.

Lastly, I have to thank my wife, Ya-Chen. We were separated by the Pacific Ocean for three years, but you were willing to keep us well-connected

via the camera, I know it was hard for long-distance relationship, but I am really appreciated it. We shared our life every day, good and bad, and finally we could be married in the middle of my graduate school. I wish us all the best, and we will keep exploring our journey, and creating more of our memories together.

Jiun-Min Hsu

09/21/2020

ABSTRACT

How injury or neurodegenerative disease alter neural circuit function remains unclear. In this thesis, I explored how axotomy affects severed axons and adjacent uninjured "bystander" neurons in a simple *in vivo* nerve preparation. Following axotomy, I observed rapid suppression of transport in all axons, whether uninjured or not, and decreased sensory signaling in intact bystander neurons. Unexpectedly, the axon death gene *dsarm* was required for early changes in bystander neuron cell biology, as were the voltage-gated calcium channel Cacophony (Cac) and MAP kinase signaling. Bystander neurons later recovered, while severed axons degenerated via dSarm/Axundead signaling, and independently of Cac/MAP kinase. Interestingly, suppression of bystander neuron function required Draper receptor and JNK/MMP-1 signaling in glia, indicating glial cells actively suppress bystander neurophysiology. This work identifies a new role for Cac/dSarm/MAPK signaling and glia in the broad suppression of neural circuit function after injury, and defines two genetically and temporally separable phases of dSarm signaling in the injured nervous system.

CHAPTER I: Introduction

Introduction 1.1- Architecture of nervous system, and neural circuit.

Neurons are highly polarized cells, with compartmentalized functions in different domains. Typically, a neuron contains dendrites for receiving input from neighboring cells, a soma to help interpret and process signals, and axons for sending output to downstream neurons. The axon is a huge compartment in a neuron relative to the dendrite or cell body. The length of an axon can be many thousand times longer than the width of the cell body. For example, the longest axon in humans can extend ~1 meter in length, from the root of the sciatic nerve to the big toe of each foot, and the cell body width to axon length ratio is ~1:20,000. Axons are not thought to produce most of the factors required for survival, such as growth factors, RNA or proteins, so axons are believed to rely heavily on nutrients supplied by the cell body (De Vos et al., 2008; Millecamps and Julien, 2013). Thus, axon transport is critically important for delivering proteins and organelles to the axon to maintain homeostasis (De Vos et al., 2008). Axon transport is a dynamic process driven by a host of motor proteins, including myosin, kinesin, and dynein, and cytoskeletal proteins such as tubulins and actin, that transport cargos such as proteins, vesicles, and organelles. Given the remarkable lengths of axons, and the fact that transmission of action potentials along axons uses enormous amounts of ATP, the maintenance of

the axon is a highly energetically demanding process (Millecamps and Julien, 2013). Indeed, defects in axon transport are associated with an array of human neurological diseases (De Vos et al., 2008); however, while our knowledge of the motors that control axon transport is deep, mechanisms that regulate axon transport along the axon's length remain poorly defined.

Introduction 1.2- Nervous system injury, axon pathology.

Severe nervous system injury is one of the most devastating neurological conditions with profound, long-lasting, and irreversible effects on nervous system function. There are many types of injuries in central nervous system (CNS) and peripheral nervous system (PNS), including mechanical injury (e.g. traumatic brain injury), chemotherapy induced peripheral neuropathy (CIPN), metabolically-induced neuropathy (e.g. diabetic-induced peripheral neuropathy), viral infection induced axon degeneration, and various neurodegenerative diseases such as Parkinson's and Alzheimer's diseases. A shared feature of these injuries and diseases is axon degeneration, where connectivity between neurons is broken due to the loss of axonal connections, which in turn disrupts neural circuit signaling. Axon degeneration and synapse loss are among the best correlates of functional

loss in patients with brain injuries or neurological diseases (Burke and O'Malley, 2013; Hill et al., 2016; Kasahara et al., 2010; Kneynsberg et al., 2017). In addition, there is a complex interaction between brain injury and neurodegenerative disease that we do not yet understand: for example, a single episode of TBI appears to be associated with increased risk for later onset neurodegenerative diseases, including Alzheimer's disease (Chen et al., 2009; Johnson et al., 2013).

Introduction 1.3- Wallerian degeneration and the *slow Wallerian degeneration* mutant.

When an axon is injured, the portion distal to the injury site undergoes fragmentation, which was first identified by Augustus Waller in 1850, as such, this phenomenon is called Wallerian degeneration (WD) (Coleman, 2005; Waller, 1850). This fragmentation was thought to be a passive process, the consequence of disrupted axon transport, thereby preventing delivery of nutrients, proteins, cellular organelles from the cell body to the axon (De Vos et al., 2008). However, this idea was challenged by the discovery of *slow Wallerian degeneration* (*Wld*^{s}) mice, a mutant in which severed axons remain morphologically intact for weeks after injury (rather

than hours) without any connection to cell body (Lunn et al., 1989). This finding revealed that, under some circumstances, axons can survive for very long periods of time without a cell body. This observation also led to the suggestion that Wallerian degeneration is an active process in the axon compartment regulated by an unknown molecular pathway.

Michael Coleman's group ultimately identified the genomic lesion in *Wld*^{S} mutant mice as a gene fusion event that led to the production of a chimeric protein composed of a nuclear isoform of nicotinamide adenine dinucleotide (NAD^{+})-biosynthetic enzyme nicotinamide mononucleotide adenyltransferase 1 (Nmnat1) and a 70-amino-acids of the N-terminal sequence from the E3 ubiquitin ligase UBE4B (N70). Expression of Wld^{s} alone can protect distal axon fibers from sciatic nerve lesion for periods equal to that of the *Wld*^{S} mutant mouse (Conforti et al., 2007). Wld^{s} also displayed the same protective effect in rats, fruit flies, zebrafish, and human primary neuronal cultures, indicating that the Wld^{s} neuroprotective function is evolutionarily conserved (Adalbert et al., 2005; Kitay et al., 2013; Lunn et al., 1989; MacDonald et al., 2006; Martin et al., 2010).

The precise mechanism by which Wld^{s} suppresses axon degeneration is still unclear, but a unifying hypothesis is that Wld^{S} functions by

redistributing the normally nuclear NAD^+ biosynthetic enzyme (Nmant1) to the cytoplasm and axons via the N70 domain, and thereby maintaining NAD^+ levels after injury. Consistent with this notion, cytosolic localization directed by the N-terminal sequence, and enzymatic activity of Nmnat1 are both critical for its protective function (Avery et al., 2009; Conforti et al., 2009). At the same time, studies in the Bellen lab identified that Nmnat1 has chaperone activity, similar in function to heat-shock protein 70 (Hsp70), where it is thought to maintain proteostasis and protect neurons from degeneration (Zhai et al., 2008). Precisely how this chaperone activity might be involved in suppression of Wallerian degeneration is not clear, as chaperone activity did not require enzyme activity (although suppression of Wallerian degeneration did).

Introduction 1.4- Axon survival factor Nmnat and NAD^+ metabolism.

The requirement of cytosolic localization and NAD^+ biosynthetic activity of Wld^s implies that axon degeneration may be caused by loss of cytosolic NMNAT activity or NAD^+. In mammals, Nmnat consists of three isoforms that are located in different cellular compartments: Nmnat1 is in the nucleus, Nmnat2 is in the cytosol, and Nmnat3 is associated with mitochondria

(Raffaelli et al., 2002; Zhang et al., 2003). Although they all possess similar NAD^+ biosynthetic activities *in vitro*, Nmnat2 acts as the critical survival factor in neurons (Gilley and Coleman, 2010). Nmnat2 is the most labile Nmnat isoform, with short half-life (~45 minutes), thus the pool of axonal Nmnat2 requires constant resupply from the cell body via anterograde axon transport (Gilley et al., 2013; Milde et al., 2013a). A reduction in the level of Nmnat2 in superior cervical ganglion neuron cultures precedes Wallerian-like axon degeneration and neuronal death, and knockdown by RNA interference can induce degeneration (Fang et al., 2012; Gilley and Coleman, 2010; Neukomm et al., 2017). Homozygous *nmnat2* mutant mice die perinatally with short axons (Gilley et al., 2013), indicating that Nmnat2 is both required for neuron development and maintenance. These observations led to the model that axonal transection interrupts the cell body-derived supply of Nmnat2, the labile pool of axonal Nmnat2 is depleted, which in turn results in axon degeneration. Wld^s, which is much more stable than Nmnat2, is thought to protect axons by functionally substituting for the loss of Nmant2 NAD^+ biosynthetic activity in the axon.

The degradation of Nmnat2 is mediated by the ubiquitin-proteasome system (UPS). Suppressing proteasome activity by inhibitors delays axon degeneration, likely through increased preservation of Nmnat2. Highwire

(*hiw*) is a key E3 ubiquitin ligase thought to target Nmnat2 for UPS degradation. The absence of *hiw* increases the stability of both dNmnat and ectopically expressed mammalian Nmnat2, and strongly suppresses axon degeneration after axon crush or axotomy, but not axon degeneration induced by dNmnat depletion (Xiong et al., 2012). Loss of Phr1, the mammalian homolog of Highwire, also suppresses axon degeneration and increased the stability of Nmnat2, suggesting conserved role in regulating the degradation of Nmnat2/dNmnat2 in neurons.

Previous studies showed that Nmnat2 is associated with the Golgi apparatus and vesicles in HeLa cells (Mayer et al., 2010; Milde et al., 2013b). In neurons, Nmnat2 colocalizes in axons with Golgi and synaptic vesicle markers (Mayer et al., 2010; Milde et al., 2013b). Nmnat2 is palmitoylated on its C164/C165 residues, which is required for its vesicular localization. Nmnat2 variants lacking palmitoylation are more stable than wild-type Nmnat2, and delay axon degeneration, arguing that palmitoylation contributes to the fast turnover of Nmnat2. However, much of the data supporting a Hiw/Phr1-mediated degradation of Nmnat2 is indirect, and so why this critical survival factor is so unstable remains an open question.

How does loss of Nmnat2 induce axon degeneration and neuron death? As its NAD^+ biosynthetic activity is important for Wld^s and Nmnat2 to protect axons from degeneration, it is possible that loss of Nmnat2 reduces the NAD^+ supply, which in turn results in a catastrophic energy loss. Indeed, axonal NAD^+ is progressively reduced after nerve transaction, and the initiation of axon degeneration occurs immediately after depletion of NAD^+ (Wang et al., 2005). NAD^+ is a critical co-factor for various metabolic pathways in cells, serving as a key bioenergetic intermediate. It is not hard to image that loss of NAD^+ might be extremely harmful to cells, and the maintenance of its supply is pivotal. However, simply increasing the level of NAD^+ by suppressing the other NAD^+ consuming proteins, CD38 and PARP1, does not suppress axon degeneration (Sasaki et al., 2009), arguing that the signaling mechanisms driving WD are likely more complicated than a simple loss of NAD^+. In mammals, most NAD^+ is produced via a salvage pathway, where NAD^+ is converted by Nmnat from nicotinamide mononucleotide (NMN) and ATP (Berger et al., 2005). Loss of Nmnat2 blocks the salvage pathway, resulting in not only reduction of NAD^+, but also accumulation of NMN. Recent work has led to the proposal that Nmnat or Wld^s protects axons via reducing NMN accumulation rather than supplementing NAD^+, leading the authors to suggest that NMN is actually

the toxic factor promoting axon degeneration after axotomy (Di Stefano et al., 2014). NMN synthesis is dependent on the nicotinamide phosphoribosyltransferase (NAMPT). Pharmacologically blocking NAMPT with FK866 can prevent NMN accumulation and suppress axotomy-induced axon degeneration. This suppression can be reverted by exogenous NMN introduction, supporting a pro-degenerative role of NMN. In addition, overexpression of the bacterial enzyme NMN deamidase, which degrades NMN, showed prominent protection of axon degeneration in cultured mouse neurons and *in vivo* in zebrafish and mice, further supporting the idea that NMN promotes axon degeneration. However, there is also data that conflicts with a simple NMN toxicity model. Another group showed that increasing NMN through the combination treatment of nicotinamide riboside kinase (NRK) overexpression and nicotinamide riboside (NR) application, which is another route to produce NMN levels ~14-fold in cultured neurons, did not induce axon degeneration (Sasaki et al., 2016). This result argues that simple NMN accumulation is not sufficient to activate axon degeneration, and that we need to probe more deeply to understand how NAD^+ and NMN regulate axon degeneration.

Introduction 1.5- dSarm and Axed are key molecules of the axon pro-degenerative program

Axon degeneration is regulated by an injury-induced molecular pathway specific to the axon compartment (Buckmaster et al., 1995; Raff et al., 2002). Upon injury, the axon initiates self-destructive processes independent of the apoptotic cell death pathway (Burne et al., 1996; Deckwerth and Johnson, 1994; Finn et al., 2000). To explore whether axon degeneration is indeed genetically controlled, a forward genetic screen in *Drosophila* identified the sterile α/Armadillo/Toll-interleukin receptor homology domain (dSarm) molecule as essential for axon auto-destruction—loss of dSarm completely blocked Wallerian degeneration (Osterloh et al., 2012). The same level of protection of axon degeneration after axotomy was also observed in the *in vitro sarm1* knockout mice neurons, as well as the *in vivo* injury models (Gerdts et al., 2013; Osterloh et al., 2012), indicating a conserved role of Sarm1/dSarm in triggering axon degeneration after injury.

Sarm1-dependent axon death mechanisms are also involved in the pathology of some diseases. Loss of Sarm1 suppressed axon degeneration and early onset neurological deficits in mouse models of TBI or repetitive mild close head injury (Henninger et al., 2016), chemical- or diabetic-

induced peripheral neuropathy, (Geisler et al., 2019; Turkiew et al., 2017), axon degeneration in the pathogenesis of rabies virus (Sundaramoorthy et al., 2020), and TDP-43-linked motor neuron degeneration (White et al., 2019). Sarm1 inhibition is thus an exciting potential approach for blocking axon loss and neuroinflammation in human disease (Wang et al., 2018). Interestingly, *sarm1* knockout mice have normal lifespan, without obvious defects, and confer life-long rescue of axonopathy (Gilley et al., 2017; Kim et al., 2007). Therefore, Sarm1 has become a compelling therapeutic target for neurological disorders (Geisler et al., 2019).

Both in mammals and *Drosophila*, the Sarm1/dSarm gene encodes a protein with Armadillo/HEAT (ARM) domain, two sterile alpha motifs (SAM), and a Toll/interleukin-1 receptor homology (TIR) domain (Gerdts et al., 2013). To understand the mechanism of Sarm1 mediated axon degeneration, we and others performed domain analysis and found that deletion of the ARM domain, which was proposed to be autoinhibitory in *C. elegans* (Chuang and Bargmann, 2005). The truncated isoform of Sarm1/dSarm (termed gain-of-function Sarm1/dSarm, $Sarm1^{GOF}$/$dSarm^{GOF}$) could actively trigger neuron cell body and axon degeneration, with or without the presence of wild-type dSarm. dSarm/Sarm1 has been studied primarily in the nervous system as a positive regulator of axonal

degeneration, and the mechanisms have been delineated. The major role of dSarm/Sarm1 is proposed to lead to axonal NAD^+ depletion and metabolic catastrophe in severed axons (Gerdts et al., 2015) through a Sarm1 intrinsic NAD^+ hydrolase activity in the TIR domain (Essuman et al., 2017). In these studies, homodimerization of the TIR domain activates its enzymatic activity, a result similar to other TIR domain-contain proteins where dimerization of the TIR domain is required for signal transduction (Gerdts et al., 2015; Yang et al., 2015). The crystal structure of Sarm1 TIR domain and SAM domain shows that SAM domain forms an octameric ring (Horsefield et al., 2019). Disruption of SAM oligomerization fails to rescue axon degeneration in *sarm1*$^{-/-}$ SCG neurons, suggesting that octamerization is required for Sarm1 function (Avery et al., 2009).

How dSarm/Sarm1 is activated after axotomy is still unclear. Nmnat2 loss somehow activates Sarm1, given that *sarm1* knockout mice suppress the lethality of *nmnat2* null mutations (Gilley et al., 2015). As mentioned above, Nmnat2 loss leads to the accumulation of NMN. Interestingly, a recent study showed that Sarm1 NAD^+ hydrolase activity appears to be activated directly by the NAD^+ precursor, NMN, presumably through allosteric conformational changes in Sarm1 upon NMN binding (Zhao et al., 2019). Taken together, the emerging model of axon degeneration is that axotomy

leads to depletion of labile Nmnat2 in axons by disconnecting the axon from the cell body, degradation of the axonal Nmnat2 pool, which ultimately causes NMN accumulation and activation of Sarm1. Sarm1 is believed to then further degrade axonal NAD^+ below the threshold needed for maintaining axon integrity, eventually resulting in axon destruction. This NAD^+ depletion model has been proposed as the primary mechanism by which Sarm1 drives axon loss, and to explain the mechanistic basis of protection by a number of other neuroprotective molecules (Gerdts et al., 2016).

This simple NAD^+ depletion model fits with much of our current knowledge about dSarm/Sarm1 function, but there are important caveats that argue against it. We recently reported that all known dSarm pro-degenerative function requires the BTB and BACK domain molecule Axundead (Axed) (Neukomm et al., 2017). How Axed executes dSarm pro-degenerative activity is unclear, and the simple NAD^+ depletion model is difficult to reconcile with observations regarding the role of Axed on axon destruction. First, it is clear that loss of Axed suppresses axon degeneration caused by loss of dNmnat (even in null clones). Second, Axed can suppress the axon death induced by activation of dSarm (i.e. driving NAD^+ consumption by overexpressing $dSarm^{GOF}$). Although there is as yet no

sufficiently sensitive indicator that will allow for quantification of the levels of NAD^+ in these manipulations in the axons, these results still challenge the NAD^+ depletion model, and suggest that axon degeneration is likely not as simple as loss of NAD^+.

Introduction 1.6- Role of Ca^{2+}/Sarm1/MAPK signaling in axon degenerative pathways.

In addition to the involvement of NAD^+ metabolism, elegant genetic studies in *C. elegans* demonstrated that TIR-1 (the worm homolog of dSarm/Sarm1) is part of a signaling cascade downstream of the voltage gated calcium channel UNC -36 and CamK-II, and signals via the MAP kinase (MAPK) signaling cascade (Chuang and Bargmann, 2005).

Channel-mediated influx of extracellular calcium is important for the onset of Wallerian degeneration, given that reducing extracellular Ca^{2+} levels with low-Ca^{2+} medium, or bath application of the calcium chelator EGTA suppresses the initiation of calcium degeneration (George et al., 1995). Consistent with a role for Ca^{2+} in axon loss, axonal Ca^{2+} increases after injury were alleviated by Wld^s overexpression, and exogenous addition

of Ca^{2+} was sufficient to re-initiate axon degeneration in Wld^s axons (Avery et al., 2009; Glass et al., 1994). One role for calcium is likely the activation of the serine-threonine protease calpain, which is capable of cleaving neurofilament and microtubule associated proteins to disrupt axonal structure, which could be activated by injury-induced Ca^{2+} signals (Billger et al., 1988; Knoferle et al., 2010). However, blockade of calpain activity with inhibitors only provides mild protection of axon degeneration after axotomy, which is significantly weaker than Ca^{2+} chelation (George et al., 1995). Therefore, the downstream signals activated by Ca^{2+} remain to be identified, although the initial work in *C. elegans* supports the notion that Sarm1/Tir-1 is one of the downstream targets of Ca^{2+} signaling that activates axon degeneration (Chuang and Bargmann, 2005).

How MAPK signaling might drive axon degeneration remains unclear. Activation of MAPK signaling (i.e. phosphorylation of MAPK pathway members) were found in axons within 15-30 minutes after axotomy, were Sarm1-dependent (Yang et al., 2015), and partial suppression of axon degeneration was observed after simultaneous blockade of multiple MAPK components (Walker et al., 2017; Yang et al., 2015). But how MAPK signaling modulates axon degeneration, particularly in the context of Sarm1 signaling, remains controversial as one study proposed MAPK

signals downstream of Sarm1 (Yang et al., 2015), while another argued Sarm1 was upstream of MAPK signaling (Walker et al., 2017), and the neuroprotective phenotypes resulting from MAPK blockade do not approach levels afforded by loss of Sarm1 *in vivo*.

Introduction 1.7- The effects of injury on bystander neurons.

The response of neurons and their axons to injury is not restricted to the injury site. Emerging evidence supports the notion that the injured or diseased neuron might also alter the functional properties of neighboring healthy "bystander" neurons (i.e. those not damaged or expressing disease-associated molecules). If true, this might change how we think about the effects of injury on the nervous system—if the physiology of bystander neurons is radically altered by their damaged neighbors, this would force us to reconsider the notion that strict loss-of-physical-connectivity is required for functional loss in neural circuits when the nervous system is traumatized.

A limited number of studies support the notion that bystander neurons can radically change their physiology in response to their neighbors being injured. For instance, mouse L5 spinal nerve transection results in the

degeneration of distal L5 afferents in sciatic nerve alongside intact L4 C fiber afferents. Within one day after L5 lesion, L4 C fibers develop spontaneous activity that lasts for at least a week and appears to mediate injury-induced pain and hyperalgesia behaviors (Wu et al., 2001). Uninjured neurons can therefore detect and respond to nerve injury, but how remains a mystery. Similar mechanisms could be in place in the CNS. In mouse models of mild TBI, on one day after injury, the pyramidal neurons with severed axons and intact bystander neurons both exhibited similar injury-induced changes in action potential firing and after hyperpolarization. Injured neurons failed to recover while bystander neurons exhibited a return to normal firing properties (Greer et al., 2012).

In some cases, TBI also led to broader development of axonal pathology in non-injured neurons, which was termed "diffused axonal injury (DAI)" (Johnson et al., 2013). The DAI pathologies include termination of axon transport, axon swelling, and Wallerian degeneration (Johnson et al., 2013). Depending upon the severity of injury, DAI was also found to lead to clinical symptoms such as immediate loss of consciousness, persistent coma, and cognitive dysfunction (Johnson et al., 2013). Interestingly, neurological deficits that develop after TBI are Sarm1-dependent (Henninger et al., 2016; Marion et al., 2019). After TBI in *sarm1* knockout mice, animals exhibited

fewer ß-amyloid precursor protein aggregates in axons, reduced plasma concentration of phosphorylated axonal neurofilament, and preservation of behaviors correlated with neurological functions (Henninger et al., 2016; Marion et al., 2019). Curiously, even very early events like paresis and other behavioral changes were also suppressed in *sarm1* knockout animals as early as 2 hours after injury. Given that Wallerian degeneration does not occur until at least 36 hours after injury, the early role for Sarm1 in these behavioral changes suggests that Sarm1 function early after injury may be separable from its roles in axon degeneration.

Introduction 1.8- Glia and neuroinflammatory responses.

Although it is clear that bystander neurons can detect local injury and change their physiology, it remains unclear how bystander neurons receive injury signals. One possibility is that glia play important roles in the response of neural circuits to injury or disease pathology. Four major types of glia have been identified in the vertebrate nervous system, including astrocytes, microglia, and oligodendrocytes in the CNS, and Schwann cells in the PNS. Astrocytes are ubiquitously distributed across the CNS and regulate a variety of neural circuit activities (Herculano-Houzel, 2014);

microglia function as the CNS immune cells together with other immune cells to respond to injuries (Li and Barres, 2018) and remodel synaptic connections (Schafer et al., 2012; Stevens et al., 2007); oligodendrocytes are mainly required for myelination–the structure enwrapping axons to optimize axon structure and accelerate the axon conduction velocity, and trophic support of axons (Boulanger and Messier, 2014). In PNS, Schwann cells myelinate or ensheath neurons to support the neuronal structure and function (Freeman et al., 2003; Freeman and Doherty, 2006).

In addition to their roles in regulating the healthy nervous system, glia also potently respond to injury, including TBI and spinal cord injury (SCI) (Gaudet and Fonken, 2018; Greenhalgh et al., 2020). Some glial-driven responses are beneficial. For example, astrocytes promote scar formation to prevent secondary damage (Wanner et al., 2013); oligodendrocytes perform activities that are required for remyelination and axon regeneration (Kondiles and Horner, 2018); and Schwann cells in the PNS initiate adaptive responses to nerve injury to help axon regeneration and remyelination (Guest et al., 2005). However, the role of glia can also be detrimental and promote disease progression after injury. Neuroinflammatory responses, which are mainly mediated by microglia and astrocytes, lead to the release of a mixture of inflammatory signals in the injured nervous system (Gaudet

and Fonken, 2018; Greenhalgh et al., 2020). Glia rapidly upregulate tumor necrosis factor-alpha (TNF-α), interleukin-1β (IL-1β), and IL-6, and promote immune cells infiltration to drive acute post-trauma inflammation (Gaudet and Fonken, 2018; Greenhalgh et al., 2020; Hwang et al., 2006; Johnson et al., 2013; Kyrkanides et al., 1999). This massive release of cytokine, chemokine, and inflammatory mediators leads to the disruption of blood-brain barrier (BBB), recruitment more leukocytes, as well as induction of necroptotic cell death and DAI. This cytokine storm can lead to dysregulated inflammation and severe damage in the CNS (Gaudet and Fonken, 2018; Greenhalgh et al., 2020).

Matrix metalloproteinase (MMP) MMP-2 and MMP-9, the secreted-type of MMPs, are elevated and released by glia in regions surrounding the injury after ischemia, stroke, and in multiple sclerosis (MS) (Esparza et al., 2004; Fujioka et al., 2012; Noble et al., 2002; Weaver et al., 2005). The MMP family is associated with increases in the permeability of BBB, which in turn opens routes for extravasation of immune cells into the brain parenchyma (Bell et al., 2012; Candelario-Jalil et al., 2011). Ectopic injection of activated MMP-9 can cause demyelination and axonal damage (Newman et al., 2001). Strangely, *mmp-9* null mice recover better from spinal cord injury (Noble et al., 2002), suggesting a negative role of MMPs

in the pathology of nervous system injuries—this highlights the complexity of responses of the CNS to injury or disease.

Introduction 1.9 – Role of Draper/MEGF10 in nervous system injury.

Glia are also involved in axon debris clearance after axon injury, which is regulated by the key engulfment receptor Draper (Freeman et al., 2003; MacDonald et al., 2006). After injury, axon debris is not properly cleared in *draper*$^{-/-}$ flies, instead axonal debris lingers in the CNS for weeks after axotomy (MacDonald et al., 2006; Neukomm et al., 2014). The mammalian ortholog MEGF10 is also required in glia for driving neuron debris clearance (cell corpses, synapses, and axon debris) during developmental neuronal remodeling (Wu et al., 2009). Draper can signal through the Src kinase Src42A, the non-receptor tyrosine kinase Shark, and the Rac family of small GTPases (Rac1) to activate the transcription factor Stat92E to further upregulate *draper* expression, and promote glial membrane extension to the regions of axon debris for engulfment (Doherty et al., 2009; Doherty et al., 2014; Ziegenfuss et al., 2008). Draper also requires the PTB domain-containing protein dCed-6, which functions as adaptor proteins, to activate glial phagocytosis independent of Stat92E (Awasaki et al., 2006; Doherty et

al., 2009; Doherty et al., 2014). In addition to driving target internalization, Src/Shark/Rac1/Stat92E signaling also signal to the nucleus to upregulate *draper* expression, thereby creating a positive feedback loop that coordinates the levels of Draper on the membrane with the severity of the axonal injury (Awasaki et al., 2006; Doherty et al., 2009; Doherty et al., 2014). Activation of Draper-mediated glial responses is downstream of axon degeneration, since glial activation is blocked by overexpressing Wld^{s} or knocking out *hiw* (Lu et al., 2017; MacDonald et al., 2006).

Draper-Shark interactions occur through an immunoreceptor tyrosine-based activation motif (ITAM) in the Draper intracellular domain (Logan et al., 2012), which is reminiscent of B- and T-cell receptors and Fcγ receptors (Underhill and Goodridge, 2007). ITAM signaling in these receptors can be inhibited by the immunoreceptor tyrosine-based inhibitory motif (ITIM) (Daeron et al., 2008; Pinheiro da Silva et al., 2008). Interestingly, three Draper isoforms have been identified that are generated by alternative splicing termed Draper-I, -II, and -III (Logan et al., 2012). Draper-I contains ITAM and is upregulated after axon injury to drive glial engulfment. In contrast, Draper-II is the shorter alternative splice variant upregulated later, which potently suppresses Draper-I signaling through ITIM-like domain and tyrosine phosphatase Corkscrew (Csw), thereby terminating glial responses

after nerve injury (Logan et al., 2012). Ectopic expression of Draper-II strongly suppresses the engulfment of axon debris, but does not affect Draper-I expression, suggesting that Draper-II directly inhibits Draper-I function, instead of interfering with upstream regulation of Draper levels (Doherty et al., 2009; Doherty et al., 2014; Logan et al., 2012).

Draper can also signal via TNF receptor associated factor 4 (TRAF4) and c-Jun N-terminal Kinase dJNK (Bsk) signaling to activate transcription via *Drosophila* active protein 1 (dAP-1), a heterodimer of Jra (c-Jun) and Kayak (c-Fos) (Lu et al., 2017). This signaling is upstream of Stat92E in the regulation of Draper (Doherty et al., 2014), but how these pathways connect is not clear. Matrix metalloprotease 1 (MMP-1) in glia is one of the downstream targets of Draper-JNK that promotes glial engulfment. MMP-1 is quickly upregulated following nerve injury to promote glia membrane extension to injury sites (Purice et al., 2017). There are only two proteins in the MMP family in flies, MMP-1 and MMP-2. MMP-1 is the secretory form whereas MMP-2 is the GPI-anchored form of MMP family (Page-McCaw, 2008). The mechanisms and downstream targets of MMP-1 remain to be defined, but their conserved activation in glia after injury further support the notion that glial responses to axon degeneration are conserved in mice and flies.

Introduction 1.10 – Thesis overview.

In this thesis, I describe my work exploring the mechanism by which axon injury leads to axon loss and suppression of function. In Chapter II, I use a partial nerve injury model to characterize early changes in the physiology of severed axons and neighboring uninjured bystander neurons. I show that axotomy of even a small subset of neurons leads to rapid blockade of axon transport in all axons, and suppression of sensory signal transduction in bystander neurons. Surprisingly, this early blockade of axon transport and sensory signal transduction required dSarm, but not Axed, in both severed axons and uninjured bystander neurons, where it signaled with the conserved UNC-36/MAPK signaling pathway first identified in *C. elegans*. In Chapter III, I describe my findings that Sarm1 NADase activity is enhanced by NMN, and suppression of bystander neuron function was not modulated by NMN, nor induced by depletion of dNmnat. These data support the notion that early responses to axon injury via dSarm are mechanistically different from later events in axon death where dSarm drives axon degeneration through Axed. In Chapter IV, I describe work where I discovered that this early spreading of injury signals to bystander neurons required the Draper

receptor in surrounding glia, which signals through JNK, dAP-1, and MMP-1 in glia, indicating that glia, through the Draper signaling pathway, actively inhibit the function of bystander neurons.

In addition to the main chapters, I describe the result of a dNmnat RNAi suppressor screen in appendix I. I found that *Drosophila* homolog of Nudt9, CG4098, is required for dNmnat RNAi induced neuronal death. I also describe experiments investigating the roles of gain-of-function Sarm1/dSarm in non-neuronal cells, including HEK293T cells and *Drosophila* salivary glands.

My work identifies new roles for dSarm in modifying axon function early after injury and a new role for UNC-36/MAPK signaling in promoting dSarm-dependent changes after axon injury. I propose that two genetically separable phases of dSarm signaling exist that differentially mediate early reversible changes in neurophysiology versus later axon degenerative events in injured neural circuits.

CHAPTER II: Widespread injury-induced changes in neuronal physiology are mediated by a Cac/dSarm/MAPK signaling pathway

In this chapter, Owen Peters identified the axon transport suppression after injury in the wings, and the maintained axon transport in *dSarm* mutants; Danielle Methieson performed calcium imaging analysis after wing neuron laser ablation, and I conducted all additional experiments.

The following manuscript is in revision for publication:

Injury-induced inhibition of bystander neurons requires dSarm and signaling from glia

Jiun-Min Hsu, Yunsik Kang, Megan Corty, Danielle Methieson, Owen Peters, Marc Freeman

Chapter II: Abstract

This chapter describes my work using a simple *in vivo* nerve injury preparation, I explored how axotomy changes the physiology of severed axons and adjacent uninjured "bystander" neurons. We observed a suppression of axon transport in both severed axons and bystander neurons within hours after injury, and decreased mechano- and chemosensory signal transduction in local intact sensory neurons. I showed that the axon death molecule dSarm was required for all of these early responses to injury, including blockade of sensory signaling in uninjured neurons, as was the voltage-gated calcium channel Cacophony (Cac) and the MAP kinase signaling cascade. Intact neurons recovered within 12 hours after injury and survived, while severed axons executed axon death through dSarm/Axed signaling, independent of MAPK. This work identifies a new, early and broad role for dSarm in promoting injury-induced changes in neurophysiology, showing that dSarm functions even in intact neurons after injury without driving axon destruction, and identified a new role for Cac/dSarm/MAPK signaling pathway in the spreading of signals that modify neural circuit function after injury.

Chapter II: Results & Discussion

Result 2.1 - Nerve injury blocks vesicle trafficking in both severed and intact axons.

I wished to examine immediate injury-induced changes in neurophysiology in severed axons along with neighboring intact neurons. To accomplish this, I used a partial axotomy model in the adult *Drosophila* wing. The L1 wing vein nerve houses ~220 sensory neurons whose cell bodies are aligned along the anterior wing margin, with all axons projecting medially and synapsing in the thoracic ganglion (Fang et al., 2012; Neukomm et al., 2014). Sensory axons are ensheathed by glial cells along their entire length (Neukomm et al., 2014). Transecting the wing nerve at its midpoint severs the axons of approximately half of the sensory neurons (Figure 2.1): those with cell bodies distal to the injury site are axotomized, while those with cell bodies proximal to the injury site remain intact and survive for weeks after injury. Severed axons undergo Wallerian degeneration ~8-10 hours after axotomy and neuronal debris is cleared by surrounding glial cells with 5-7 days (Neukomm et al., 2014).

I live imaged axon transport in the L1 wing vein as a first step toward determining how axon biology changes in response to nerve injury. Sensory

neurons were sparsely labeled using the mosaic analysis with a repressible cell marker (MARCM) approach (Lee and Luo, 1999; Neukomm et al., 2014), which allowed for the GAL4/UAS-dependent labeling of single cell clones with membrane tethered GFP. After surgical removal of the distal half of the wing, we directly compared the phenotypes of severed axons alongside remaining intact neighboring neurons (Figure 2.1). For examination of changes in axon transport, we labeled four different types of axon cargoes: autophagosomes (*UAS-mCherry-atg8a*), lysosomes (*UAS-GFP-lamp*), synaptic vesicles (*UAS-syt-GFP*), and mitochondria (*UAS-mito-GFP*). In uninjured wings, autophagosomes were transported in anterograde and retrograde directions along axons, with almost 80% of the total population exhibiting movement (both anterograde and retrograde) during the 3-minute observation window (Figures 2.2A, B). In severed axons, the number of autophagosomes moving decreased to ~25% within 1 hour, and continued to decrease at each hour timepoint until it was <4% at 4 hours after injury (Figures 2.2A, B). To my surprise, I also found that the percent of moving autophagosomes dropped significantly in the axons of neighboring intact bystander neurons at 3 hours after injury (Figures 2.2A, C), and partially recovered by 6 hours after axotomy. Although we did not find a statistical difference between uncut group when comparing to other

time points (1, 2, 4, 6, and 24 hrs), the average autophagosome transport percentage on the axons was still reduced as much as 10% to 20%. The high variations in each group may explain the lack of a statistical difference. We observed a similar time course for suppression of axonal transport of lysosomes (Figures 2.3A, B) and synaptic vesicles (Figures 2.3C, D), with a near full blockade of transport in severed axons, and partial suppression in bystander neurons. Mitochondria were largely stationary in adult post-mitotic neurons, so they were not examined further.

I sought to determine whether the proximity of neuronal cell bodies of bystander neurons to the injury site affected the severity of axon transport blockade, or whether blockade of axon transport was uniform throughout the wing nerve. I lesioned the L1 wing nerve distally, removing only ~20 neuronal cell bodies from the tip of the wing, and then imaged the transport of autophagosomes in intact bystander neurons at 3 hours after injury at two sites along the wing nerve, one distant from (Site A) and one closer to (Site B) the injury site (Figure 2.4). I found that regardless of the distance of the cell body from the lesion site, or even the reduced number of severed axons in the more distally injured nerve preparation (~20 in the distal lesion, versus ~110 with midpoint lesions), the suppression of autophagosome transport was similar in bystander neurons and approximated that observed when we

lesioned the midpoint of the wing. These data indicate that nerve injury efficiently suppresses axon transport throughout the L1 wing nerve within 3 hours after injury, even with relatively small (~20 neuron) injuries. Because the axons of uninjured cells also exhibited this phenotype, I conclude that bystander neurons can detect nerve injuries even at a distance, and respond by suppression of axon transport.

Result 2.2 - dSarm, but not Axed is required for the blockade of vesicle trafficking in both severed and intact axons after injury.

Approximately 8-10 hours after axotomy of the L1 wing vein, axon death is driven cell autonomously by dSarm in severed axons (Neukomm et al., 2014). While dSarm is primarily thought to drive axon death at these later stages, we assayed *dsarm* mutant clones to determine whether dSarm was also required for this early suppression of axon transport. I found normal rates of axon transport of autophagosomes (Figure 2.5A, B) and lysosomes (Figure 2.7) in axons in $dsarm^{896}$ null mutant clones before injury. However, in contrast to wild-type clones, $dsarm^{896}$ null clones exhibited normal rates of axon transport of autophagosomes in severed axons for at least 6 hours after axotomy (Figures 2.5C). This was confirmed using the

independent null allele *dsarm*^{4705} (Figure 2.5B) and using markers for lysosomes (Figure 2.7). In addition, I also found that introducing the Bacterial Artificial Chromosome (BAC) that covers the dSarm genomic locus could rescue the axon transport blockade phenotype (Figure 2.5B). I conclude that dSarm is required within the first few hours after axotomy for blockade of axon transport in severed axons.

I next examined axon transport in adjacent uninjured *dsarm* null mutant clones and found, unexpectedly, that transport of autophagosomes was also maintained at normal levels in bystander neurons (Figures 2.5A, B, and D). This was also confirmed using the *dsarm*^{4705} allele (Figure 2.5B), and by examination of lysosome transport (Figure 2.7). This observation indicates that dSarm is required in bystander neurons to detect nerve injury and suppress axon transport. To our knowledge, this is the first description of a cell autonomous role for dSarm/Sarm1 after nerve injury in changing the physiology of uninjured neurons.

Loss of Axed suppresses axon degeneration at levels equivalent to loss of dSarm (Neukomm et al., 2017). To determine whether dSarm functions to suppress axon transport through Axed, I assayed axon transport in *axed* null mutant clones before and after nerve injury. I found normal

rates of axon transport for autophagosomes (Figure 2.6A, B) and lysosomes (Figure 2.7) before axon injury in *axed* null clones. However, in both severed and bystander neurons, we found that loss of Axed did not maintain axon transport after nerve injury (Figures 2.6A, B), and axon transport was suppressed within 1 hour after axotomy (Figure 2.6C, D). This was confirmed with a second null allele of *axed* (Figure 2.6B), and similar results were found with lysosomes (Figure 2.7). I conclude that Axed is not required for nerve injury-induced blockade of axon transport, despite its critical role at later stages in executing dSarm-dependent axon degeneration (Neukomm et al., 2017).

Result 2.3 - Cacophony and the TIR-1-like-MAPK signaling pathway promote blockade of vesicle trafficking after nerve injury.

C. elegans TIR-1 (worm dSarm/Sarm1) signals downstream of the voltage-gated calcium channel (VGCC) UNC-36 and activates a conserved MAP kinase cascade (Figure 2.8A) (Chuang and Bargmann, 2005). In injured mouse DRG axons, the MAPKK MKK4, and the MAPKs JNK (1,2,3), are phosphorylated within 15 min in a Sarm1-dependent fashion (Yang et al., 2015), arguing for an early role in injury-induced changes in axon biology.

To determine whether dSarm might signal through a VGCC/dSarm/MAPK-like cascade early in axonal injury signaling, we first visualized axon transport in mutants for cacophony, which encodes the *Drosophila* ortholog of UNC-36. We found in MARCM clones of cac^{K}, similar to *dsarm* null mutants, that axon injury failed to suppress the transport of autophagosomes (Figure 2.8B) and synaptic vesicles (Figure 2.8C) in both severed and bystander neuron axons. Similar results were found with a second strong loss of function allele of *cac*, cac^{F} (Figures 2.8B, C), which is a channel conductance mutant (Tian et al., 2015), arguing for a role for ion conductance in promoting suppression of axon transport.

I next assayed for roles of the MAPKKKs Ask1 and Slpr, and the MAPKKs Lic, Mkk4, and Hep. We found that MAPK signaling components were required for potent suppression of axon transport after axotomy in severed and intact bystander neurons (Figures 2.9), although their phenotypes did not appear as strong null alleles of *dsarm* or *cac*, possibly due to the partially redundant nature of the MAPK cascade. Despite these clear roles in early blockade of axon transport, even strong loss-of-function alleles of *cac* and MAPK components genes failed to suppress axon degeneration at later stages at any level (Figure 2.10). I conclude that dSarm signals with the VGCC Cac and through the MAPK signaling cascade within

the first few hours after axonal injury to suppress axon transport, while loss of this signaling pathway does not suppress later phases of axon death signaling, where dSarm signals with Axed to execute axon destruction.

The involvement of the VGCC Cac led us to test whether initial calcium influx after axotomy was altered by manipulation of Cac or dSarm, and might thereby be suppressing blockade of axon transport. I sparsely labeled control and *cac* mutant MARCM clones with GCaMP6, laser-ablated a subset of axons in the L1 wing nerve, and then live imaged GCaMP6s fluorescence in clones following ablation. I found strong GCaMP signal induction in the cell bodies of severed axons and bystander neurons across all the genotypes we tested within seconds of injury (Figure 2.11). I found no differences in the maximum amplitude or time to maximum amplitude in either severed or bystander neurons when we compared controls to *dsarm* or *axed* mutants (Figure 2.11A-C). However, I did observe a significant decrease in maximum amplitude and increase in time to maximum amplitude for GCaMP6s signals in injured neurons lacking Cac, although this change was small (Figure 2.11A-C). I conclude that while Cacophony may partially contribute to initial calcium influxes after axon injury, it plays a relatively minor role in total Ca^{2+} influx immediately after

axotomy despite its potent role in suppression of axon transport within the following 1-2 hours.

Result 2.4 - Axon injury leads to a dSarm-dependent reversible suppression of sensory signaling in bystander neurons.

I sought to determine whether bystander neurons exhibited changes in their functional properties beyond suppression of axon transport. I therefore examined the effects of L1 wing nerve injury on mechanosensory-driven behaviors. Stimulation of mechanosensory neurons in the wing (Figure 2.12A) with a gentle touch leads to a kicking response that is thought to represent a type of grooming behavior (Li et al., 2016). I stimulated mechanosensory bristles in control wings and wings lesioned at the midpoint of the L1 nerve and found that 3 hours after axotomy there was a significant reduction (~40%) in kicking responses in injured wings (Figure 2.12B). By 6 hours after axotomy responses had recovered to control levels (Figure 2.12B). I found this injury-induced decrease in mechanosensory function could be suppressed by RNAi-mediated knockdown of *dsarm* in sensory neurons (Figure 2.12C), suggesting that this impairment of mechanosensation is dSarm-dependent.

To directly assay the sensitivity of other intact sensory neurons I live imaged L1 wing vein chemosensory neuron activity using the Ca^{2+} indicator GCaMP6s (expressed pan neuronally with tub-Gal4) in response to bath application of 200 mM glucose (Raad et al., 2016). Glucose exposure led to a robust activation of sugar-sensitive wing sensory neurons, which was potently suppressed within 3 hours post axotomy, but recovered by 6 hours post axotomy (Figures 2.13A, B). Taken together, our data suggest that partial wing injury not only suppresses the axon transport but also impairs the functions in the bystander sensory neurons.

Chapter II: Material and Methods

Axotomy assays

Adult flies were anesthetized on a CO_2 pad, and the wings were cut manually with MicroPoint Scissors at the indicated location (Figure 2.1). Flies were returned to vials and incubated at 25°C. The remaining wings were either left attached on the fly body for behavioral assays or dissected for imaging at the appropriate time point.

Live imaging of Vesicle trafficking

Intact or injured wings were dissected and mounted in Halocarbon oil 27 beneath a coverslip and imaged immediately. Images of vesicle trafficking were acquired on a spinning disc microscope (Zeiss Examiner Z1) with a 63X oil-immersion objective at the location indicated (Figure 2.1). Time-lapse images were acquired with CCD camera (Hamamatsu Orca Flash 4.0) using Zen software (Zeiss) for a 3-minute window. The wings were sitting in halocarbon oil no longer than 15 min before imaging. All the wings were imaged including the those with only labeled severed neurons or intact neurons.

Sensory transduction assay and calcium imaging

The procedures of sugar application and imaging were adapted from a previous study (Raad et al., 2016). Intact or injured wings (3 to 5 days old flies) were dissected and mounted in a drop of water (~1.5µl) under a coverslip, and imaged immediately. Time-lapse images were acquired on a Intelligent Imaging Innovations spinning disc microscope (Zeiss Imager X1) with a 63X oil-immersion objective, CCD camera (Hamamatsu Orca Flash 4.0) using Slidebook software at 1 frame/sec for 5 minutes. 5 µl of D-glucose solution (200 mM in water) was loaded at the edge of coverslip at indicated time point.

Laser ablation and calcium imaging

Flies (3 to 7 days old) were anesthetized on CO_2 and had the dorsal side of both wings and abdomen glued to a coverslip using a UV light-cured adhesive. Neurons were sparsely labeled and expressed GCaMP6s using a MARCM approach. Wing nerve ablation time-lapse images were taken on a 3I spinning disc confocal microscope with a Micropoint laser ablation system (430 nm). An ablation region was selected by manually drawing a line across the wing nerve at the location for ablation to occur. All cell bodies analyzed were within 200 µm from the site of ablation. Time-lapse confocal images were analyzed using Fiji (ImageJ). Cell body average

fluorescence intensity was analyzed by manually drawing regions of interest and F_0 was defined as the average fluorescence intensity for the ten seconds before ablation. Outliers for values of either max amplitude or the time to maximum amplitude were identified (ROUT method, Q=1%)

Behavioral assays

Behavior assays were adapted from (Li et al., 2016). Briefly, adult female flies (3 to 7 days old) were anesthetized on ice and decapitated with micro forceps. Decapitated flies were recovered on wet kimwipes for 10 minutes, and those flies able to stand up and respond to light touch on the body were used for behavioral tests. An eyelash was used as the probe to stimulate gentle touch and kicking response by touching the wing margin bristles for 1-2 seconds. For each animal, the wing was touched 3 times. If the animal did not respond to all 3 touches, this test was counted as no response, if it responded to any of the 3 touches, it was counted as a positive response. Each wing (intact or injured) was touched 10 times, with ~30 seconds interval between each touch. The number of kicking responses was recorded. Videos were recorded by the camera of iPhone 7.

Vesicle movement analysis

Kymographs were created in Fiji (ImageJ) for time-lapse confocal images using the multiple kymograph plugin. Lysosomes, autophagosomes, mitochondria, or synaptic vesicles were classified as stationary (no movement during the 3 minutes video), or moving (with any movement, including oscillation during the 3 minutes video). The percentage of moving or stationary vesicles in the imaged region was calculated, and similar genotypes and conditions (e.g. injured vs uninjured) were pooled. The n value represents the total number of axons scored. If too many cells were labeled in a wing for unique identification, we only included those axons were clearly identifiable as severed or intact (by connection to cell bodies).

Calcium imaging analysis

Time-lapse confocal images were analyzed by using Fiji (ImageJ). The average fluorescent intensity of GFP in three individual chemosensilla were measured in each imaged wing. The F0 was defined as the average fluorescent intensity in 20 seconds before glucose application (Figure 2.2D). Chemosensilla were identified based on morphology, or the change of fluorescent intensity upon glucose application. In injured wings, if there was no increase of the fluorescent intensity in any cell bodies, the percentage of $\Delta F/F0$ was count as 0%.

Quantification and statistical analysis

Unpaired two-tailed t-test, one-way ANOVA, and two-way ANOVA were performed in GraphPad Prism 8 for experiments as indicated in the figure legends. Error bars in bar graphs represent standard error of mean (S.E.M.). Comparison detail, number, and p value are indicated in all figure legends.

Chapter II: Figures

Figure 2.1: Schematic of partial injury model on Drosophila wings.

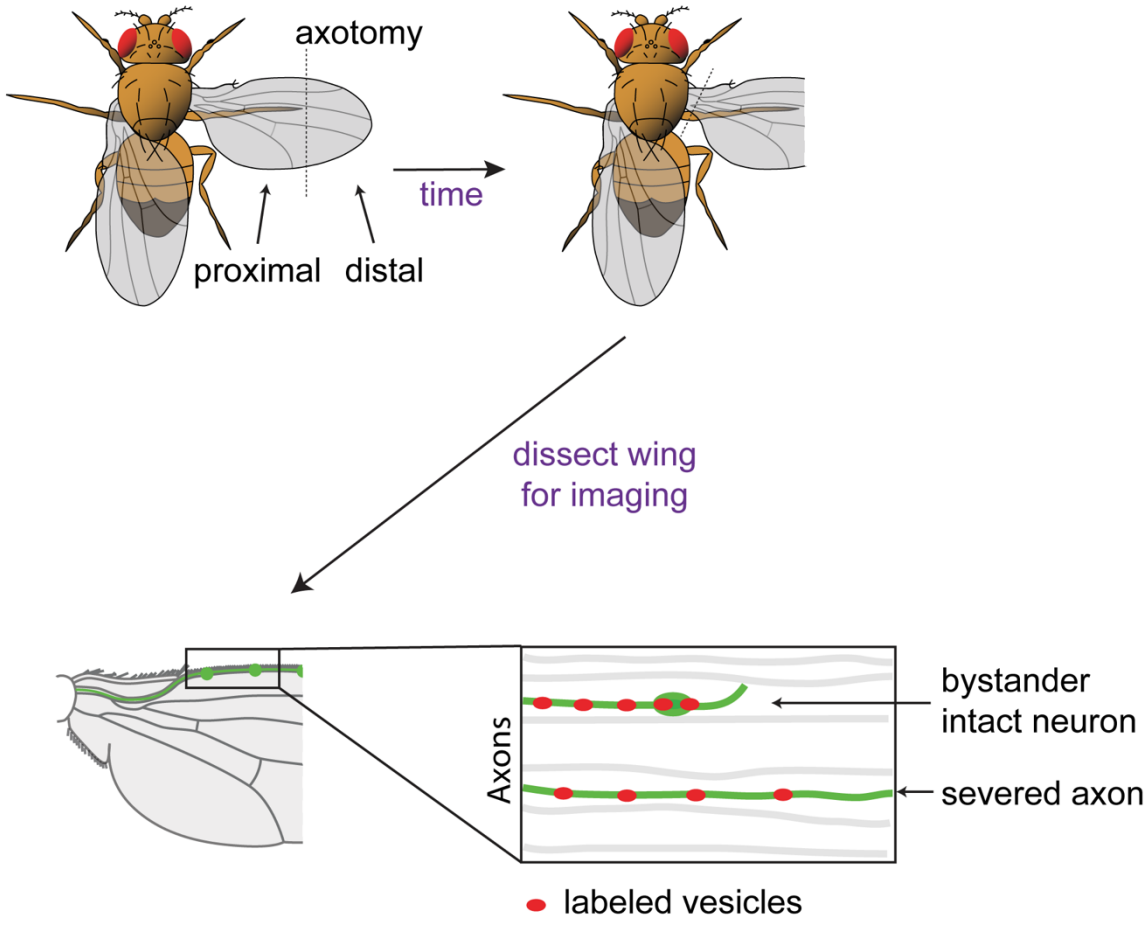

Figure 2.1:

Schematic of injury and vesicle transport assays in *Drosophila* wings. Individual clones were labeled using MARCM (green), which allowed for clonal expression of markers; severed and intact axons were discriminated by tracing to cell bodies; unlabeled neurons (gray).

Figure 2.2: Nerve injury blocks axon transport in both severed axons and intact bystander neurons.

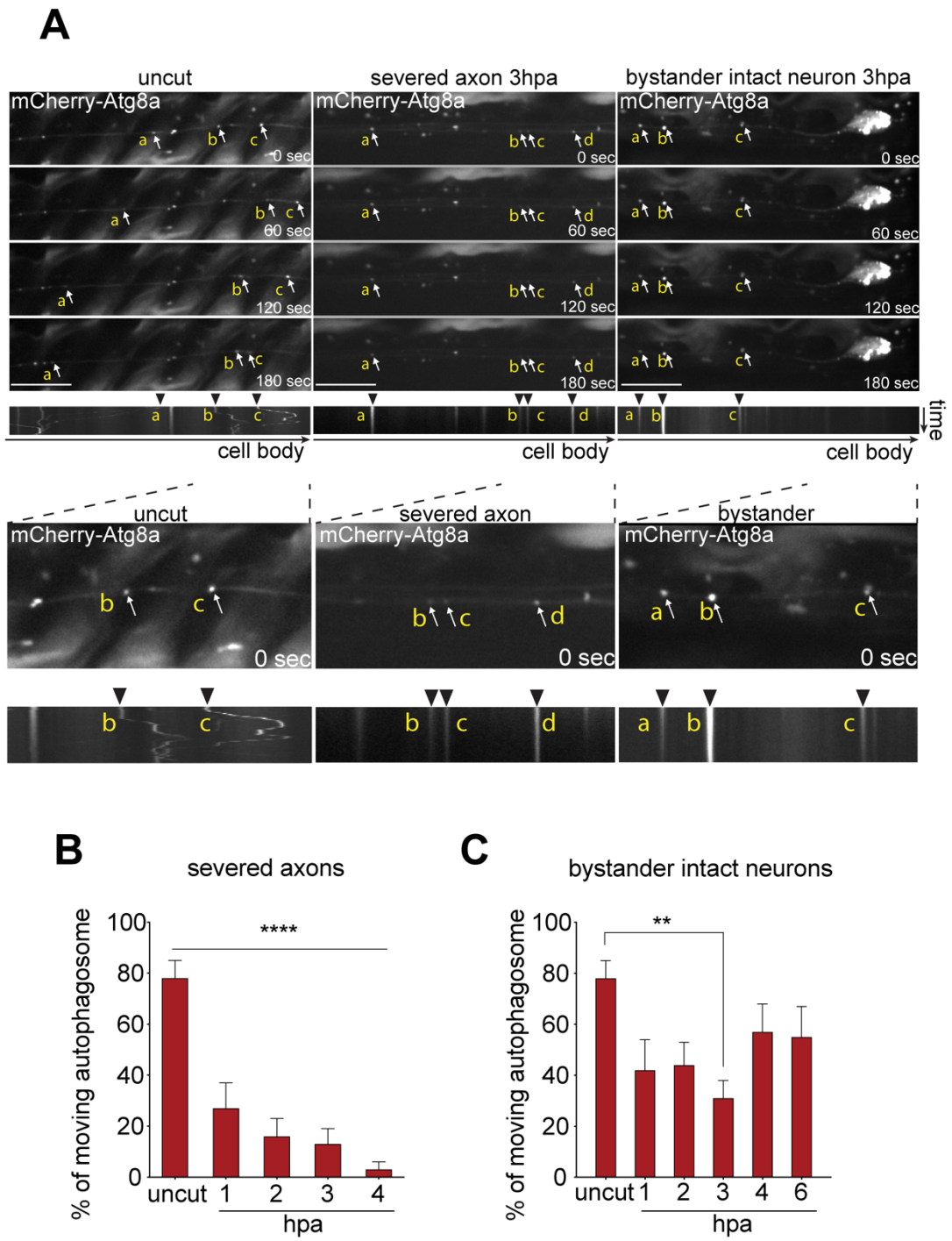

Figure 2.2:

(A) Representative time series and kymographs of mCherry-atg8a (arrows) transports in axons of uncut (left column), severed axons 3 hours post axotomy (middle column), and intact neurons 3 hours post axotomy (hpa) (right column). The insets of 0 sec images and kymographs of each column are shown. Scale bar,10 μm. Total imaging time shown is 3 minutes. Same vesicle on different images are indicated (a, b, c, and d).

(B, C) Quantification of moving autophagosomes over time in (B) severed axons or (C) proximal intact axons. Ordinary one-way ANOVA with Sidak multiple comparisons test. (*$p < 0.05$, **$p < 0.01$, ***$p < 0.001$, ****$p < 0.0001$, n = 10 animals, Error bar = SEM).

Figure 2.3: Nerve injury blocks trafficking of lysosomes and synaptic vesicles in both severed and intact axons.

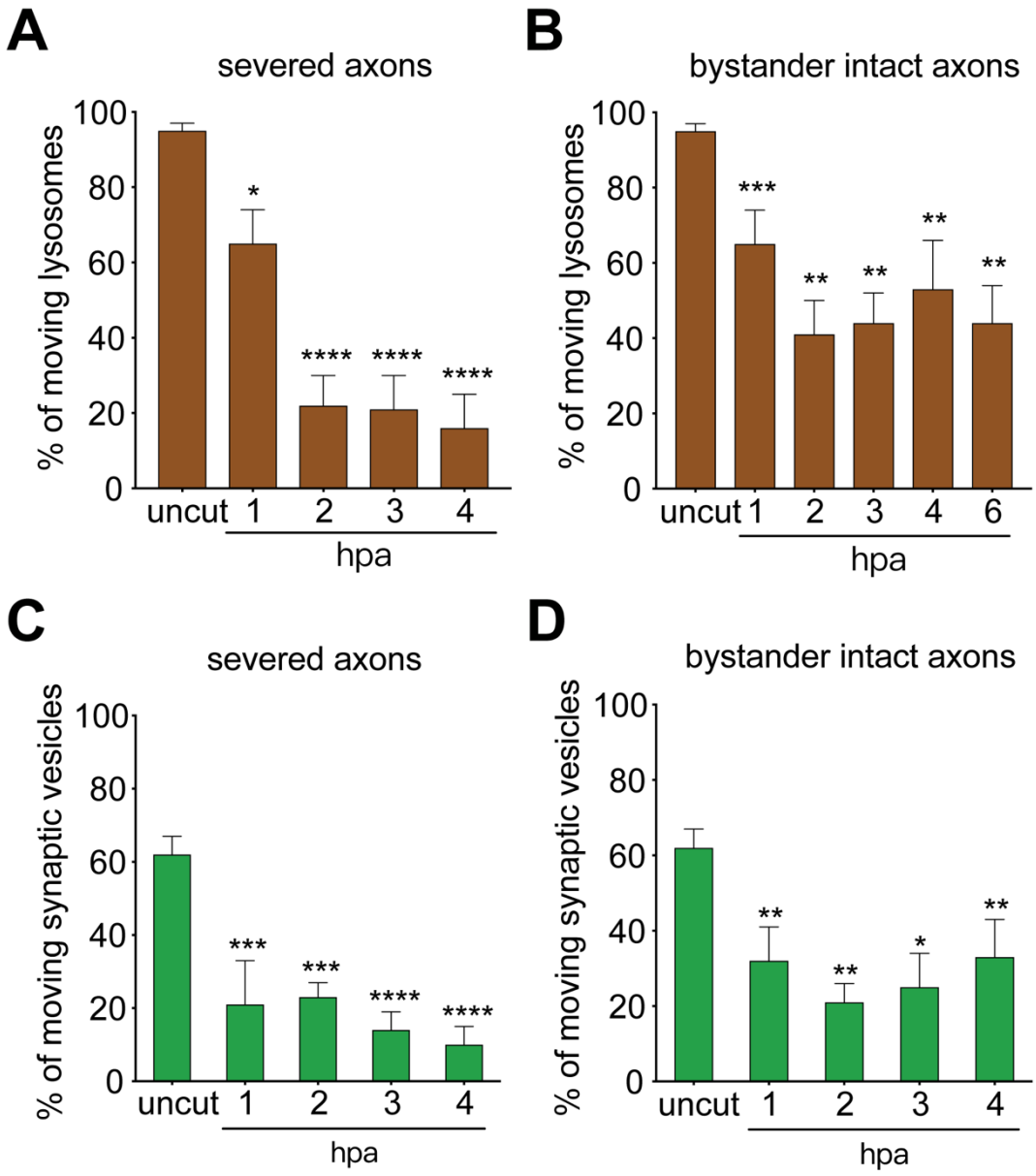

Figure 2.3:

(A, B) Injury reduced the percentage of moving lysosomes in both severed axons and proximal intact axons. (For all, ordinary one-way ANOVA with Sidak multiple comparisons test. *$p < 0.05$, **$p < 0.01$, ***$p < 0.001$, ****$p < 0.0001$, n = 10 animals, Error bar = SEM).

(C, D) Injury reduced the percentage of moving synaptic vesicles in both severed axons and proximal intact axons.

Figure 2.4: Distal wing nerve injury suppresses bystander axon transport throughout the entire wing vein.

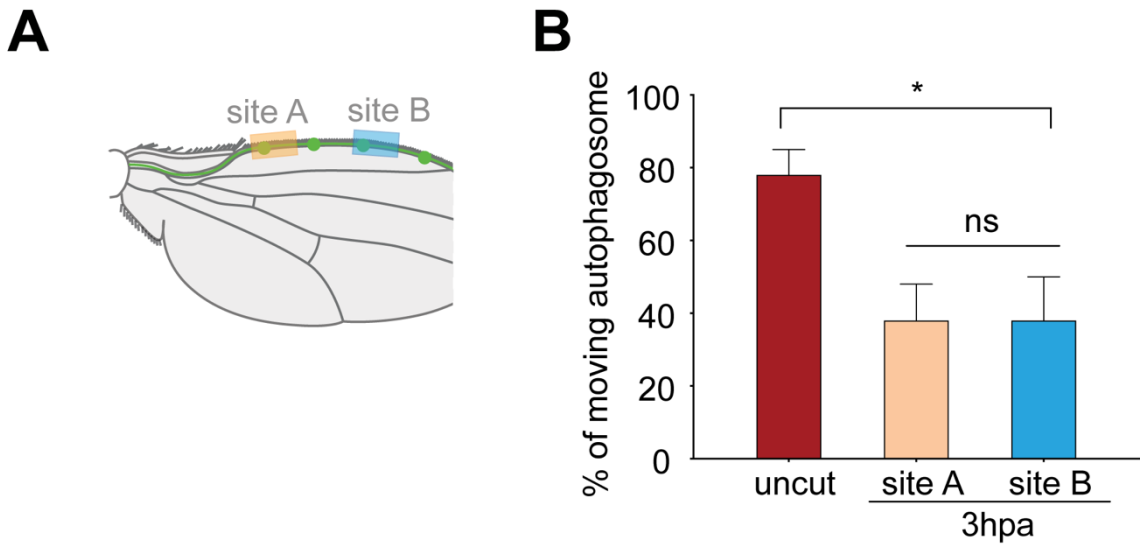

Figure 2.4:

Upper panel: Schematic showing distal wing nerve injury and sites where intact axons were subsequently imaged (site A and B) 3hpa. Lower panel: Quantification of autophagosome movement. Ordinary one-way ANOVA with Sidak multiple comparisons test. (ns = not significant, *p < 0.05, **p < 0.01, ***p < 0.001, ****p < 0.0001, n = 10 animals, Error bar = SEM).

Figure 2.5: dSarm is required for the suppression of axon transport in both severed axons and intact bystander neurons after wing injury.

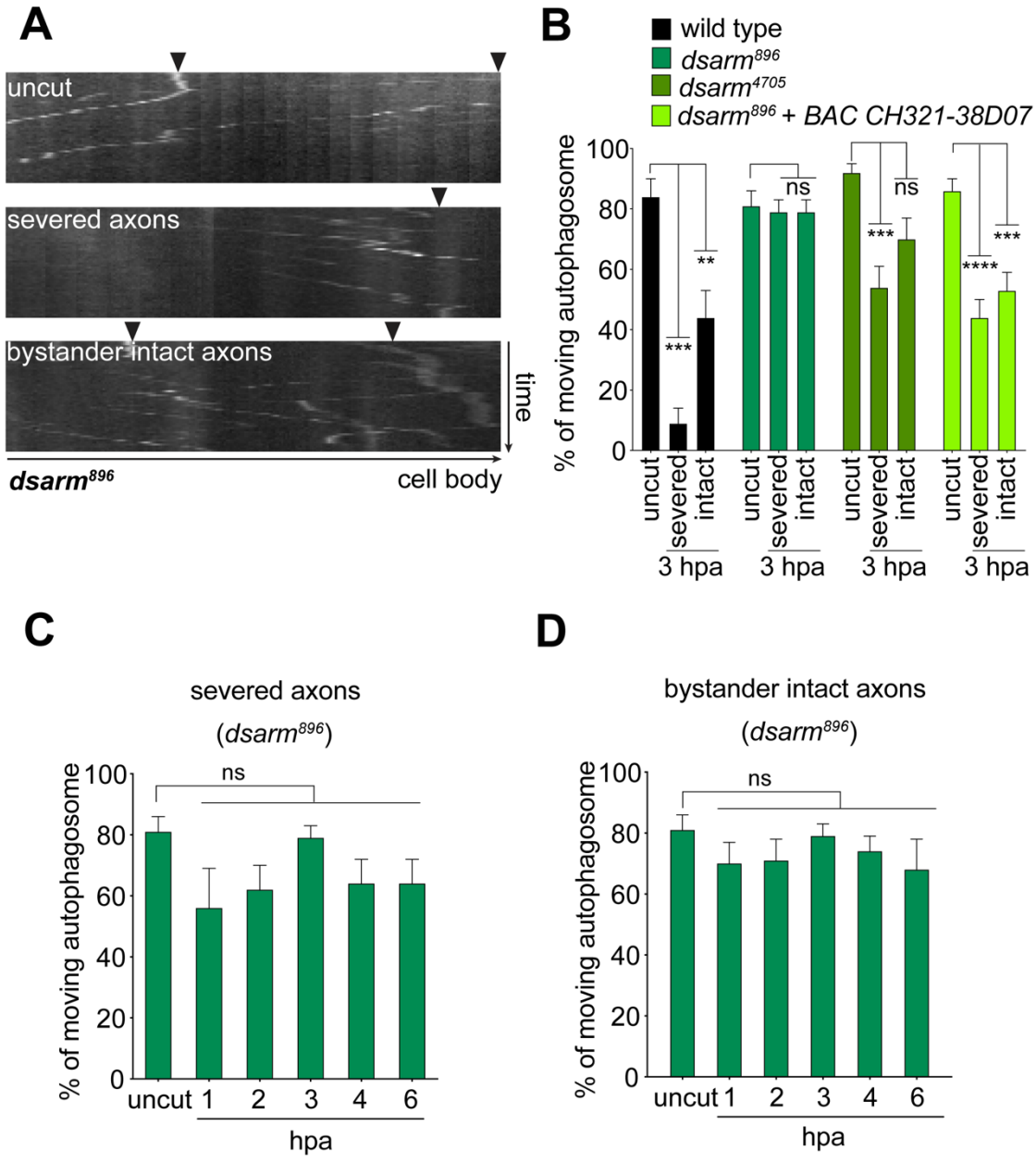

Figure 2.5:

(A) Representative kymographs of mCherry-atg8a (arrows) transports in *dsarm*^{896} axons of uncut (top), severed axons (middle), and intact neurons 3 hours post axotomy (hpa) (bottom). Total imaging time shown is 3 minutes. (B) Quantification of autophagosome movement in *dsarm* mutants (*dsarm*^{896} and *dsarm*^{4790}) 3hpa, compared to uninjured wings (uncut). Two-way ANOVA with Sidak multiple comparison. (ns = not significant, *p < 0.05, **p < 0.01, ***p < 0.001, ****p < 0.0001, n = 10 animals, Error bar = SEM).

(C, D) Quantification of autophagosome trafficking over the first 6 hours after injury in *dsarm* mutant axons. One-way ANOVA with Sidak multiple comparison. (ns = not significant, *p < 0.05, **p < 0.01, ***p < 0.001, ****p < 0.0001, n = 10 animals, Error bar = SEM).

Figure 2.6: Axed is not involved in the suppression of axon transport after wing injury.

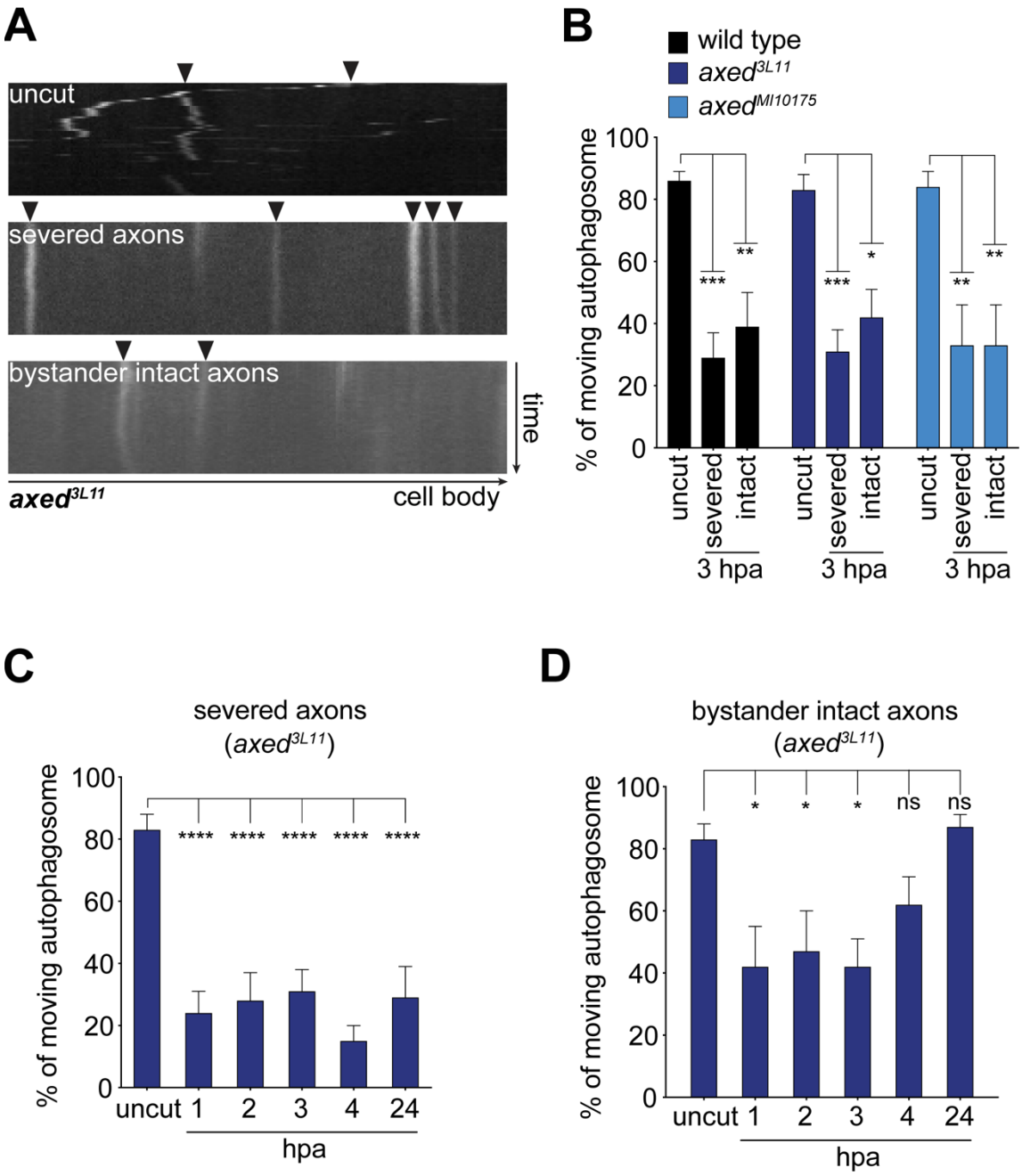

Figure 2.6:

(A) Representative kymographs of mCherry-atg8a (arrows) transports in *axed*^{3L11} axons of uncut (top), severed axons 3 hours post axotomy (middle), and intact neurons 3 hours post axotomy (hpa) (bottom). Total imaging time shown is 3 minutes.

(B) Quantification of autophagosome movement null mutants of axed (axed^{3L11} and axed^{MI10175}) 3 hpa compared uncut controls. Two-way ANOVA with Sidak multiple comparison. (For all, ns = not significant, *p < 0.05, **p < 0.01, ***p < 0.001, ****p < 0.0001, n = 10 animals, Error bar = SEM).

(C, D) Quantification of autophagosome trafficking over the first 6 hours after injury in axed mutant axons. Ordinary one-way ANOVA with Sidak multiple comparisons test. (For all, ns = not significant, *p < 0.05, **p < 0.01, ***p < 0.001, ****p < 0.0001, n = 10 animals, Error bar = SEM).

Figure 2.7: dSarm, but not Axed, is required for suppression of lysosome transport after injury.

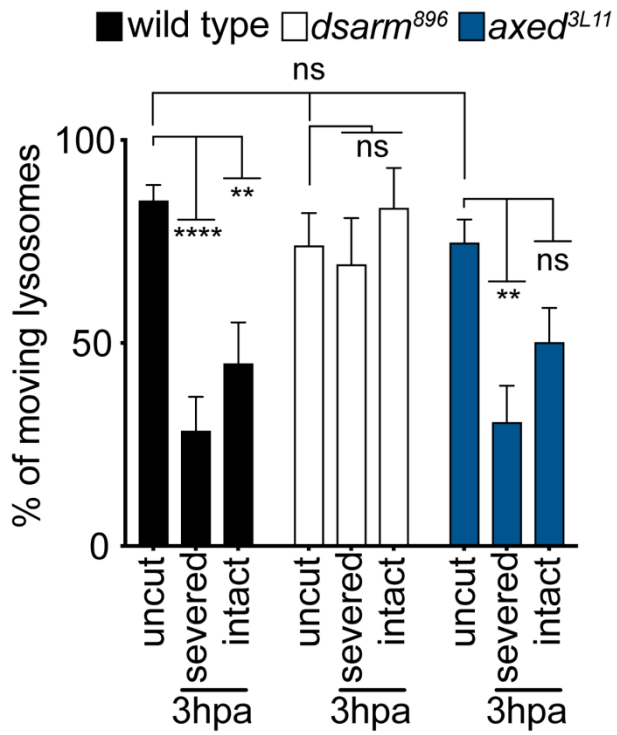

Figure 2.7:

Lysosome trafficking in axons was suppressed in control and axed (*axed*^{3L11}) mutant animals 3hpa, but not in *dsarm* (*dsarm*^{896}) null mutants. Two-way ANOVA with Sidak multiple comparisons test. (ns = not significant, ***p < 0.001, ****p < 0.0001, n = 10 animals, Error bar = SEM).

Figure 2.8: Cacophony in the TIR-1-like MAPK signaling pathway suppress axon transport after nerve injury.

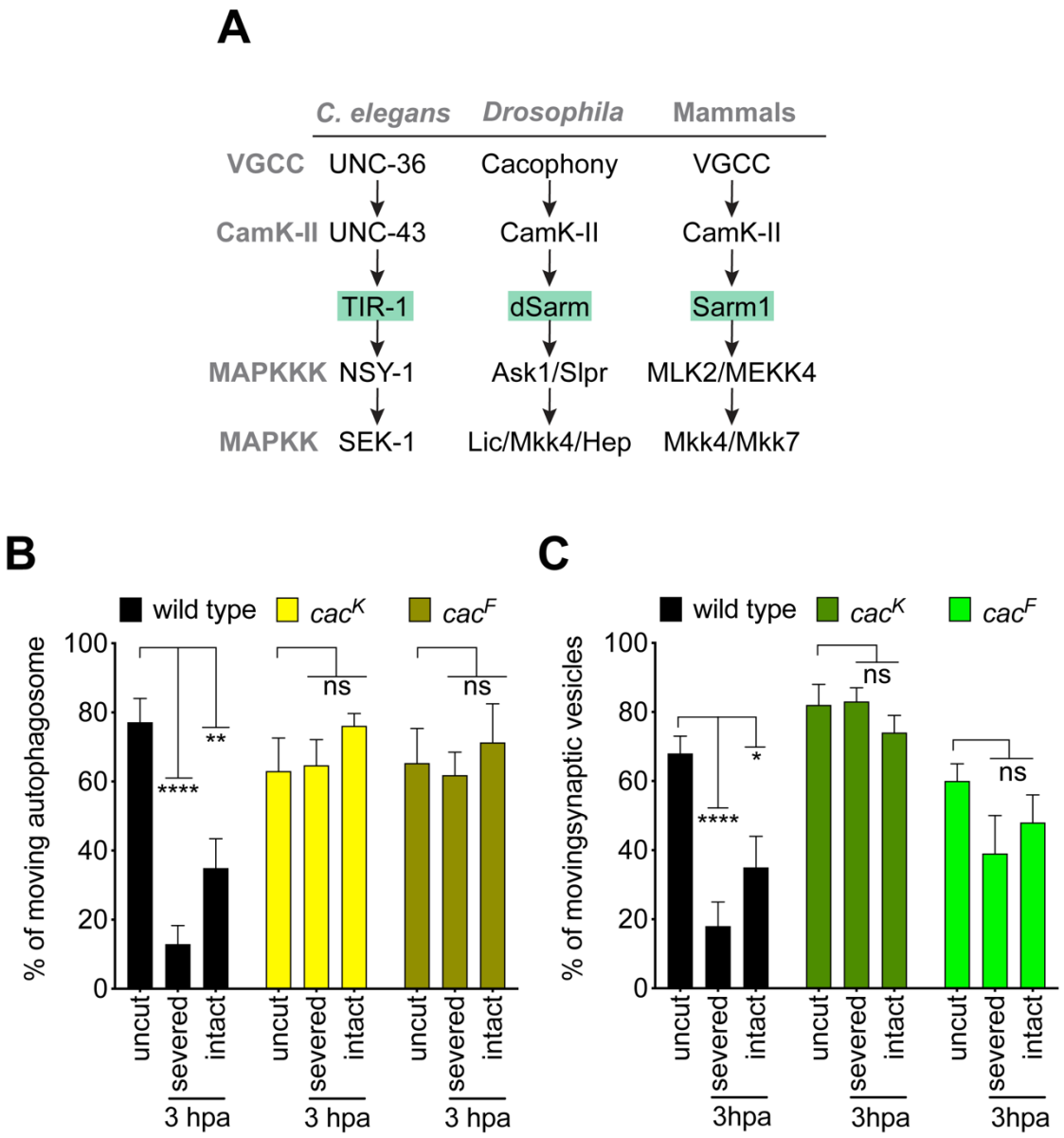

Figure 2.8:

(A) The Tir-1/MAPK signaling pathway and conservation in flies and mammals.

(B) Quantification of autophagosome movement in two *cac* mutants (cac^{K} and cac^{F}) in severed or proximal intact axons 3hpa compared uncut controls. (Two-way ANOVA with Sidak multiple comparisons test. ns = not significant, **p < 0.01, ***p < 0.001, ****p < 0.0001, n = 10 animals, Error bar = SEM).

(C) Synaptic vesicle movement in the two independent alleles of *cac* mutants (cac^{K} and cac^{F}) in both severed axons and proximal intact axons in injured wings (3hpa). (Two-way ANOVA with Sidak multiple comparisons test. ns = not significant, *p < 0.05, ****p < 0.0001, n = 10 animals, Error bar = SEM).

Figure 2.9: MAPK in the TIR-1-like MAPK signaling pathway is involved in axon transport suppression after nerve injury.

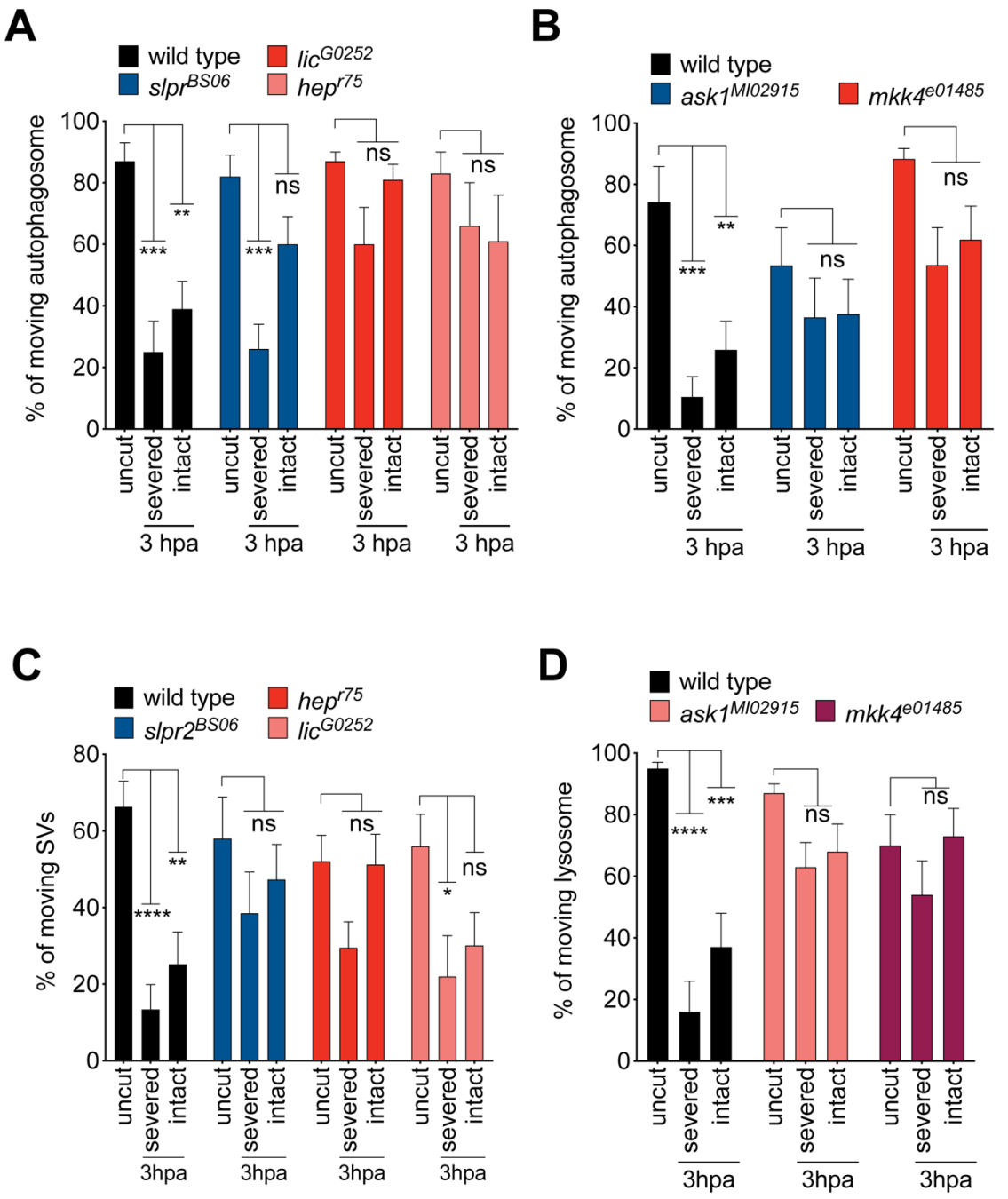

Figure 2.9:

(A) Quantification of autophagosome movement in *mkk4* and *ask1* mutants (*mkk4*^{e01485}, and *ask*^{MI02915}) in both severed axons or proximal intact axons in injured wings (3hpa) compared to that in uninjured wings (uncut).

(B) Quantification of autophagosome movement in *slpr*, *lic*, and *hep* mutants (*slpr*^{BS06}, *lic*^{G0252}, and *hep*^{r75}) in both severed axons or proximal intact axons in injured wings (3hpa) compared to that in uninjured wings (uncut).

(C) In severed axons, synaptic vesicle movement was not significantly changed in *slpr* or *hep* (*slpr*^{BS06} and *hep*^{r75}) mutant axons (3hpa) compared to uninjured wings (uncut). An allele of *lic*, (*lic*^{G0252}) showed a mild reduction in trafficking after injury compared to uninjured wings.

(D) Strong alleles of *mkk4* and *ask1*, (*mkk4*^{e01485}, and *ask*^{MI02915}) exhibited normal lysosome transport in both severed axons in injured wings 3hpa compared to uninjured wings.

Figure 2.10: MAPK components are not involved in axon degeneration.

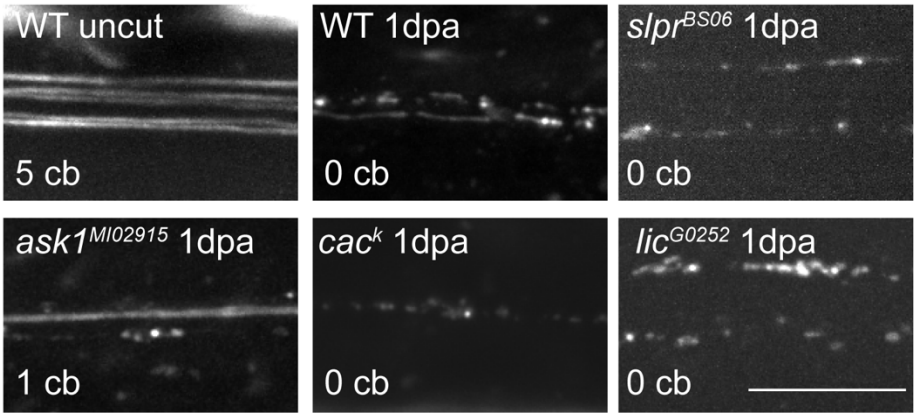

Figure 2.10:

Loss of function mutations in *slpr*, *ask1*, *cac*, and *lic* are unable to suppress axon degeneration even at 1day post axotomy (dpa). The number of remaining cell bodies (cb), and therefore predicted axon number were indicated at lower left corner. Scale bar = 10 μm.

Figure 2.11: Increase of calcium influx in severed and intact axons after axotomy is mildly reduced in cacophony mutants.

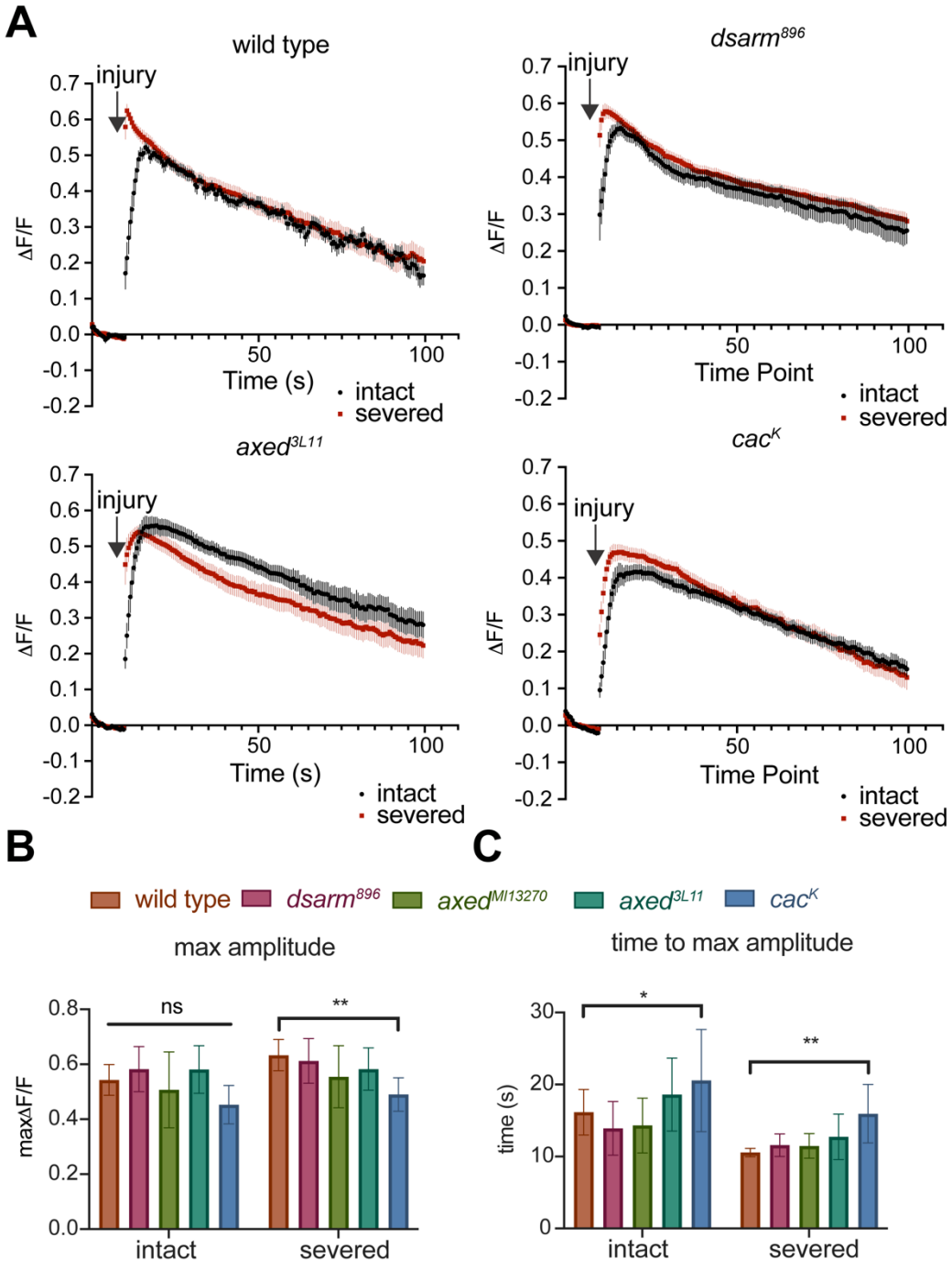

Figure 2.11:

(A) The GCamp6s intensity in different genotypes over time after injury is plotted. (Error bar = SEM, n = 9-15 wings).

(B, C) Maximum amplitude (B) and time to max amplitude (C) of GCamp6s intensity after injury in different genotypes. Two-way ANOVA with Sidak multiple comparisons test. (ns = not significant, *$p < 0.05$, **$p < 0.01$, n = 9-15 wings. Error bar = SEM).

Figure 2.12: Wing injury leads to a dSarm-dependent reversible suppression of mechanosensation.

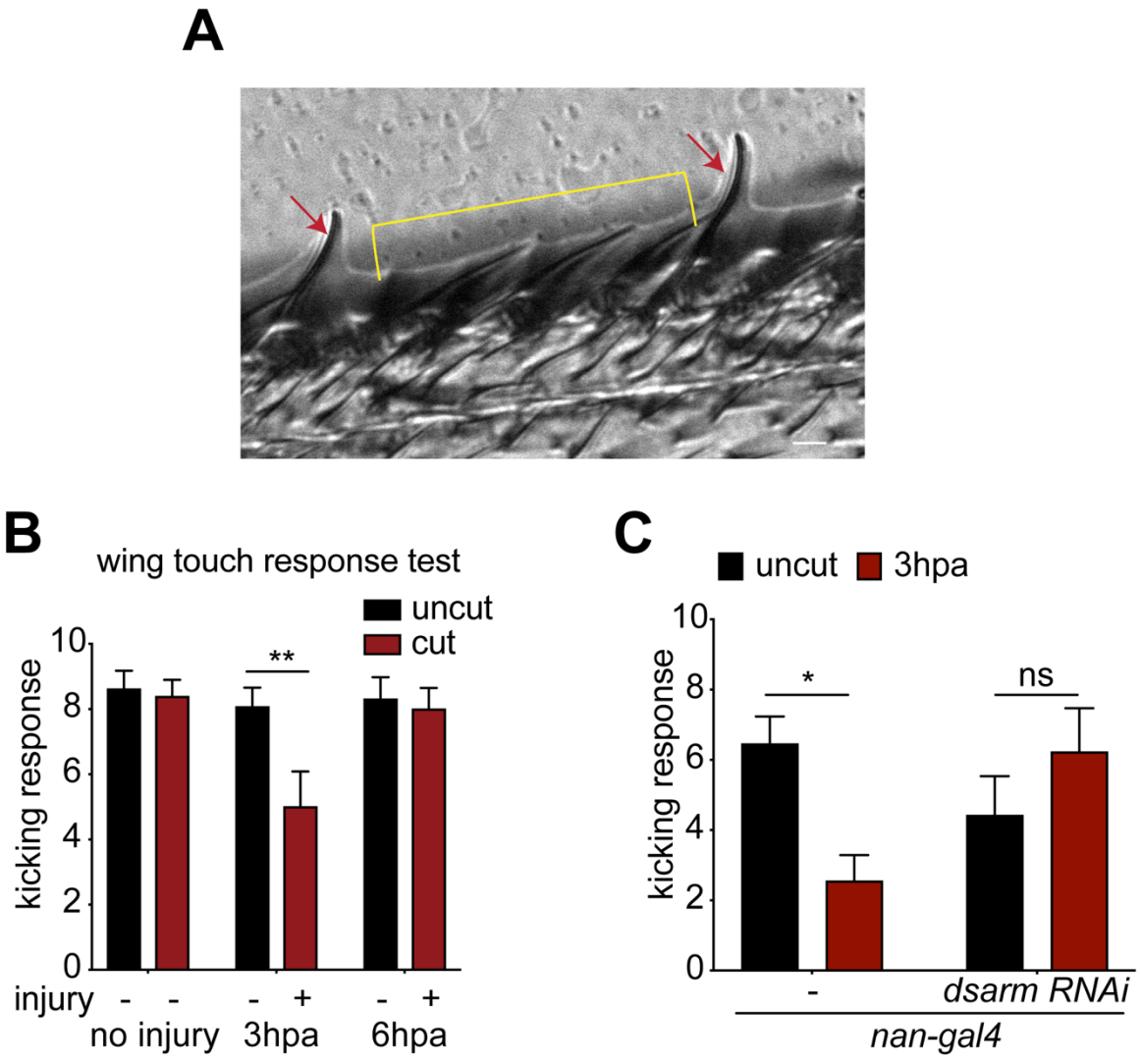

Figure 2.12:

(A) Representative image of chemosensory (red arrows) and mechanosensory (yellow bracket) bristles on the fly wing margin.

(B) Injury reduced the number of kicking responses upon bristle stimulation at 3 hours post axotomy (3hpa) of injured wings (left wings) in w^{1118} control animals, which recovered by 6 hpa. Two-way ANOVA with Sidak multiple comparisons test. (**$p < 0.01$, n = 13~14 animals of each, Error bar = SEM).

(D) Knocking down of *dsarm* in Nan+ neurons resulted in normal kicking responses 3 hpa. Unpaired two-tailed t-test. (ns = not significant, *$p < 0.05$, n = 10~14 animals, Error bar = SEM).

Figure 2.13: Wing injury leads to reversible suppression of chemosensation in bystander neurons.

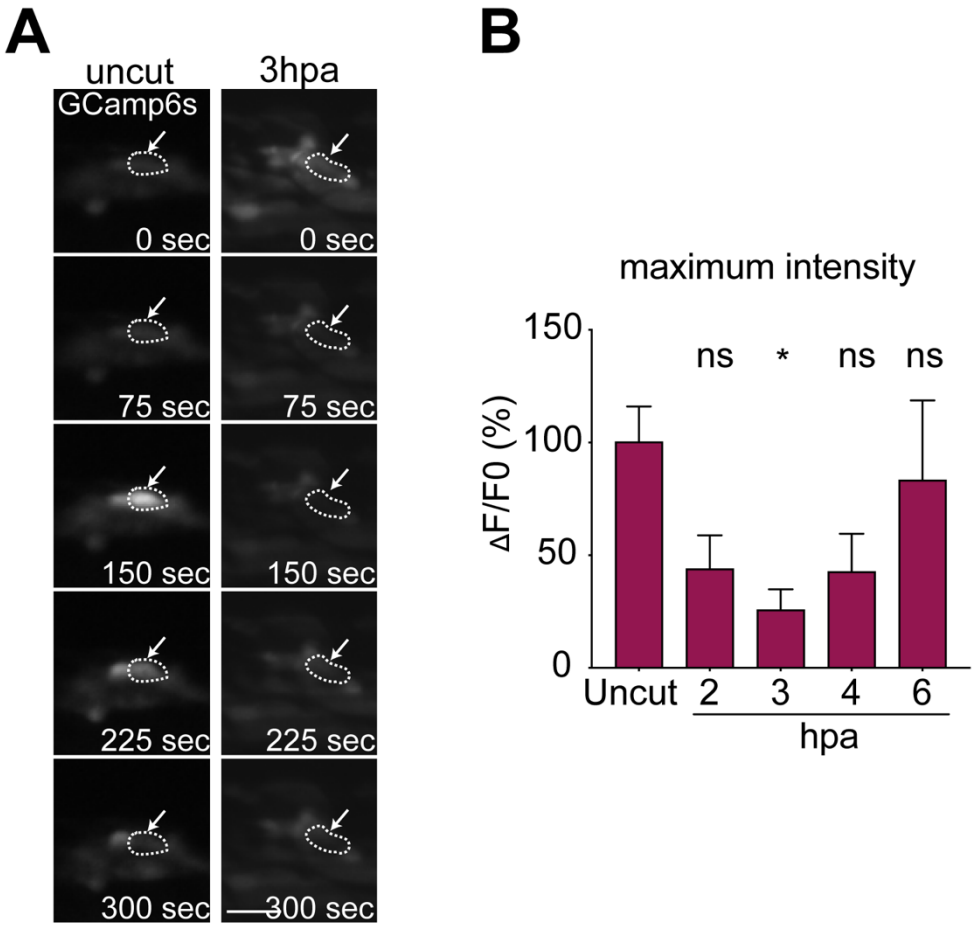

Figure 2.13:

(A) GCamp6s signals are increased in the wing chemosensilla of *UAS-GCamp6s/+*; *tub-gal4/+* flies in response to 200mM glucose application, but this response was suppressed by nerve injury (3hpa), arrows point the representative chemosensillar. Scale bar, 10 μm. Dash line circled the chemosensilla with responses upon stimulation.

(B) The average maximum intensity (maximum ΔF/F0%) of GCamp6s fluorescence stimulated by glucose was significantly reduced at 3hpa, but recovered by 6hpa. F0 was defined as the average of fluorescent intensity of 100-120 seconds. Ordinary one-way ANOVA with Sidak multiple comparisons test. (ns = not significant, *$p < 0.05$, n = 10 animals, Error bar = SEM).

CHAPTER III: Suppression of axon transport is independent of the accumulation of NMN or the depletion of dNmnat.

In this chapter, Paul Meraner cloned and purified Sarm1 recombinant protein and designed *in vitro* NAD^+ hydrolysis assay, and I conducted all additional experiments.

Part of the work in this chapter is included in the following publication:

Injury-induced inhibition of bystander neurons requires dSarm and signaling from glia

Jiun-Min Hsu, Yunsik Kang, Megan Corty, Danielle Methieson, Owen Peters, Marc Freeman

Chapter III: Abstract

In previous chapter, I described that the early global suppression of axon transport after wing injury is mediated by Cac/dSarm/MAPK signaling pathway, but not Axed. These observations suggest that there are two phases of dSarm signaling in response to axonal injury – an early broad suppression of neurophysiology, and a later phase of explosive axon degeneration. The late axon degeneration phase is known to be regulated by dSarm and Axed. dSarm/Sarm1 is activated to drive axon degeneration when Nmnat levels are depleted. In this chapter, I show that NMN can act as a direct activator to enhance Sarm1 NADase activity, but neither NMN accumulation nor dNmnat depletion are involved in the early dSarm-dependent suppression of axon physiology. These results further support the notion that there are two distinct dSarm/Sarm1 dependent pathways that differentially mediate early and late axonal responses to partial nerve axotomy.

Chapter III: Results

Result 3.1 – NMN functions as a Sarm1 activator to promote NAD^+ hydrolase activity.

According to the NAD^+ depletion model, Sarm1 is activated when axonal Nmnat2 levels are low (Gilley et al., 2015). It was not clear how Nmnat2 depletion might activate Sarm1. NMN accumulates when Nmnat2 is depleted, which correlates well with activation of Sarm1-dependent axon degeneration (Di Stefano et al., 2014; Loreto et al., 2015). We tested the possibility that NMN is an activator of Sarm1 using an *in vitro* NAD^+ hydrolysis assay. I used ε-NAD, an NAD^+ fluorescent analog in which the ADP-ribose group is attached with the fluorophore, ethanoadenine ring, as the substrate. In ε-NAD, the nicotinamide group quenches the fluorescence of the ethanoadenine ring. Upon hydrolysis of ε-NAD by an NADase, the nicotinamide group is separated from the ethanoadenine ring, and its fluorescence intensity increases ~10-fold (Barrio et al., 1972). I measured the relative NADase activity of purified recombinant Sarm1 using *in vitro* incubation with ε-NAD substrate and by monitoring the time course of fluorescent intensity changes. I found without NMN, the fluorescent intensity exhibited a slight increase over time, this is presumably reporting

as basal Sarm1 NADase activity (Figure 3.1A). In contrast, incubation of Sarm1 with NMN resulted in a dramatic increase of fluorescent intensity from the reaction (Figure 3.1), suggesting that Sarm1 NADase activity is enhanced by NMN. To further investigate whether Sarm1 NADase activity can also be enhanced by the molecules with similar structures, I tested Sarm1 NADase activity in the presence of nicotinamide (NAM) and nicotinic acid mononucleotide (NaMN). Interestingly, neither NAM nor NaMN were capable to enhance Sarm1 NADase activity (Figure 3.2).

To explore whether this was a result of NMN I used Nmnat to deplete NMN from the reaction. Nmnat requires ATP and $MgCl_2$ for transferring NMN to NAD^+ (Werner et al., 2002; Zhai et al., 2006; Zhou et al., 2002). I found that addition of purified Nmnat1/Nmnat2 with ATP and $MgCl_2$ could suppress this NMN-mediated Sarm1 NADase activity enhancement, while removing ATP or $MgCl_2$ suppressed this effect (Figure 3.3), arguing that Nmnat1/Nmnat2 suppresses Sarm1 activity by converting NMN to NAD^+, rather than through a direct physical interaction. These data further support the notion that NMN is a selective activator of Sarm1 capable of enhancing its NADase activity, and thereby promoting axon degeneration.

Result 3.2 - Suppression of axon transport is not caused by the accumulation of NMN or the depletion of dNmnat.

dSarm/Sarm1-dependent explosive axon degeneration observed during Wallerian degeneration is believed to be driven by Nmnat loss, NAD^+ depletion, and activation of Sarm1 by NMN to drive further NAD^+ depletion and ultimately catastrophic energy failure. We wished to determine whether these events were also required for early suppression of axon transport in severed and bystander neurons *in vivo*, early after nerve injury. Overexpression of *E. coli* NMN deamidase, which degrades NMN, has been shown to partially protect the axons from degeneration after axotomy (Figure 3.4A) (Di Stefano et al., 2014; Loreto et al., 2014). I generated transgenic *Drosophila* that express NMN deamidase (NMNd) under the control of Gal4-UAS system. I found that overexpression of NMNd led to strong suppression of axon degeneration for 3-5 days after axotomy (Figure 3.4B), arguing that NMN is also involved in axon degeneration in *Drosophila*. I note, however, that this suppression is not nearly as strong as the suppression of axon degeneration afforded by *dsarm* null mutations. In addition, I also overexpression of NMNd failed to suppress $dSarm^{GOF}$ induced neuronal death (Figure 3.4C, D), supporting the notion that NMN is acting upstream of dSarm in the axon death signaling.

To explore potential roles for NMN in suppression of axon transport early after injury, I utilized LexA-LexAop system, a second binary system to label neurons and internal vesicles, while NMNd was driven by the Gal4-UAS system. I used a construct that allows for sparse, FLP/FRT-dependent activation of the pan-neuronal *brp-LexA* driver (Chen et al., 2014) to expresses *LexAoP-mCD8-GFP* and *LexAoP-rab3-mcherry* or *LexAoP-mcherry-atg8* in small subsets of neurons and vesicles. Sparse labeling was accomplished by using modified variant of heat shock FLP, hsFLP$^{D5.fco}$ (Nern et al., 2011). Animals were grown at 25^{o}C to restrict the expression level of *hs-FLP*, and we found that average about 5 sensory neurons were labeled in the L1 wing vein. We next assayed whether expression of NMNd could suppress the axotomy-induced blockade of axon transport. We found that NMNd expression failed to sustain the transport of synaptic vesicles in both injured axons and bystander neurons 3 hours after axotomy (Figure 3.4C). These data argue against a role for NMN in activating dSarm in the context of early blockade of axon transport in response to nerve injury.

Depletion of dNmnat in intact neurons also causes spontaneous axon degeneration that can be suppressed by loss of dSarm or Axed (Gilley et al., 2015; Neukomm et al., 2017). Is dNmnat depleted in neurons within hours after nerve injury? To explore this possibility, I utilized a dNmnat allele that

is endogenously tagged with GFP (Nmnat-GFP-Nmnat^{WT}) (Li-Kroeger et al., 2018) to visualize the level of dNmnat before and immediately after axotomy. I found no discernable change of the dNmnat-GFP in cell bodies of intact neurons when I compared intact nerves to samples 3 hours after axotomy (Figures 3.5A, B). Finally, there is only one Nmnat molecule encoded in the fly genome, dNmnat, and its loss causes spontaneous axon degeneration and cell death (Fang et al., 2012; Neukomm et al., 2017; Xiong et al., 2012). However, *dnmnat* null clones can survive in *axed* mutant backgrounds (Neukomm et al., 2017). *axed, dnmant* double mutants thereby allowed us to examine axon transport in *dnmnat* nulls, while preserving axonal integrity. *axed* mutants do not alter the blockade of axon transport 3 hours after axotomy (see above). Similarly, I found that compared to the wild type and *axed* single mutant clones, *axed, dnmnat* null clones did not spontaneously block axon transport (Figure 3.5C). Together these data support the notion that early blockade of axon transport is not mediated by Nmnat loss or NMN accumulation.

Result 3.3 – Combining NMNd overexpression with *cac* mutations enhances axon protection.

The aforementioned results argue that dSarm/Sarm1 has multiple activators upon axon injury: calcium signal through Cac to activate the early axon transport suppression, and the late NMN accumulation to drive dSarm/Sarm1 dependent axon degeneration. I also noticed that NMNd only provides partial axon protection from degeneration (Figure 3.4B) up to 5 days, unlike the lifespan protection offered by Wld^s. In addition to the prevention of NMN accumulation (Di Stefano et al., 2014), Wld^s is also found to suppress initial Ca^{2+} spike from enhancing mitochondria Ca^{2+} buffering (Avery et al., 2012). I therefore attempted to determine whether axon protection can be enhanced by combining NMNd overexpression and suppression of Ca^{2+} influx (via *cac* mutation). I found that expression of NMNd in *cac* mutants increased percentage of surviving axons at 5 days post axotomy, up to 7 days post axotomy (Figure 3.6), compared to no suppression in *cac* single mutants and controls. These data support the notion that NMN and Ca^{2+} signaling converge to activate dSarm to promote axon degeneration.

Result 3.4 - Overexpression of Wld^s or increasing the level of dNmnat is sufficient to rescue axon transport defects after nerve injury.

Wld^s is thought to suppress axon degeneration by substituting for the axon survival factor Nmnat2 after its depletion (Gilley and Coleman, 2010). Our data above argue against a role for dNmnat depletion or NMN accumulation in modulating axon transport immediately after injury, and predict, according to the NAD^+ depletion model, that Wld^s overexpression or loss of Hiw/Phr1 should not alter the early injury-induced blockade of axon transport. However, we found that expression of Wld^s or dNmnat, was indeed sufficient to suppress the axotomy-induced inhibition of axon transport in both severed axons and intact bystander neurons 3 hours after axotomy (Figure 3.7). Likewise, we found axon transport was maintained 3 hours after axotomy in *hiw* mutant clones in both severed axons and intact bystander neurons (Figure 3.8). The ability of Wld^s to suppress axon transport blockade required its enzymatic activity (Figure 3.7A, B). The partial suppression by $Nmnat^{WR}$ could be due to the remaining enzymatic activity (Figure 3.7). We conclude that early blockade of axon transport in injured nerves is sensitive to Wld^s and Hiw/Phr1. Given the lack of evidence supporting roles for NMN and Nmnat at this early time point, our data argue that the NAD^+ depletion model is not sufficient to explain these early modulatory effects of Wld^s and Hiw/Phr1.

Result 3.5 – Overexpression of Wld^s, or increasing the level of dNmnat, is sufficient to restore sensory signaling in bystander neurons.

We sought to determine whether injury-induced decrease in mechanosensory and chemosensory function can be regulated by NMN deamidase or Wld^s/dNmnat. We found that impairment of mechanosensation could not be suppressed by neuronal expression of NMN deamidase, but could be fully suppressed by neuronal expression of Wld^s or dNmnat (Figure 3.9A). $hiw^{\Delta N}$ mutants showed defective kicking response even without any injury (Figure 3.9B), possibly due to the changes of synaptic growth during development (Collins et al., 2006), so we were unable to test its potential role in suppressing mechanosensory behavior. Likewise, injury-induced inhibition of sensory neuron activity was not modified by neuronal expression of NMN deamidase, but was suppressed by Wld^s, dNmnat (Figure 3.10A) or $hiw^{\Delta N}$ mutants (Figure 3.10B). Together these data demonstrate that nerve injury profoundly alters the physiological responsiveness of bystander neurons within 3 hours, and that this reversible modification of neurophysiology is modulated by dSarm and other components of the axon death signaling cascade.

Chapter III: Material and Methods

Axotomy assays & Vesicle movement image and analysis & sensory transduction assay

See Material and Methods of Chapter II.

In vitro NAD^+ hydrolysis assay

Sarm1 recombinant protein was a gift from Paul Meraner. For the in vitro NAD^+ hydrolysis assay, varying concentrations of β-NMN (Sigma N3501) or 100μM of NaMN (Sigma N7764) or NAM (Sigma N3376) (as indicated in the figures) were incubated with 50μM of ε-NAD substrate (Sigma N2630) in the 96-well plate (Thermo Fisher #237108) in the buffer (50mM KH_2PO_4 pH7.2, 150mM NaCl, ddH_2O). NAD^+ hydrolysis was initiated upon the addition of Sarm1 recombinant protein with the final concentration 1mg/ml. The fluorescent was measured in the plate reader with 280nm excitation and 400nm emission. The results at different time points were collected. For Nmnat1/Nmnat2 test, 0.5 to 0.05 μg of Nmnat1/Nmnat2 protein (Novus biological) were incubated with ε-NAD substrate, 15mM $MgCl_2$ (Sigma) and 2mM ATP (Sigma A26209).

Quantification of Nmnat-GFP-$Nmnat^{WT}$ fluorescent intensity

Confocal images were analyzed by using Fiji (ImageJ). 5 neuronal cell bodies were chosen in each wing, and we calculated the average fluorescent intensity of green channel, 20 wings were quantified for both injured and uninjured wings.

Transgenesis

The constructed NMN deamidase plasmids were cloned from *E. Coli* NMN deamidase cDNA (Liu et al., 2018) with the primer pairs listed in Key Resource Table, and were used for transgenesis (Bestgene).

Chapter III: Figures

Figure 3.1: Addition of NMN enhanced Sarm1 NAD^+ hydrolase activity.

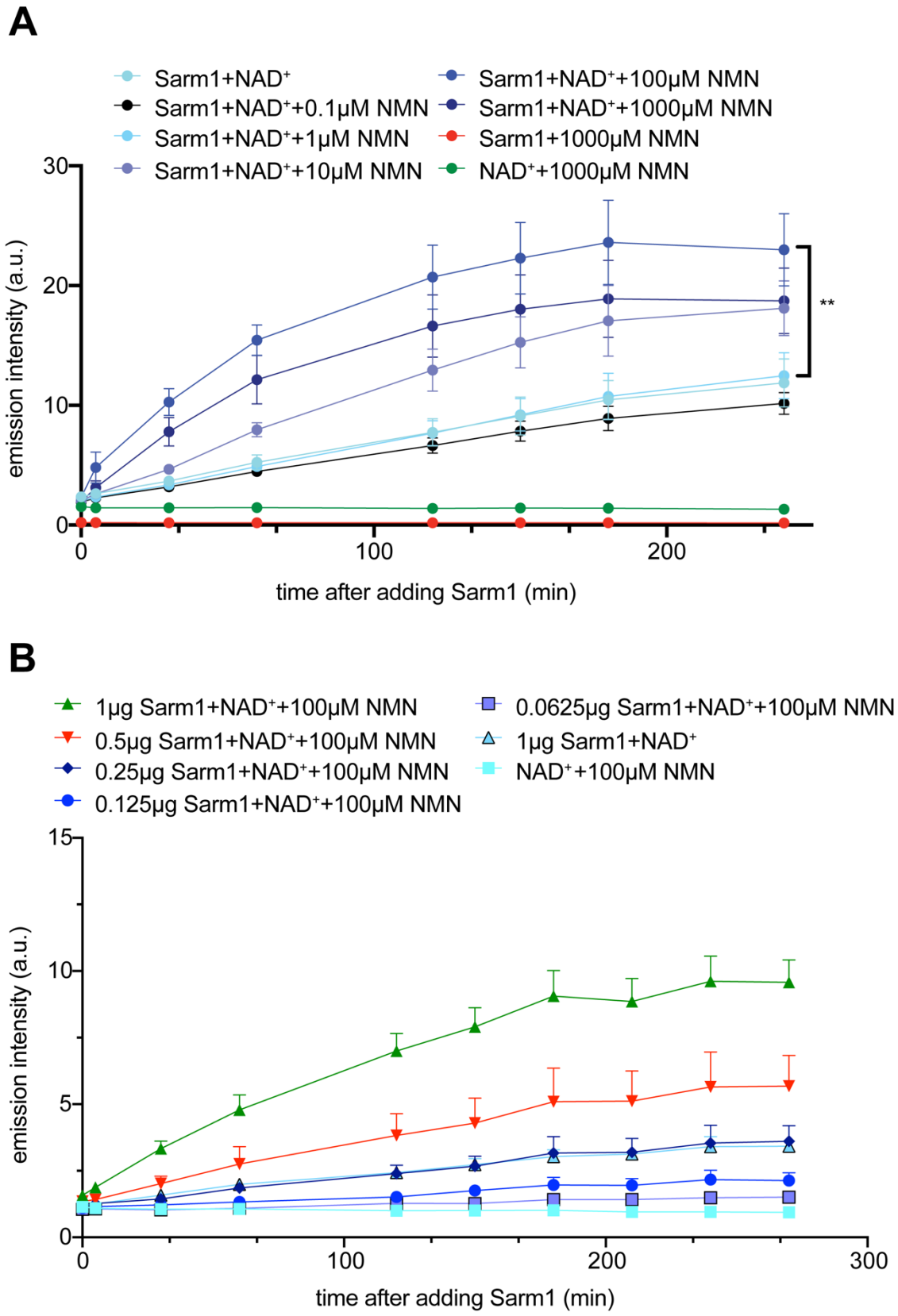

Figure 3.1:

(A) Time course *in vitro* NAD^+ hydrolysis assay with purified Sarm1 recombinant protein (1mg/ml), 50 μM ε-NAD (NAD^+), indicated concentrations of NMN. The y-axis indicates the artificial unit (a.u.) of the fluorescent intensity emission of ε-NAD hydrolization.

(B) Time course *in vitro* NAD^+ hydrolysis assay with different concentrations of purified Sarm1 recombinant protein, 50 μM ε-NAD (NAD^+), and 100μM NMN. Ordinary one-way ANOVA with Dunnett multiple comparisons test. (*p < 0.05, **p < 0.01, ***p < 0.001, ****p < 0.0001, n = 4 replicates, Error bar = SEM).

Figure 3.2: NMN is possible the allosteric Sarm1 NAD^+ hydrolase activator.

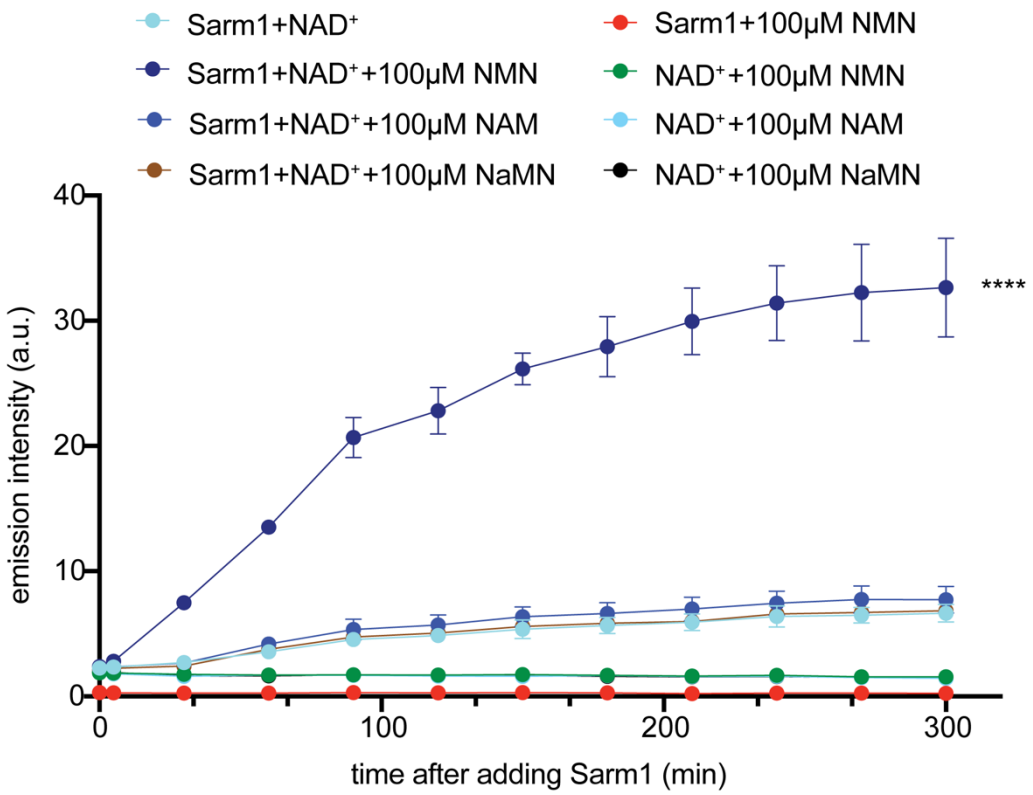

Figure 3.2:

(A) Time course *in vitro* NAD^+ hydrolysis assay with purified Sarm1 recombinant protein (1mg/ml), 50 μM ε-NAD (NAD^+), and 100 μM of NMN, NaMN, and NAM. The y-axis indicates the artificial unit (a.u.) of the fluorescent intensity emission of ε-NAD hydrolysis. Ordinary one-way ANOVA with Dunnett multiple comparisons test. (*$p < 0.05$, **$p < 0.01$, ***$p < 0.001$, ****$p < 0.0001$, n = 4 replicates, Error bar = SEM).

Figure 3.3: Nmnat1/2 suppressed the enhanced Sarm1 NAD⁺ hydrolase activity possibly by degrading NMN.

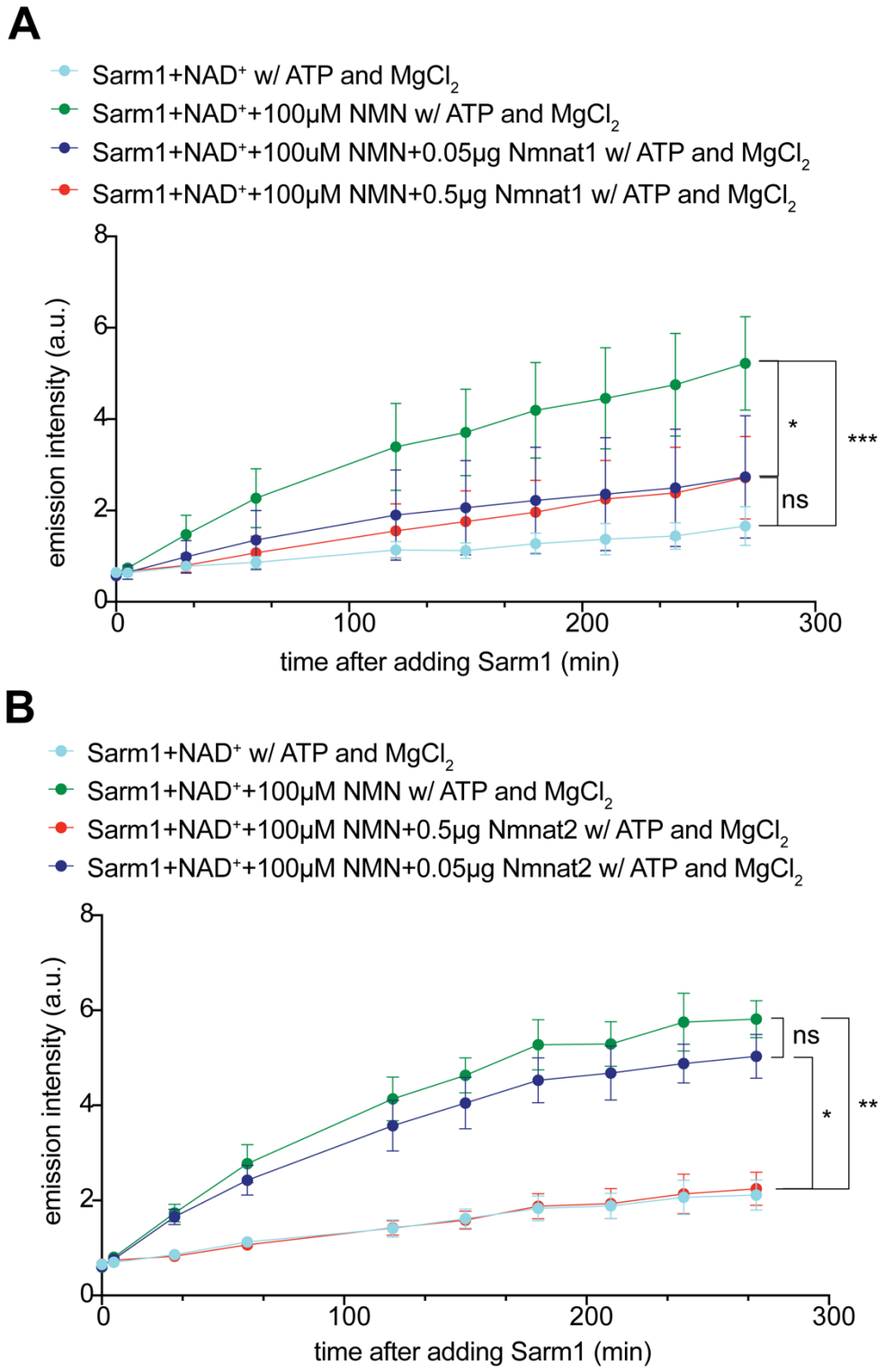

Figure 3.3:

(A) NAD^+ hydrolysis assays with purified Sarm1 recombinant protein (1mg/ml), purified Nmnat1 protein with indicated amounts, 50 μM ε-NAD (NAD^+), and 100μM NMN. The y-axis indicates the artificial unit (a.u.) of the fluorescent intensity emission of ε-NAD hydrolyzation.

(B) NAD^+ hydrolysis assays with purified Sarm1 recombinant protein (1mg/ml), purified Nmnat2 protein with indicated amounts, 50 μM ε-NAD (NAD^+), and 100μM NMN. The y-axis indicates the artificial unit (a.u.) of the fluorescent intensity emission of ε-NAD hydrolyzation. Ordinary one-way ANOVA with Dunnett multiple comparisons test. (ns = not significant, *$p < 0.05$, **$p < 0.01$, ***$p < 0.001$, ****$p < 0.0001$, n = 4 replicates, Error bar = SEM).

Figure 3.4: Overexpression of NMNd was able to suppress axon degeneration after axotomy, but not dSarm^{GOF} induced neuronal death.

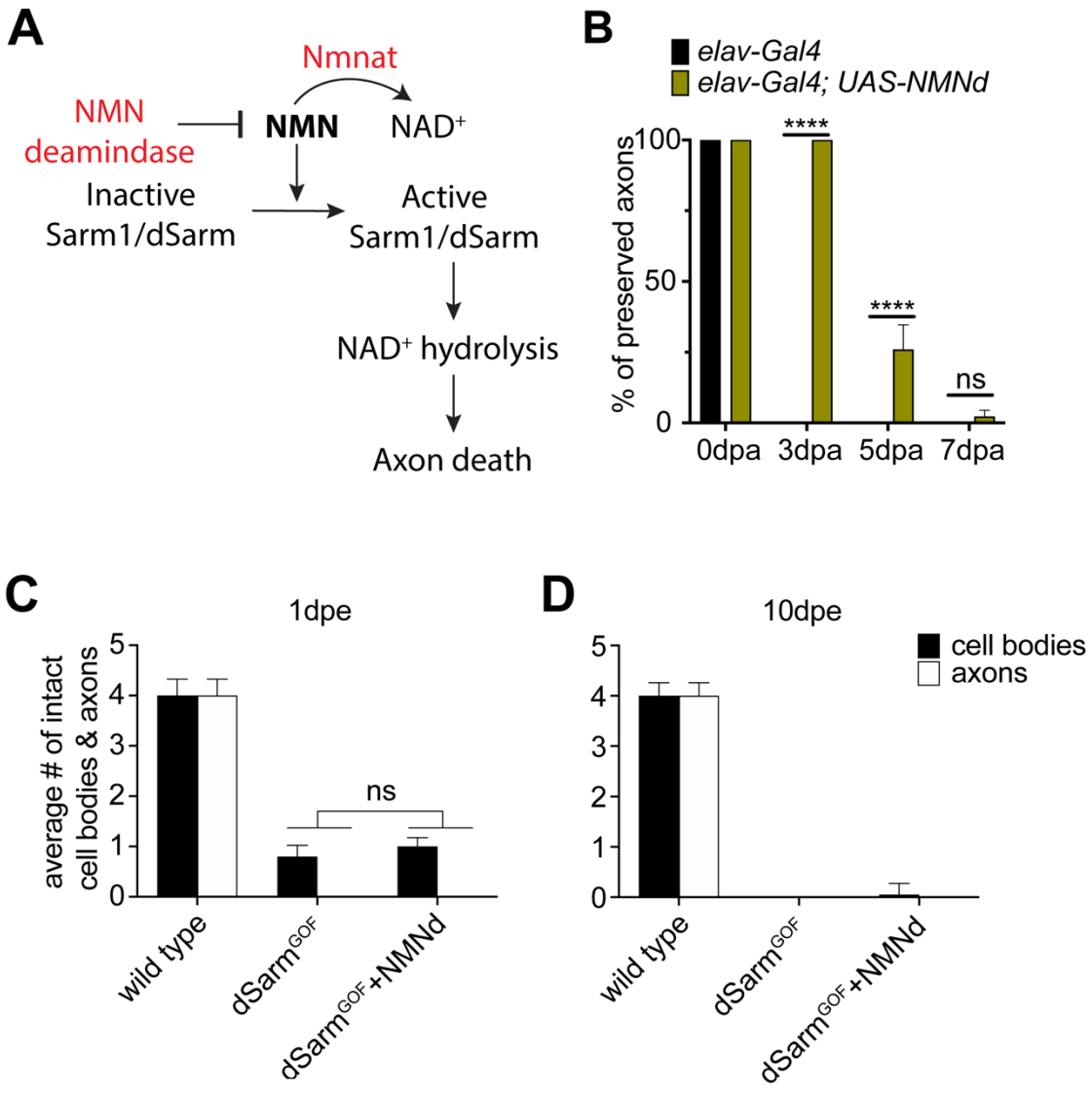

Figure 3.4:

(A) Model for NMN induced Sarm1 NAD^+ hydrolase activity.

(B) Quantification of axon preservation after axotomy. dpa, days post axotomy. Two-way ANOVA with Sidak multiple comparisons test. (ns = not significant, ****$p < 0.0001$, n = 25 animals for each, Error bar = S.E.M.).

(C, D) Quantification of neuron preservation (cell body and axon) in wild type (*ok371-Gal4)*, and $dSarm^{GOF}$ (*ok371-Gal4, UAS-dSarm^{GOF}-GFP)*, and $dSarm^{GOF}$+NMNd (*ok371-Gal4, UAS-dSarm^{GOF}-GFP, UAS-NMNd-T2A-mCherry)* expressing neurons at different time points (1 and 10 days post eclsion, dpe). Two-way ANOVA with Sidak multiple comparisons test. (ns = not significant, ****$p < 0.0001$, n = 25 animals for each, Error bar = SEM).

Figure 3.5: Overexpression of NMNd failed to maintain axon transport after nerve injury.

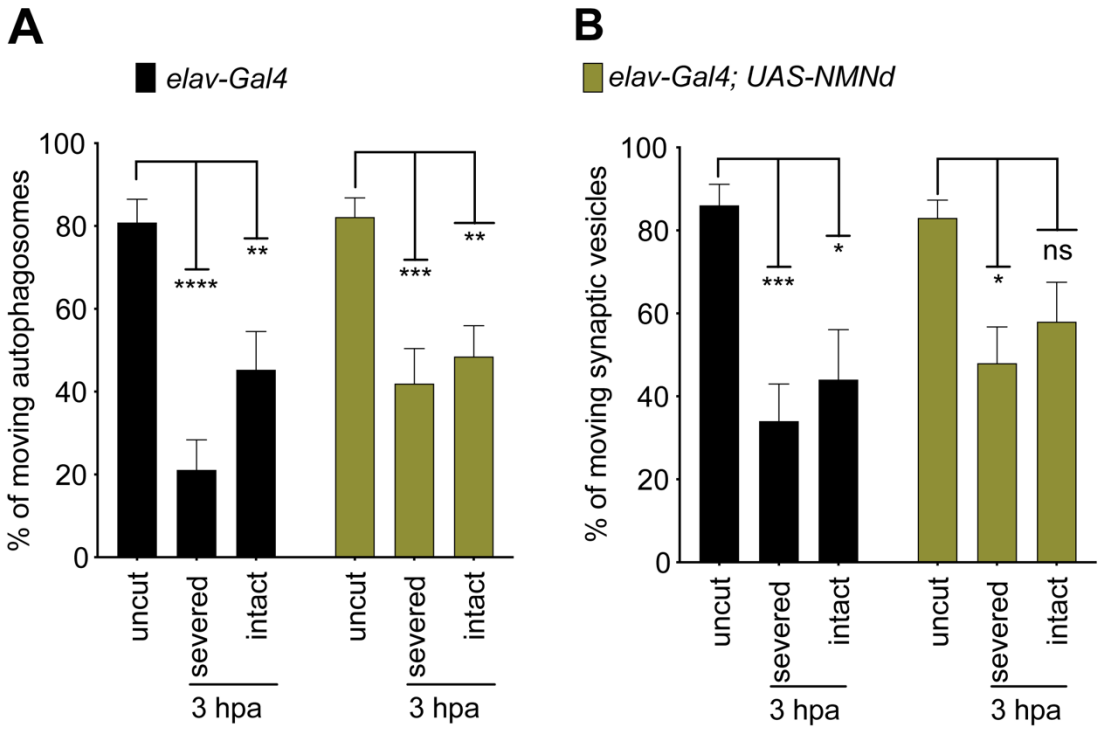

Figure 3.5:

(A, B) Severed and intact axons expressing NMN deamidase (NMNd) showed decrease of autophagosome transport (A), and partial decrease of synaptic vesicle transport (B) after axonal injury 3hpa compared to that in uninjured wings. Two-way ANOVA with Sidak multiple comparisons test. (ns = not significant, ****$p < 0.0001$, ***$p < 0.001$, **$p < 0.01$, *$p < 0.05$, n = 10~20 animals, Error bar = SEM).

Figure 3.6: Overexpression of NMNd in cacophony mutants mildly extended axon protection after axotomy.

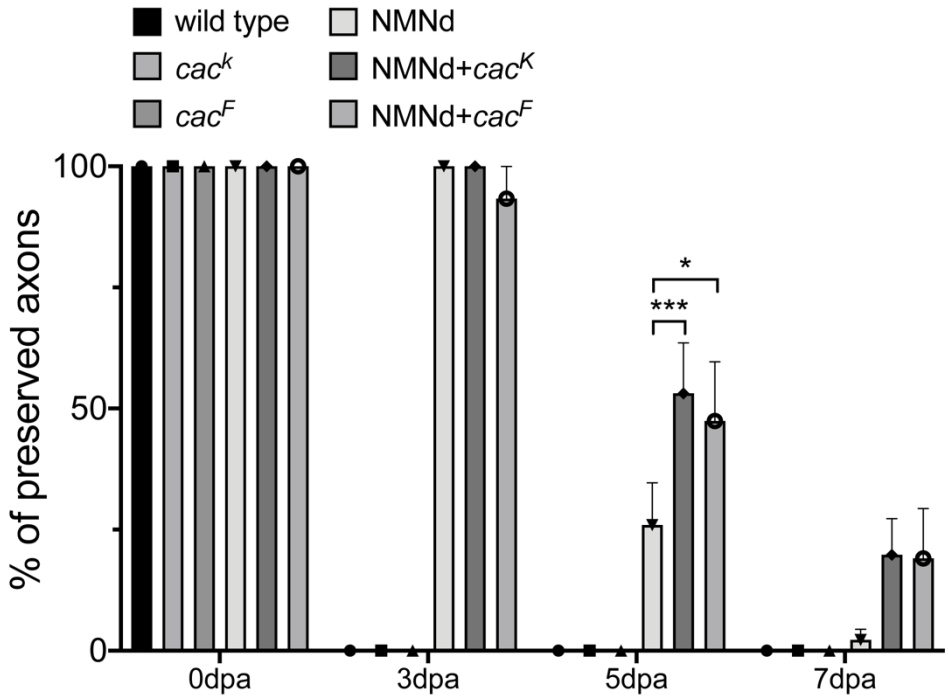

Figure 3.6:

Quantification of axon preservation after axotomy with indicated genotypes. Genotypes: wild type (*ok371-Gal4*), cac^K (*ok371-Gal4,* cac^K), cac^F (*ok371-Gal4,* cac^F), NMNd (*ok371-Gal4, UAS-NMNd-T2A-mCherry*), NMNd+cac^K (*ok371-Gal4, UAS-NMNd-T2A-mCherry,* cac^K), and NMNd+cac^F (*ok371-Gal4, UAS-NMNd-T2A-mCherry,* cac^F). dpa, days post axotomy. Two-way ANOVA with Sidak multiple comparisons test. (ns = not significant, ****p < 0.0001, ***p < 0.001, **p < 0.01, *p < 0.05, n = 10~20 animals, Error bar = SEM)

Figure 3.7: Overexpression of Wlds/dNmnat resulted in maintained axon transport after nerve injury.

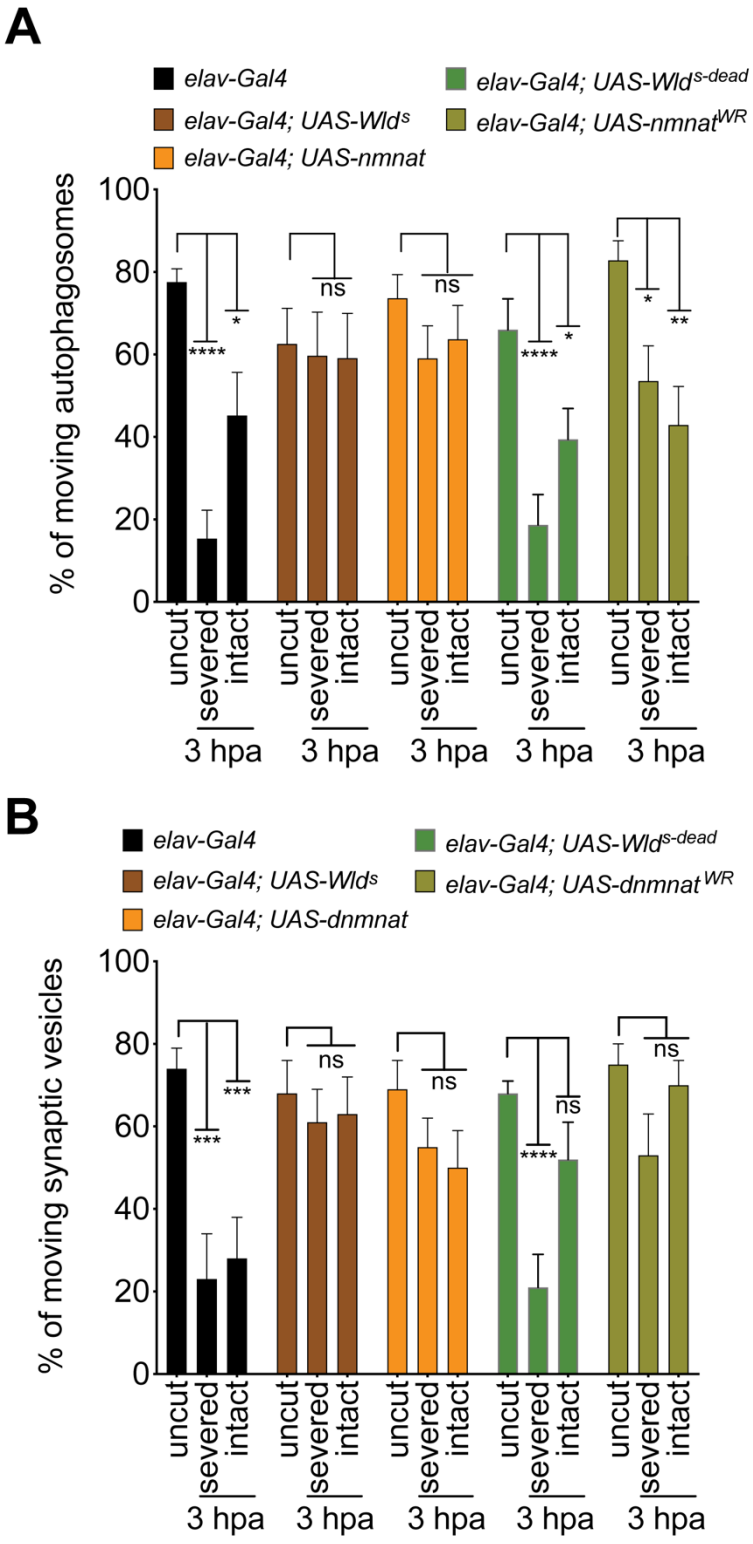

Figure 3.7:

(A, B) Autophagosome transport (A), synaptic vesicle transport (B) of severed and intact axons expressing Wld^{S}, dNmnat, $Wld^{S\text{-}dead}$, and $dNmnat^{WR}$, compared to that in uninjured wings. Two-way ANOVA with Sidak multiple comparisons test. (ns = not significant, ****$p < 0.0001$, ***$p < 0.001$, **$p < 0.01$, *$p < 0.05$, n = 10 animals, Error bar = SEM)

Figure 3.8: hiw was required for suppression of axon transport after nerve injury.

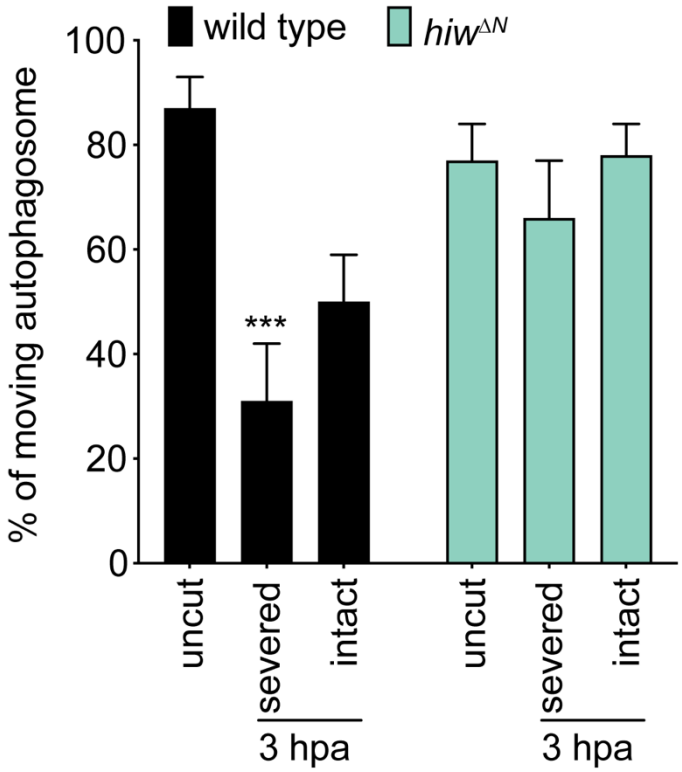

Figure 3.8:

Severed and intact axons of *hiw*$^{\Delta N}$ mutant clones 3hpa compared with uninjured wings. Two-way ANOVA with Sidak multiple comparisons test. (ns = not significant, ***$p < 0.001$, n = 10 animals, Error bar = SEM).

Figure 3.9: Overexpression of Wld^S/dNmnat, but NMNd, is sufficient to restore mechanosensation.

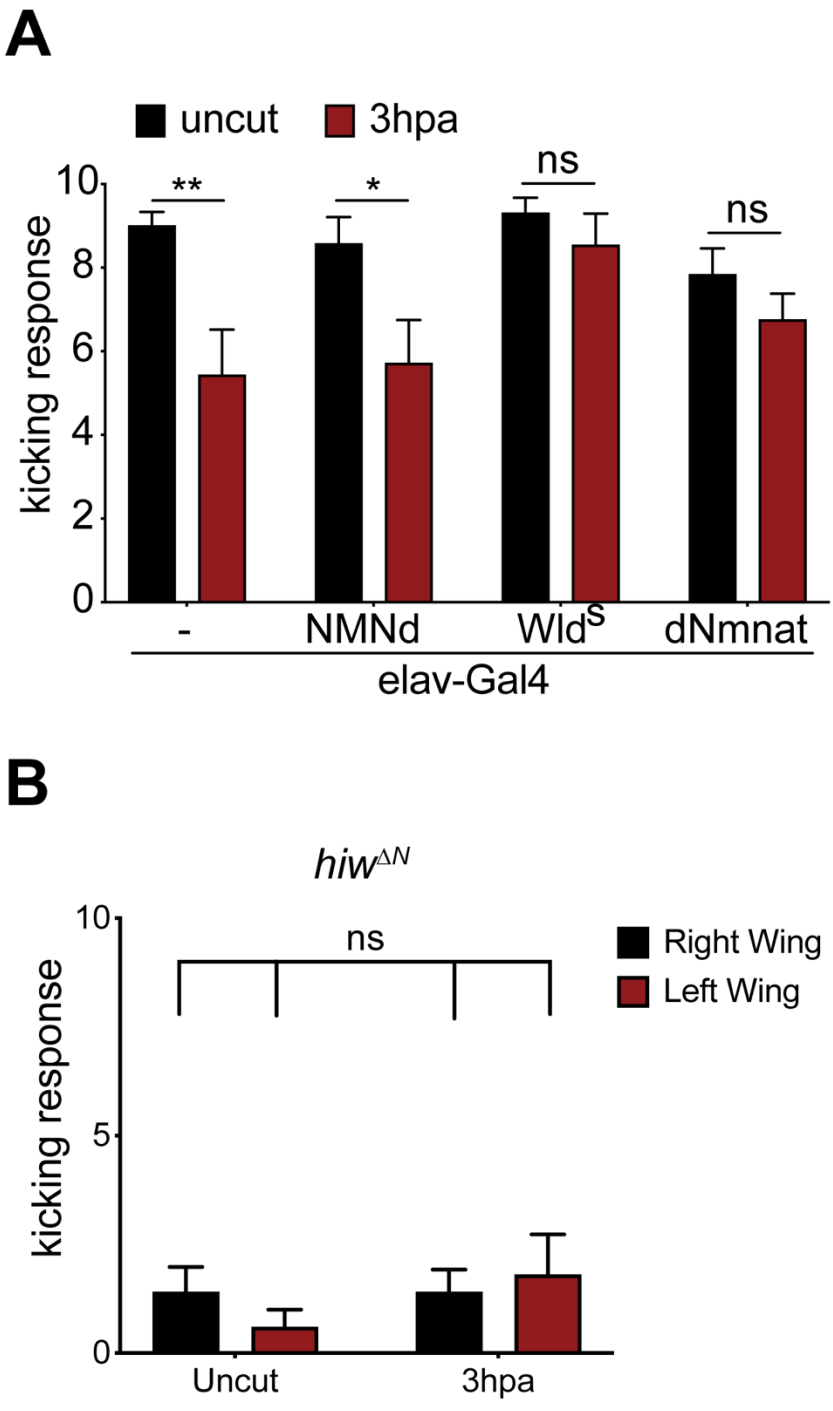

Figure 3.9:

(A) Overexpression of NMNd, Wld^S, dNmnat or driver only by pan-neuronal driver *elav-Gal4*. Two-way ANOVA with Sidak multiple comparisons test. (ns = not significant, *p < 0.05, **p < 0.01, n = 10~14 animals, Error bar = SEM).

(B) Uncut: Both side of the wings are intact. 3hpa: Right wings are intact, but the left wings are injured. $hiw^{\Delta N}$ mutant showed defective kicking responses upon bristle stimulation even in the animals without any injury. Two-way ANOVA with Sidak multiple comparisons test. (ns = not significant, n = 13~14 animals of each, Error bar = SEM).

Figure 3.10: Overexpression of Wld^S, or increase the level of dNmnat, was sufficient to restore chemosensation in bystander neurons.

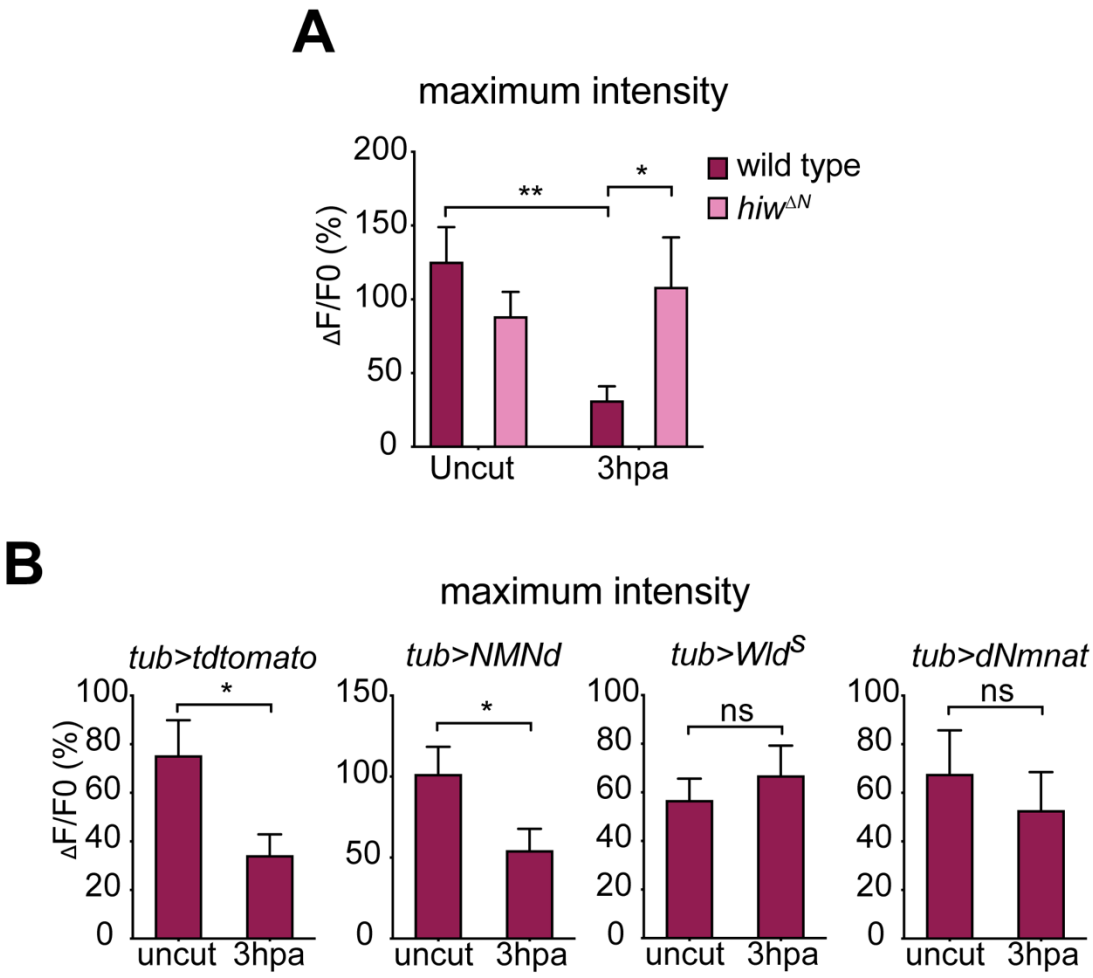

Figure 3.10:

(A) The average maximum intensity (maximum ΔF/F0%) of GCamp6s fluorescence stimulated by glucose was significantly reduced at 3hpa, but recovered by 6hpa. F0 was defined as the average of fluorescent intensity of 100-120 seconds. In *hiw*$^{\Delta N}$ homozygous mutant animals, the average maximum GCamp6s intensity is comparable in the uninjured and injured wings. Two-way ANOVA with Sidak multiple comparisons test. (**p < 0.01, *p < 0.05, n = 10~18 animals of each, Error bar = SEM).

(B) Overexpression of tdTomato, NMNd, Wld^{s} or dNmnat by tub-Gal4. Unpaired two-tailed t-test. (ns = not significant, n = 15 animals, Error bar = SEM).

CHAPTER IV: Glia are required for suppressing axon transport in bystander neurons through Draper/JNK/MMP-1 signaling.

In this chapter, Megan Corty generated the *Drosophila* transmission electron microscopic images of the wing, and I conducted all additional experiments.

Part of the work in this chapter is included in the following publication:

Injury-induced inhibition of bystander neurons requires dSarm and signaling from glia

Jiun-Min Hsu, Yunsik Kang, Megan Corty, Danielle Methieson, Owen Peters, Marc Freeman

Chapter IV: Abstract

In this chapter, I describe a novel role for glia in spreading injury signals within the nerve to suppress bystander axon transport. Using transmission electron microscopy, we first show that axons in the *Drosophila* L1 wings vein are fully enthsheathed by glial process. Surprisingly, we also found that suppression of bystander neuron function required signaling through glia. Loss of glial Draper, or the downstream signaling molecules JNK, c-Jun and MMP-1 in glia suppressed the ability of nerve injury to block axon transport in bystander neurons, while distal severed axons exhibited a potent blockade of transport. These observations reveal a novel role for glial Draper signaling in active suppression of bystander neurophysiology.

Chapter IV: Results

Result 4.1 - Draper functions in glia to suppress axon transport in neighboring intact neurons.

How are injury signals spread to bystander neurons? The *Drosophila* L1 wing vein houses ~280 sensory neurons that project into the thoracic ganglion. Megan Corty in Freeman lab examined the morphology of this nerve and found that individual sensory neuron axons were fully ensheathed by glial processes (Figures 4.1), suggesting they are not in direct contact with one another. It is plausible that severed axons signal to glia, and then glia alert bystander neurons to alter their axonal physiology. Alternatively, glia could be damaged during the nerve injury and signal directly to neurons that an injury has occurred. To begin to explore these possibilities we assayed for blockade of axon transport in *draper* null mutants. Draper is a receptor required for glial phagocytic function (Freeman et al., 2003; MacDonald et al., 2006), as is its mammalian ortholog MEGF10 (Wu et al., 2009), but Draper/MEGF10 also plays additional roles in cell-cell signaling in the activation of autophagy and starburst amacrine cell tiling (Kay et al., 2012; McPhee et al., 2010). We labeled autophagosomes in control and *draper* null mutants ($drpr^{\Delta 5}$) and assayed transport in severed axons and

bystander neurons. We found that axon transport was suppressed in severed axons in *draper* mutants, similar to controls (Figure 4.2A). However, axon transport in bystander neurons was maintained in *draper* mutants (Figure 4.2A). To confirm this represented a role for Draper in glia, we knocked down *draper* with RNAi selectively in glia using the pan-glia Gal4 driver line *repo-Gal4* and assayed axon transport. We found that glial depletion of Draper was sufficient to maintain axon transport in bystander neurons, but not severed axons (Figure 4.2B). These data demonstrate that glial Draper is required for active spreading of injury signals to bystander neurons, while suppression of axon transport in severed axons occur in a Draper-independent manner.

Result 4.2 - JNK and MMP-1 function in glia to suppress axon transport in the intact neurons.

Draper is thought to function as a receptor that senses injury signals and then promotes glial engulfment process through the stimulation of positive auto-regulatory transcriptional loop in the glia, and multiple downstream molecules of Draper receptor have been identified (Awasaki et al., 2006; Doherty et al., 2009; Doherty et al., 2014; Logan et al., 2012; Lu et

al., 2017; Purice et al., 2017). To explore the mechanism by which Draper spreads the injury signal and suppress axon transport in bystanders, we performed glial knock-down of key molecules known to act downstream of Draper to drive glial engulfment. First, I found that axon transport in bystander neurons was still suppressed at 3 hours after axotomy after glial knockdown of Shark and dCed-6, both of which directly associate with Draper receptor (Doherty et al., 2009), (Figure 4.3A). We note that there appeared to be a partial effect of Shark knockdown, suggesting that Shark may play a minor role. Overexpression of Draper-II, a Draper isoform that functions as a potent suppressor of Draper-I and can terminate Draper signaling after injury and block glial phagocytic responses (Logan et al., 2012), did not maintain bystander axon transport after injury (Figure 4.3A). These data argue that Draper-II/ITIM signaling via Corkscrew (Shp1/2) cannot regulate glial suppression of bystander neuron physiology. Interesingly, I found impairment of JNK signaling by knocking down of the JNK, Bsk, or overexpression of a dominant-negative Jra molecule, was sufficient to maintain bystander axon transport (Figure 4.3A). Given that Bsk is the only JNK in the *Drosophila*, and *jra* encodes c-Jun, which is one of the members of dAP-1 complex, these results argue that JNK signaling plays a central role in glia to suppress bystander axon transport. I next

explored the potential role of Mmp-1 in glial suppression of bystander neuron function. Previous work has shown that *mmp-1* is regulated by JNK signaling in the glia after nerve injury to promote glial phagocytic function (Purice et al., 2017). I found that Mmp-1 knockdown also suppressed the ability of glia to block transport in bystander neurons (Figure 4.3A). Together these data indicate that Draper is required to spread injury signals throughout the nerve, and does so via JNK/AP-1/MMP-1 signaling.

Finally, I assayed for roles for PI3K signaling in glial suppression of bystander neuron function. Raptor is a key component of the TOR complex in *Drosophila*. I found that knockdown Raptor also restored bystander axon transport 3 hrs after injury (Figure 4.3A). In previous work Raptor was found to be required to maintain the basal level of Draper via a transcriptional cascade involving dAP-1 and STAT92E (Doherty et al., 2014), although Draper upregulation was still observed in response to axon injury in Raptor RNAi animals. These data further support the notion that a transcriptional cascade downstream of Draper, involving JNK, dAP-1, and PI3K/Raptor signaling is required for glial suppression of bystander neuron function after partial nerve injury (Figure 4.3B).

Chapter IV: Material and Methods

Transmission electron microscopy

Wings were prepared for TEM using microwave-assisted tissue processing as follows. Wings were dissected from anesthetized 5 dpe female flies and immediately placed in fresh modified Karnofsky's fixative (2% glutaraldehyde, 4% paraformaldehyde, 0.1M sodium cacodylate buffer, pH 7.4). Primary fixation, secondary fixation with additional 2% OsO4 and imidazole, en bloc UA staining, dehydration, and resin infiltration of samples was carried out in a Pelco laboratory microwave following the procedure for zebrafish larvae described in previous study (Cunningham and Monk, 2018). After resin infiltration, wings were flat embedded between two sheets of Aclar plastic. After overnight polymerization at 60C, the Aclar was removed and flat-embedded wings were trimmed to access the ROI and remounted in fresh resin for sectioning on an Ultramicrotome (Leica). 70nm sections were collected on Formvar coated grids, counterstained with 5% uranyl acetate for 20 minutes, and Reynold's lead citrate for 7 minutes before being imaged on an FEI Technai T12 operating at 80kV with an Advanced Microscopy Techniques camera.

Axotomy assays & Vesicle movement image and analysis

See Material and Methods of Chapter II.

Chapter IV: Figures

Figure 4.1: Axons in the wing vein are individually wrapped by glia.

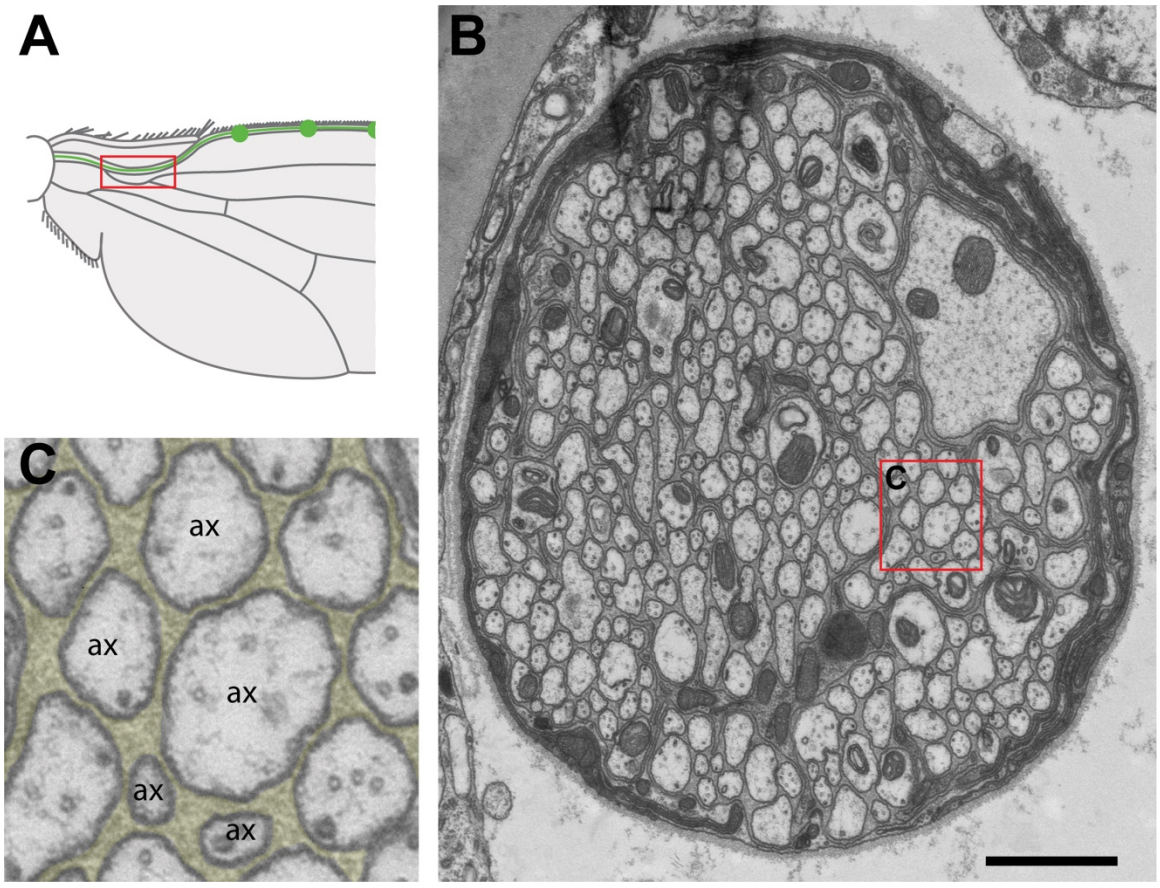

Figure 4.1:

(A) Schematic shows that the region where TEM image was taken (red rectangle).

(B) TEM of the nerve in L1 wing vein. Red rectangle indicates the selected region of (C). Scale bar = 1μm.

(C) 5x magnified TEM image from the indicated region on (B). Glia are pseudocolored. ax = axon.

Figure 4.2: Draper in glia was required for suppressing axon transport in bystander neurons.

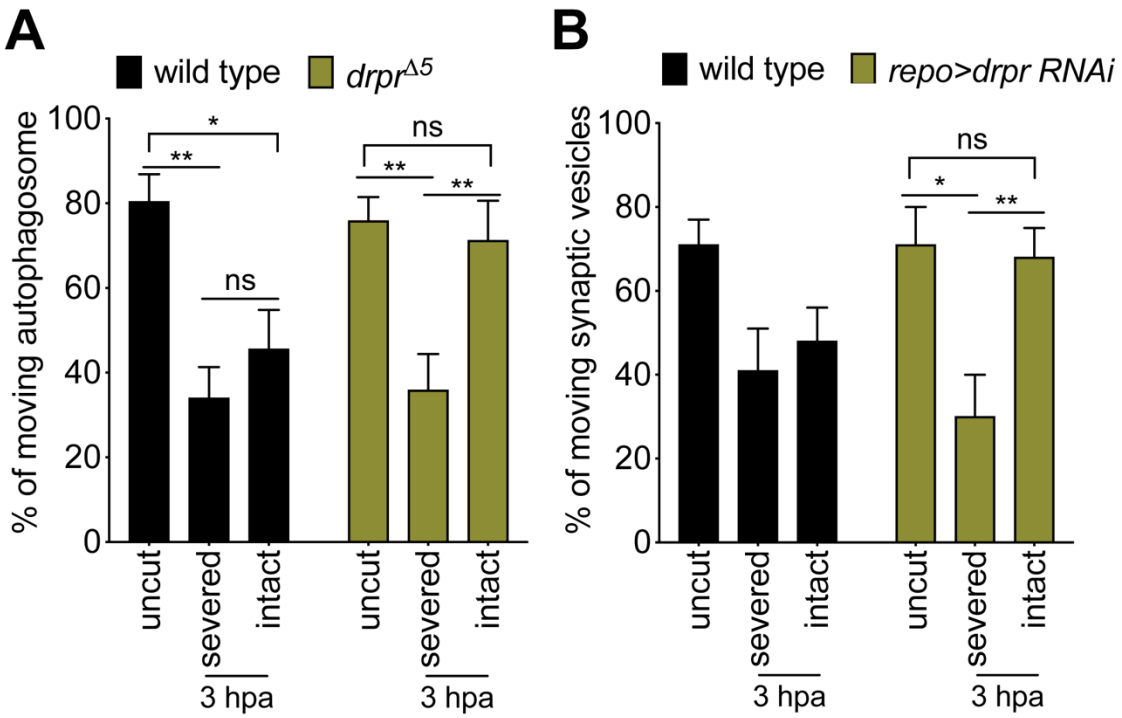

Figure 4.2:

(A) Severed axons, but not intact axons, showed decrease of axon transport after axonal injury 3hpa in drpr$^{\Delta 5}$ homozygote flies. Two-way ANOVA with Sidak multiple comparisons test. (ns = not significant, **p < 0.01, *p < 0.05, n = 10~20 animals, Error bar = SEM).

(B) Severed axons, but not intact axons, showed decrease of axon transport after axonal injury 3hpa in glial-specific draper knockdown flies (repo-gal4, uas-drpr RNAi). Two-way ANOVA with Sidak multiple comparisons test. (ns = not significant, **p < 0.01, *p < 0.05, n = 10~20 animals, Error bar = SEM).

Figure 4.3: JNK/MMP-1 signaling in glia was required for suppressing bystander axon transport.

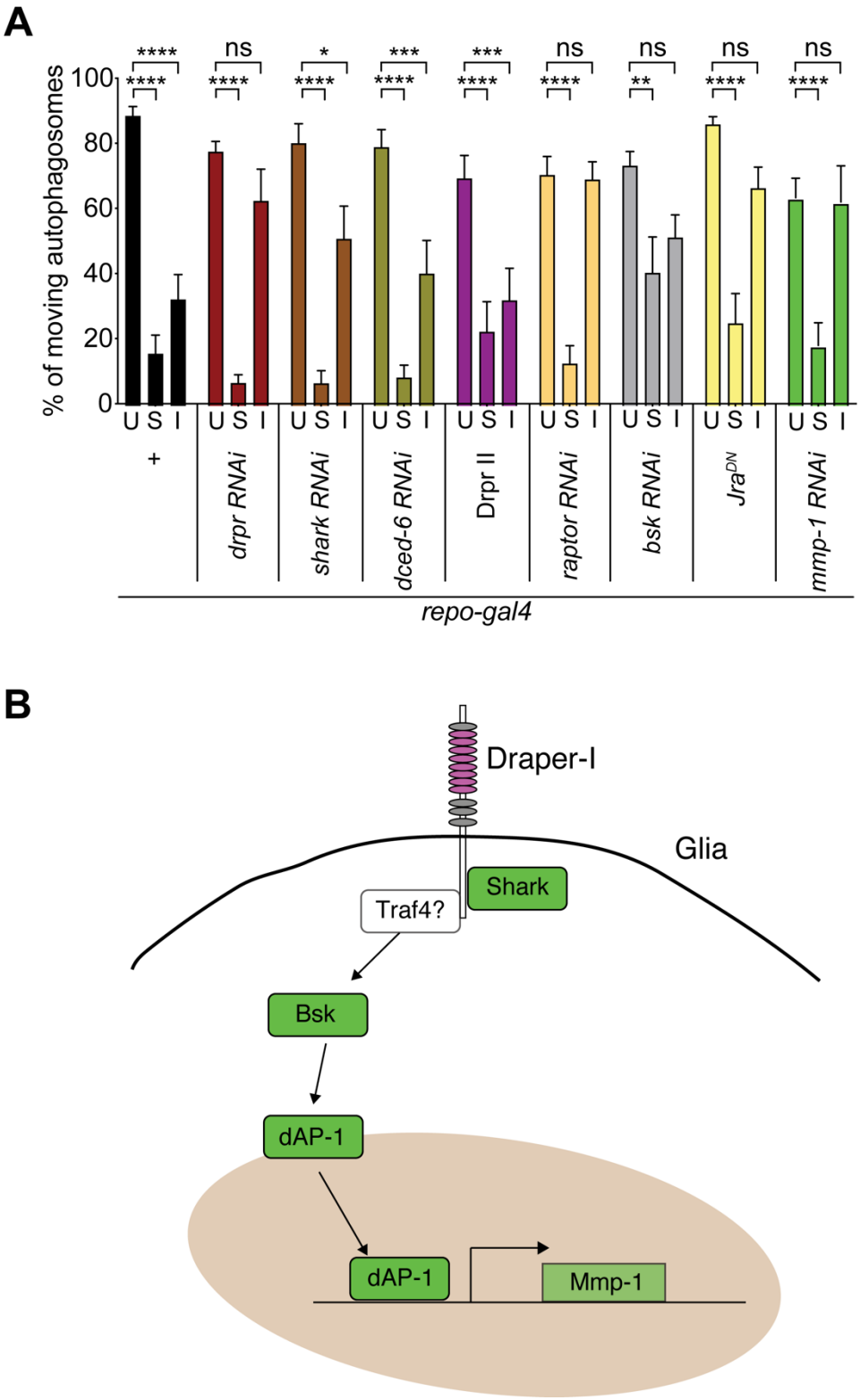

Figure 4.3:

(A) Axon transport of uncut (U), severed axons (S). and intact neurons (I) after axonal injury 3hpa in glial-specific knockdown flies. Two-way ANOVA with Sidak multiple comparisons test. (ns = not significant, ****p < 0.0001, ***p < 0.001, **p < 0.01, *p < 0.05, n = 10~20 animals, Error bar = S.E.M.).

(B) Proposed model of Draper-mediated glial responses to nerve injury. Draper is cell-autonomously required for glia and possibly upregulates JNK signaling cascade and MMP-1, likely through the activation of Shark, or Traf4, to suppress bystander axon transport.

CHAPTER V: Discussion

Discussion 5.1 - Injury signals spread efficiently across the injured nerve through Cac/dSarm/MAPK signaling.

My data support the notion that widespread signaling occurs between cells in injured neural tissues immediately after injury, and that injury signals can radically alter neuronal function. Severing even a small number of axons led to a blockade of axon transport within hours in all axons in the adult wing nerve, even in uninjured bystander neurons. Beyond axon transport, local uninjured bystander sensory neurons also exhibited a disruption of mechano- and chemosensory signal transduction, which was partially reversible within a few additional hours. These observations indicate that even a very small injury can have far-reaching effects on nerve function. This is a not result of particular injury (i.e. wing cutting) since similar responses are observed in other, less damaging settings including wing margin crush without cutting off the large portion of the wing, and laser ablation, which minimizes the size of the injury.

Surprisingly, we found that dSarm is required cell-autonomously in bystander neurons to alter axon transport and nerve function in response to injury. This indicates that dSarm function is required in bystander neurons to receive this injury signal from other cells. Reception of this injury signal in

the bystander neuron (and severed axons) requires the voltage gated calcium channel Cac and the MAPK signaling cascade, similar to Tir-1 signaling in C. elegans, but not Axed. Reciprocally, Cac and MAPK components are not required for Wallerian degeneration at later stages. Based on the timing of these different events (i.e. changes in neuronal function versus frank degeneration) and our genetic studies indicating they are separable, we propose a two-phase model for dSarm signaling in injured neural tissues: early dSarm-dependent changes in axon biology and neurophysiology that occur within hours are mediated by the Cac/dSarm/MAPK signaling cascade, but not Axed; and late stage axon degeneration is driven by dSarm signaling through Axed, while Cac/MAPK signaling is dispensable for this step.

To date dSarm/Sarm1 has been thought of primarily as a cell autonomous regulator of explosive axon degeneration, but our work shows that dSarm can also drive important changes in circuit function through altering neuronal cell biology and neurophysiology in intact neurons. That bystander neurons recover and remain viable also demonstrates that activation of dSarm after injury does not necessarily lead to axon death. Defining how dSarm is alternatively activated in each of these contexts will be an important for our understanding of how dSarm governs neural

responses to injury. For instance, these distinct signaling events may involve different conformational activation states of dSarm (e.g. partial versus full activation), and they may depend on the recently identified dSarm/Sarm1 NAD^+ hydrolase activity (Essuman et al., 2017).

We found significant Ca^{2+} influx appeared not just in the injured axons, but also in the bystanders right after nerve injury. These results may indicate that calcium functions as the initial signal to activate dSarm-mediated early phenotypes. However, we did not see obvious reduction of Ca^{2+} influx after injury in the *cac* loss-of-function mutants, but removal of Cac was sufficient to suppress early phase phenotype at levels similar to *dsarm* mutants. One of the *cac* alleles (cac^F) we tested included a point mutation without affecting major protein structure, which has been shown to reduce depolarization amplitude, suggesting that calcium influx is reduced (Tian et al., 2015). As this *cac* allele also showed maintained axon transport (Figure 2.8), it indicates that the calcium influx and current transduction activity of this calcium channel is required to block axon transport after injury. These data suggest that Cac functions as the specific channel to initiate early axon transport suppression, but is not the major mediator of injury-induced Ca^{2+} increases after axotomy. Cac encodes the primary α1 subunit of voltage-gated calcium channel (Smith et al., 1998), which is the

fly ortholog of the N-type calcium channel or P/Q-type calcium channel. L-type channels have previously been assigned roles in the process of axon degeneration, as blockers of L-type, but not N-type calcium channels, can significantly delay axon degeneration after axotomy (George et al., 1995). Together this work supports a model where early functional changes in neurons receiving injury signals are mediated by N-type channels, while late degenerative events are driven by L-type channels.

Discussion 5.2 - Roles for axon death molecules in suppression of neuronal function in bystander neurons.

A compelling case exists for the NAD^+ depletion hypothesis for dSarm/Sarm1 function in axon degeneration (Essuman et al., 2017; Gerdts et al., 2015; Gerdts et al., 2016), although arguments have been made that dSarm/Sarm1 signaling is likely more complex (Neukomm et al., 2017). In this model, depletion of Nmnat2 via Hiw/Phr1 results in the accumulation of NMN, which functions as an activator of Sarm1, with Sarm1 NAD^+ hydrolase activity driving metabolic catastrophe. We provide several lines of evidence that the above, newly-described early dSarm signaling events (i.e. suppression of axon transport and neurophysiology) are mechanistically

distinct, but are nevertheless also regulated by a subset axon death-associated molecules. First, while NMN deamidase (NMNd) can suppress axon degeneration in flies and other species (Di Stefano et al., 2014), it cannot block early suppression of axon transport or changes in bystander neuron function. Second, although limited to tagged versions of dNmnat for our analysis, we observe no depletion of dNmnat within the time frame of 6 hours after injury. Even in vitro Nmnat2 and NAD^+ depletion take 4-6 hours in mouse SCG neuron cultures (Gilley and Coleman, 2010; Wang et al., 2005). This would be inconsistent with dNmnat or NAD^+ depletion activating dSarm at this early stage. Third, Axed, which is genetically downstream of dSarm during axon degeneration (Neukomm et al., 2017), is not required for early suppression nerve responses to injury, only later axon degenerative events. Nevertheless, Wld^s or dNmant expression, and hiw mutants are all capable of suppressing early changes in axon transport and neurophysiology, even in bystander neurons. This is difficult to reconcile with a simple NAD^+ depletion model. It seems likely that at early stages dSarm is likely active by Cac signaling, as is the case with Tir-1 activation in *C. elegans* (Chuang and Bargmann, 2005), and that later stages are mediated by an NAD^+ depletion model-type signaling event. However, the ability of Wld^s or dNmnat expression or loss of Hiw to suppress these early

dSarm-mediated signaling events argues that the NAD^+ depletion model cannot fully explain the effects of any of these molecules in modulating axon transport or bystander neurophysiology.

In addition to the involvement of NAD^+ metabolism, Wld^s, dNmnat, or cytosolic Nmnat1 can suppress initial Ca^{2+} spike after axon injury in the *Drosophila* larval peripheral nerves (Avery et al., 2012). Cytosolic Nmnat1 ($Nmnat1^{CYTO}$) can reduce the injury induced MAPK activation in the mouse optic nerve crush model (Yang et al., 2015). These events are required for the early phase phenotype in our data, and such suppression could explain the role of Wld^s or dNmnat expression, or even loss of Hiw in the early dSarm-mediated signaling. That the enzymatic activity of Wld^s is required for maintaining axon transport after injury is consistent with our previous finding that it is required for early Ca^{2+} suppression. Overexpression of $dNmnat^{WR}$ (mostly enzyme dead) only partially rescued axon transport of autophagosomes and synaptic vesicles, perhaps because of that these mutations (W98G and R224A; (Zhai et al., 2006) do not fully abolish the enzymatic activity. In summary, while the emerging evidence supports an interesting connection between Ca^{2+} signaling and activation of dSarm, the precise connection remains elusive.

Discussion 5.3 - Glial Draper/JNK/Mmp-1 signaling drives suppression of bystander neuron function.

Glial cells are well-positioned to rapidly spread signals to all axons in the wing nerve. Much like Remak bundles in mammals, the *Drosophila* L1 wing nerve has glial cells that appear to fully wrap axons individually, which would imply that axon-to-axon signals must pass through glia. Our observation that selective elimination of Draper in glia is sufficient to inhibit the spreading of injury signals to bystander neurons is consistent with an axon→glia→bystander neuron signaling event, although it is also possible that glia are directly injured by the axotomy and signal directly to bystander neurons without input from the severed axons, through a Draper-dependent mechanism. Given the similarities in the response of severed axons and those of bystanders (i.e. both block axon transport on the same time scale), and the selective effects of Draper on the bystander neuron axons, we favor the former model.

How does glial Draper suppress bystander physiology? I tested most of the key signaling molecules downstream of Draper known to regulate glial engulfment responses, and interestingly, the results showed on a subset

of the signal transduction molecules known to act downstream of Draper phagocytosis, are required for glial signaling to bystander neurons. Draper signals to bystander neurons through a transcriptional JNK/dAP-1 cascade, likely activating MMP-1, to suppress bystander axon transport. The involvement of MMP-1 is intriguing given its role on neuroinflammatory responses to brain injury in mammal. It functions to break down the extracellular matrix, and permeabilize the blood brain barrier, both activities which are believed to promote diffuse axon injury (Bell et al., 2012; Candelario-Jalil et al., 2011). Other key components of the Draper signaling pathway—dCed-6 in particular, which is required for Draper signaling in all other known contexts—were not required for suppression of bystander neuron neurophysiology. Key questions for the future include: What signal to glia receive from neuron (if any)? Does direct glial injury drive the spreading of the injury signal? Which glial subtypes (i.e. wrapping, subperineurial, or astrocytic) are involved in this response? What is the mechanism by which glia block neuronal function?

Discussion 5.4 – The recovery of bystanders.

Our observation of widespread suppression of neuronal physiology after nerve injury raises several interesting questions: Why is such a mechanism present? What selective advantage does it provide? How are bystander neurons blocked functionally, and how do they recover? We envision a number of possibilities the could answer these questions. Widespread suppression may be important for the injured tissue to transiently reduce energy and trophic consumption, which might be required for neurorepair and functional recovery. However, we did not observe any overt detrimental outcomes, such as neuronal death or function impairment in the mutants without widespread suppression, including Wld^{s}/dNmnat overexpression, *hiw* mutants, or dSarm knockdown animals, although more detailed examinations are needed.

A key future question will be defining the mechanism by which glial cells suppress bystander neuron function after partial injury. This remains a black box. Bystander recovery is likely due to their maintained connections to their cell bodies, which would be predicted to supply them with a steady stream of Nmnat activity once transport has recovered, while severed axons deplete Nmant/NAD^{+} and activate axon death. There could also be key changes in gene expression in the cell body, as JNK signaling in proximal cell bodies of injured neurons has been observed to occur after axotomy in

mammals and flies (Brace and DiAntonio, 2017; Fang and Bonini, 2012; Valakh et al., 2015). To begin to explore potential changes in gene expression in bystander cell bodies I attempted to extract the mRNAs bound to ribosomes in bystander neuron cell bodies in the distal wing margin after injury. Unfortunately, the efforts failed to isolate sufficient high-quality RNA for analysis. This could be accomplished using mouse primary neuronal cultures.

Axon transport is affected in a number of contexts of injury and in neurodegenerative disease. How this occurs in each case is likely to be varied, complex and context/compartment dependent. For instance, strangely, in *C. elegans* severed proximal axons are capable of axon regeneration, and NMAT-2, the worm homolog of Nmnat2, functions negatively on axon regrowth (Kim et al., 2018). This is likely the opposite of what one might predict based on the Nmnat/NAD^+ depletion model. We speculate that axon degeneration molecules function in a complex, compartment/context-dependent manner.

Discussion 5.5 – Nmnat RNAi suppressor screening.

One of our long-term goals is to comprehensively identify molecules involved in Wallerian degeneration, and our group has therefore performed several forward genetic and molecular screens toward this end. Near saturation EMS mutagenesis screens on chromosomes 2 and 3 (representing ~80% of the fly genome) were performed over a period of 5-7 years, but only three key genes were identified as capable of fully blocking axon degeneration: dSarm, Axed, and Hiw. Pebbled was also found, although its protective effects were much weaker, and limited to glutamatergic neurons (Farley et al., 2018; Neukomm et al., 2014; Neukomm et al., 2017). These results imply there is only a limited number of molecules in the genome that can provide dSarm-like suppression of axon degeneration. We also screened for suppressors of $dSarm^{GOF}$-induced cell destruction, but we failed to identify suppressors other than Axed. It is possible that $dSarm^{GOF}$ overexpression triggers multiple signaling pathways driving axon death and cell death. In this case, the genetic redundancy of other factors with minor roles in the individual pathways might have obscured the discovery of potent suppressors.

How could one screen for axon death genes more effectively? In previous studies, Nmnat2/dNmnat depletion resulted in activation of Sarm1/dSarm and Axed dependent axon death (Gilley et al., 2015;

Neukomm et al., 2017). These results suggest that dNmnat knockdown could serve as a less devastating injury, where the cell is still attached to its cell body, but nevertheless activates dSarm signaling. In my pilot screen, I found *CG4098* out of ~800 chromosomes screened on 3L, which encodes the *Drosophila* homolog of Nudix hydrolase 9. Loss-of-*CG4098* protected axons against dNmnat RNAi induced axon degeneration, and the cell survival rate was 80%, which is robust, but still weaker than loss of dSarm or Axed. Loss of *CG4098* did not block degeneration after axotomy or $dSarm^{GOF}$, which is consistent with the notion that suppressors of Nmnat loss exist, but may not fully block axon degeneration. The analysis of such molecules could be very informative in our quest to understand axon degeneration. It is also possible that CG4098 could acting upstream of dSarm; or the genetic interaction is more complicated, and we need to remove more molecules to protect the axons (e.g. double mutants); or CG4098 may be playing a unique role on axon death induced by dNmnat RNAi, but not in dSarm dependent death pathway. The latter seems less likely given that dNmnat/Nmnat2 RNAi has been shown to highly depend on dSarm/Sarm1 signaling. Overall, this pilot screen supports the idea that dNmnat RNAi is a sensitive manipulation that could lead the identification

of more molecules involving in axon death pathways. Such large-scale screens are currently underway in the laboratory.

Nudix hydrolase is a superfamily with around 24 genes in mammals, and 20 genes in *Drosophila*, and each gene encodes a protein with specific substrates (McLennan, 2006). Among these, NUDT9 is one of the ADP-ribose hydrolases, which removes the ribose-5-phosphate from ADP-ribose and produces AMP (Lin et al., 2002). ADP-ribose is the direct product of NAD^+ depletion by the NADases such as poly(ADP-ribose) polymerases (PARPs) and CD38, as well as indirectly produced by Sir2 family (Rafty et al., 2002), while NUDT9 is one of the enzymes responsible for ADP-ribose elimination. Interestingly, Sarm1 also degrades NAD^+ and produces ADP-ribose, which in turn is partially converted to cyclic-ADPR (cADPR) (Essuman et al., 2017). ADPR can mediate Ca^{2+} mobilization through the cation channel TRPM2 (Heiner et al., 2005; Kuhn et al., 2005; Perraud et al., 2003). The intracellular domain of TRPM2 contains a NUDT9H domain , which is related to NUDT9 but with a different core motif (Kuhn and Luckhoff, 2004), with prolonged binding of ADPR, instead the hydrolysis, is required for channel gating (Heiner et al., 2005; Kuhn et al., 2005; Kuhn and Luckhoff, 2004; Perraud et al., 2003). However, there is still no direct evidence for a role for ADPR, cADPR or TRPM2 in axon degeneration.

The identification of CG4098 raises a number of important questions for the future: (i) Does CG4098 function similarly as NUDT9 in mammals? (ii) Does *dnmnat* knockdown result in ADPR accumulation? (iii) Is the accumulation of ADPR good or bad for the axon survival? (iv) What is the role of the products of ADPR hydrolysis by CG4098, including AMP and ribose-5-phosphate? Answers to these questions will require metabolic profile analysis and biochemical analysis in the context of dSarm/Sarm1 signaling, and a deep analysis of CG4098 binding partners.

Discussion 5.6 – Sarm1/dSarm function and NAD^+ depletion.

One model for axon death is that Sarm1/dSarm drives axon destruction via the energy failure, and disruption of various cellular signaling pathways by depleting NAD^+ (Gilley and Coleman, 2010). However, our studies suggested that there are caveats in this NAD^+ depletion model: First, increase in the cellular NAD^+ level by inhibiting NAD^+ consuming enzymes, including tankyrases and PARP in HEK293T cells failed to suppress the cell death in $Sarm1^{GOF}$ overexpressing cells. This is consistent with a previous study, where removing CD38 and PARP1 failed to protect axons from degeneration (Sasaki et al., 2009). Lastly, our previous

work suggests that dSarm^{GOF} requires Axed to proceed to axon destruction, and I found NAD^+ was also depleted in the glands where Axed was knocked down in the presence of dSarm^{GOF} overexpression. Thus accumulating evidence supports the notion that the NAD^+ depletion model is likely an oversimplification of the dSarm/Sarm1 mechanism of axon degeneration and cell destruction.

What are the downstream signaling partners of Sarm1/dSarm that drive axon degeneration? One model was that Sarm1/dSarm utilizes NAD^+ as the coenzyme to promote poly-ADP ribosylation in the cells, which in turns activates death signaling for execution, potentially by allowing Axed to bind its targets. To test this hypothesis, we investigated global poly-ADP ribosylation changes in salivary glands with dSarm^{GOF} overexpression, in a collaborated with Justina Sileikyte in Michael Cohen's lab. However, we failed to find any increase of poly-ADP ribosylation in the dSarm^{GOF} glands (data not shown), suggesting that NAD^+ is likely not used for such modification in these cells. However, we cannot exclude the possibility that the biochemistry of dSarm function in salivary glands is different from that in neurons. It would be useful to identify dSarm/Sarm1 binding partners, for instance using proximity labeling technology to identify the proteins surrounding dSarm^{GOF} by tagging dSarm^{GOF} with ascorbic acid peroxidase

(APEX). This approach leads to the covalent biotinylation of proteins in a radius of 20nm of the tagged molecule (Trinkle-Mulcahy, 2019). These experiments are underway and will hopefully identify substrates, adaptor proteins, or other enzymes required for dSarm/Sarm1 axon death signaling.

Discussion 5.7 – Potential role of Axed – ubiquitination?

The functional role of Axed on axon degeneration is still a mystery. Axed is a BTB/BACK domain containing protein, and this family often serves as adaptor proteins for dimerization and recruitment of E3 ubiquitin ligases (Canning et al., 2013; Zhuang et al., 2009). Previous work in our lab by Tom Burdett failed to find evidence supporting a role for the cullin family proteins, RING box regulators of cullins, E1, ubiquitin conjugating E2, or E3 ligases in axon degeneration. However, Burdett found the overexpression of the yeast de-ubiquitinating enzyme UBP2 did lead to suppression of axon death up to 7 days post axotomy. Therefore, we still cannot exclude a putative ubiquitination role for Axed or dSarm in axon death. In HEK293T cell and salivary gland studies, I found the increased levels of the ubiquitin adaptor p62/Ref(2)P upon $Sarm1^{GOF}$/$dSarm^{GOF}$ expression. This was an early event that occurred within few hours after

Sarm1^{GOF}/dSarm^{GOF} induction. Although I did not see the axon protection when removing Ref(2)P in the fly olfactory neurons or glutamatergic neurons. We also found in the dSarm^{GOF} salivary glands, knockdown Ref(2)P with RNAi preserves the normal actin structure, arguing that Ref(2)P can augment dSarm signaling. In addition, we also found Ref(2)P, ubiquitin, dSarm^{GOF} and Axed colocalized together in the glands. These results support the idea that dSarm and Axed connect functionally with the UPS or ubiquitin in important ways. Ubiquitination serves not only as the signal for protein degradation, but also for cellular signaling. It is possible that Axed functions as a scaffold protein to recruit ubiquitinated proteins, or Axed possesses enzymatic activity for ubiquitination, and drives axon death signaling, or even that Axed is recruited to ubiquitinated proteins. These are all questions for the future, and it will be important to understand the role of NADase activity of Sarm1/dSarm on recruiting p62/Ref(2)P or ubiquitinated proteins.

Discussion 5.8 – Concluding remarks and future perspectives.

The cellular and molecular basis of neural circuit dysfunction after neural injury or in neurodegenerative disease remains poorly defined. The

loss of physical connections between neurons, through synapse or axon degeneration, is thought to be a major contributor. Here we show that relatively small injuries can lead to the rapid and efficient spreading of signals across nerves that potently suppress axon transport throughout the nerve, and even inhibit functions of uninjured bystander neurons. Surprisingly, we found the same molecule required to drive explosive axon degeneration in severed axons at later stages, dSarm/Sarm1, is required for this early suppression of neuronal function, although the signaling pathways dSarm couples with at each stage appear to be different. This significantly expands the role for dSarm/Sarm1 in regulating nervous system responses to injury to even uninjured bystander neurons. Furthermore, we discovered a critical role for glial cells, through Draper, JNK, and MMP-1, in signaling to bystander neurons to inhibit their axon transport and neurophysiology. Together this work suggests that a significant amount of functional loss after neural trauma does not involve frank degeneration, but more subtle changes in neuronal function, and it occurs in uninjured neurons through glial spreading of injury signals.

How bystander neurons receive injury signals and respond has remained unclear, although injury or disease-induced effects on bystander neurons is well- documented (Ising and Heneka, 2018). In most cases this

has been explored in the context of bystander neuron cell death driven by neuroinflammatory cells. For instance, releasing of C1q, IL-1α, TNF from microglia following brain injury drive the formation of neurotoxic astrocytes which can promote the death of neurons through release of unknown toxins (Liddelow et al., 2017). Bystander neuronal cell death is also driven by brain-infiltrating inflammatory monocytes in viral encephalitis, in a way that is mediated by calpains (Howe et al., 2016), which are also important regulators of axon degeneration. Secondary axon degeneration (i.e. that occurring in neurons not damaged by the initial injury) can be driven in a way that requires intracellular Ca^{2+} release through IP_3Rs and ryanodine receptors (Orem et al., 2017). These represent extreme cases of bystander effects, where cells undergo apoptosis or their axons degeneration. Whether dSarm/Sarm1 is involved in these effects is an interesting question.

However, our results are likely most relevant to partial nerve injury, where non-autonomous changes in bystander neurons are observed (Figure 1). Whether bystander neurons in partially ligated nerves are unaffected in $Sarm1^{-/-}$ mice is an important next question. Uninjured bystander neurons in mild TBI models are certainly altered physiologically, in a reversible way, but the molecular basis of these events remain unexplored (Greer et al., 2012). It is interesting to note that in contrast to control mice, which show

significant behavioral defects for hours after mild TBI, Sarm1$^{-/-}$ animals almost immediately recover (Henninger et al., 2016), at a time point long before axon degeneration is observed. Our study places dSarm/Sarm1 at the heart of neuronal injury signaling throughout neural tissues, identifies new signaling partners for dSarm in uninjured neurons, and expands its role to regulating the responses of uninjured neurons to local tissue injury.

APPENDIX I: Forward EMS mutagenesis to identify suppressors of dNmnat RNAi-induced axon degeneration.

Appendix I: Results

Nmnat2 depletion is a key event associated with axon degeneration after axotomy in mammals (Gilley and Coleman, 2010), and Nmnat2 loss activates Sarm1-dependent axon death through unknown mechanisms. Likewise, in *Drosophila*, knockdown of dNmnat with RNAi resulted in axon degeneration in animals within days after eclosion, which was suppressed by loss of dSarm and Axed (Gilley et al., 2015; Neukomm et al., 2017). These data indicate that loss of Nmnat activity is a conserved mechanism for activation of induce Sarm-dependent axon degeneration, but how dNmnat loss activates Sarm remains unclear. To identify molecules required for dSarm activation after Nmnat loss, we designed a mutagenesis screening to find the suppressors of dNmnat RNAi induced axon degeneration. dNmnat RNAi and GFP were expressed under UAS-control sparsely in the *Drosophila* glutamatergic neurons (OK371-Gal4) in the wing using MARCM clonal technology (Neukomm et al., 2014). In my screen I used used FRT2A on the left arm of chromosome 3 (3L chr), and drove mitotic recombination early in SOP lineages with *asense-Flippase* (*ase-FLP*) to generate clones. We found consistent with our previous work, that an average of ~6 neuron clones per wing were obtained (Neukomm et al., 2014), and dNmnat RNAi expression resulted in ~90% of neurons

undergoing cell death and axon degeneration within 10 days post eclosion (10 dpe) (Appendix figure 1.1). For the most part, dead neurons and degenerated axons were cleared by 10 days (Appendix figure 1.1).

I performed a pilot screen to find possible suppressor hits that protect neurons from this dNmnat knockdown induced neuronal death. I screened ~800 mutant chromosomes on 3L and got one suppressor hit (3L184), in which up to 80% of the neuronal clones survived and maintained their axons (Appendix figure 1.2). 3L184 was recovered by balancing, it was retested to confirm the phenotype, and the genome was extracted for deep sequencing analysis. The results showed that there are potentially function altering mutations in 5 genes on 3L including: *dpr6*, *wnk*, *CG4098*, *CG45067*, and *CG44362* (Appendix table 1.1). To determine which of these 5 mutations was the causative mutation that protects the neurons from dNmnat loss, I performed bacterial artificial chromosome (BAC) rescue mapping with BACs containing each of the candidate genes. I found the BAC CH321-79A19, which includes the wild-type *CG4098* gene, could rescue the dNmnat knockdown-induced neuronal death phenotype when crossed into the 3L184 mutant background. This argues that the mutation in *CG4098* is the causative loss-of-function mutation suppresses neuronal death (Appendix figure 1.2A). *CG4098* encodes the *Drosophila* homolog of mammalian

Nudix hydrolase 9 (Nudt9). Nudt9 has ADP-ribose (ADPR) dehydrogenase activity (also called ADPR pyrophosphatase), which removes the ribose-5-phosphate from ADPR and produce AMP (McLennan, 2006). In 3L184, there is a 56 base pair deletion on the first exon of *CG4098*, resulting in frame shift and formation of premature stop codon (Appendix figure 1.3). To further confirm the role of *CG4098*, I cloned the wild-type *CG4098* cDNA (*CG4098-RA*) and ectopically expressed it into 3L184 flies with *OK371-Gal4*. The results were imaged and analyzed by the rotation student Ryan Doan, and he found that similar to BAC expression, the wild-type *CG4098* cDNA could also rescue the neuronal death phenotype (Appendix figure 1.4), suggesting that *CG4098* plays an important role on dNmnat RNAi induced neuronal death.

In the current Wallerian degeneration model, Nmnat2/dNmnat knockdown can activate Sarm1/dSarm dependent axon degeneration (Gerdts et al., 2016; Gilley et al., 2015). To understand whether *CG4098* also plays a role in this signaling pathway, I investigated $dSarm^{GOF}$-induced axon death in the wild-type and 3L184 mutant animals. However, I found same as in the wild-type animals, the 3L184 animals also showed 100% of neuronal death at 10 days post eclosion (Appendix figure 1.5B). This result suggests that CG4098 does not play a role in the *dnmnat* RNAi/dSarm dependent axon

degeneration signaling, or that CG4098 functions upstream of dSarm. To further distinguish these possibilities, I axotomized the wings of wild-type and 3L184 animals. I found that 3L184 failed to suppress axon degeneration after axotomy (Appendix figure 1.5A, C). The simplest interpretation of these data is that *CG4098* does not function in the axon death signaling, on degeneration after dNmant loss, or it acts on a parallel pathway downstream of *dnmnat* knockdown that is independent of dSarm, although additional interpretations exist.

Appendix I: Material and Methods

EMS mutagenesis

Male flies were starved for 12 hours, which was followed by the incubation with 25mM ethyl methanesulphonate (EMS) in 1% sucrose for another 12 hours. The EMS solution is dropped on kimwipes for animal consumption. Before breeding, the animals were recovered in fresh vials for at least 8 hours.

Wing imaging

See Material & Method of Chapter 2

CG4098 cDNA cloning

The cDNA of *CG4098* was cloned from cDNA clones SD14666 by PCR which was obtained from the *Drosophila* Genomics Research Center (DRGC). *The attB-pUAST* vector was linearized with *XhoI* and *XbaI*, and the PCR product of *CG4098* cDNA was inserted into the vector after *XhoI* and *XbaI* digestion. The *attB-pUAST-CG4098* were injected (Bestgene). The primers used are listed in Key Resource Table.

Appendix I: Figures

Appendix figure 1.1: F_1 mutagenesis screen for suppressors of dNmnat RNAi induced neuronal death in the Drosophila wing.

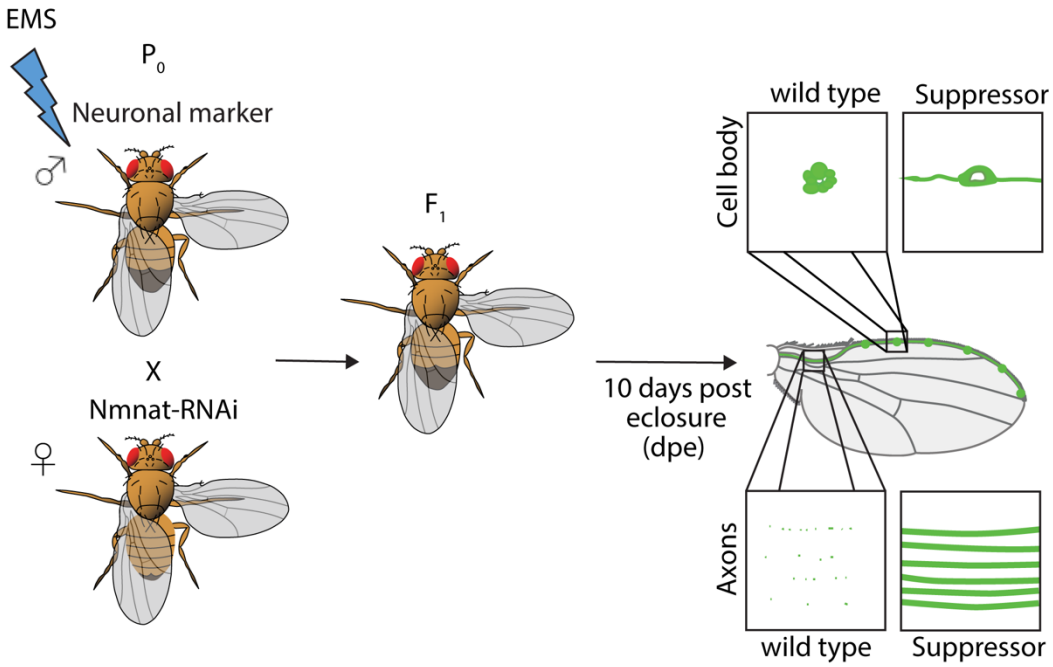

Appendix figure 1.1:

P_0 males with the neuronal marker (*ok371-Gal4, UAS-mCD8-GFP*) were fed EMS, and crossed to females carrying *UAS-dNmnat RNAi*. Both males and females carried genetic elements for MARCM. One wing of F_1 progeny was dissected for imaging on 10 days post animal eclosure; the labeled neurons should contain random EMS-induced homozygous mutations and express dNmnat RNAi. Wild type neurons degenerated and cell corpse lingered in the wing vein, in suppressor animals cell bodies and axons were retained.

Appendix table 1.1: Whole genome sequencing results showed 5 severe mutants on the 3rd left arm chromosome of 3L184 allele.

gene_name	**consequences**	**Human Ortholog**
CG45067	start_lost	Prominin
dpr6	stop_gained	LSAMP/CADM
CG44362	frameshift_variant	No ortholog
CG4098	frameshift_variant	NUDT9/TRPM2
Wnk	frameshift_variant	WNK

Appendix figure 2: 3L184 is a suppressor that protected neurons from dNmnat RNAi induced neuronal death.

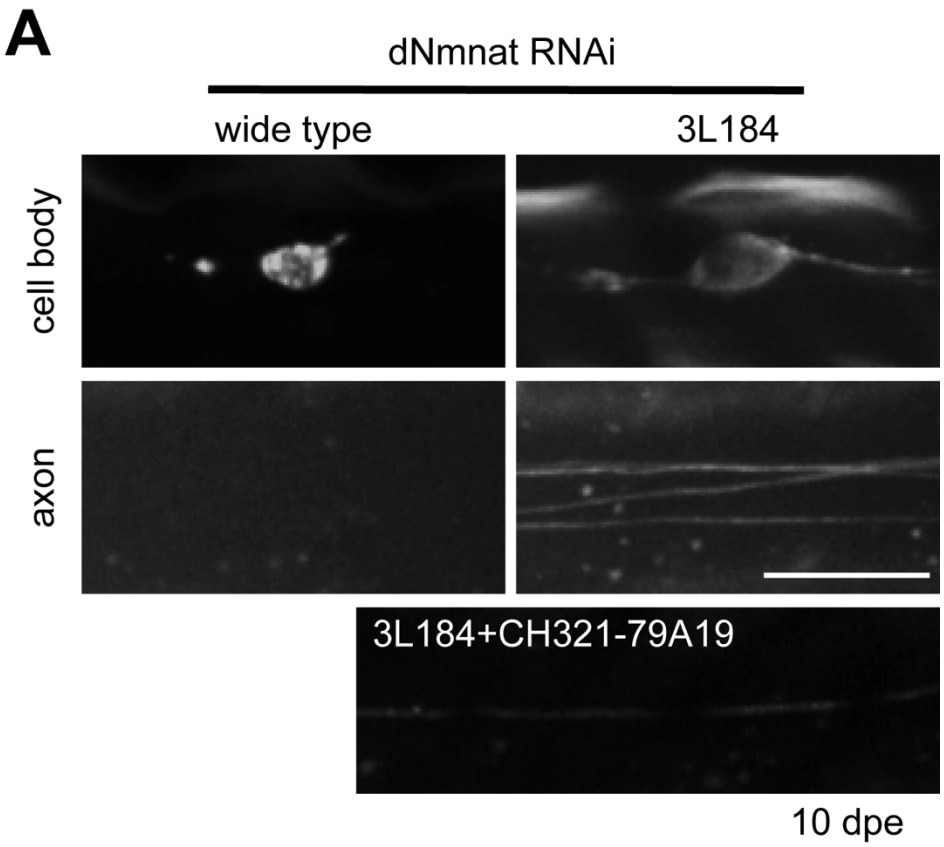

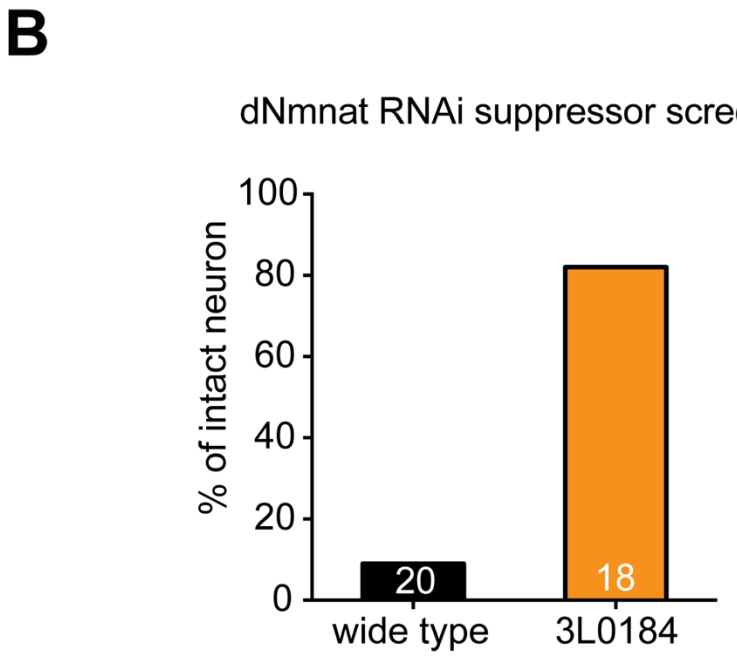

Appendix figure 1.2:

(A) dNmnat RNAi induced neuronal death on 10 days post eclosion (10 dpe) in wild type clone where the cell corpse is present in the wing. Neurons persisted in 3L184 mutant. Addition of BAC CH321-79A19, which covers CG4098 locus, reconstitutes the pro-degenerative activity of dNmnat loss. (B) Quantification of neuronal survival in wild type and 3L184 with dNmnat RNAi.

Appendix figure 1.3: 3L184 is an allele of Drosophila gene CG4098.

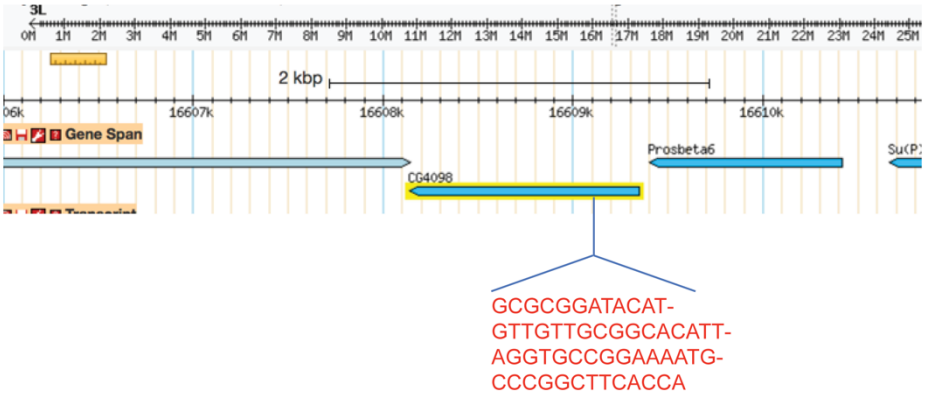

Appendix figure 1.3:

The indicated sequences in the *CG4098* gene were deleted in 3L184 allele.

Appendix figure 1.4: CG4098 cDNA overexpression rescued dNmnat RNAi induced neuronal death.

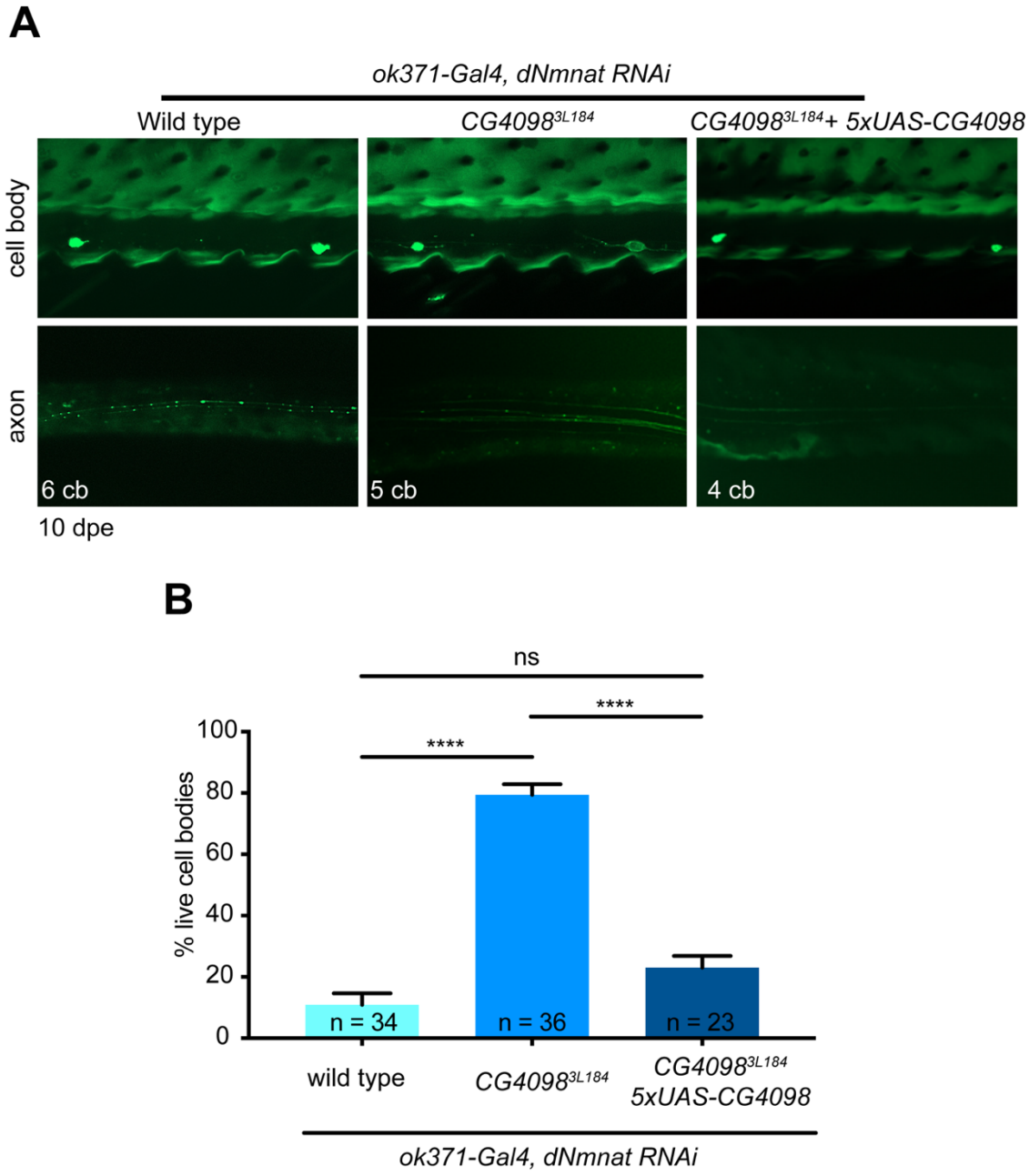

Appendix figure 1.4:

(A) Representative images show neuronal death in wild type animals with dNmnat RNAi, while the neurons persist in *CG4098*^{3L184} mutants. Overexpression of *5xUAS-CG4098* rescued the neuronal death phenotype. (CB, cell body; dpe, days post eclosion).

(B) Quantitative results of neuronal survival (represented with living cell bodies) in the animals with indicated genotypes on 10 dpe. Ordinary one-way ANOVA with Dunnett multiple comparisons test. (ns = not significant, ****$p < 0.0001$, n number is indicated on the graph, Error bar = SEM).

Appendix figure 1.5: CG4098^{3L184} did not protect neurons from axotomy or dSarm^{GOF} overexpression.

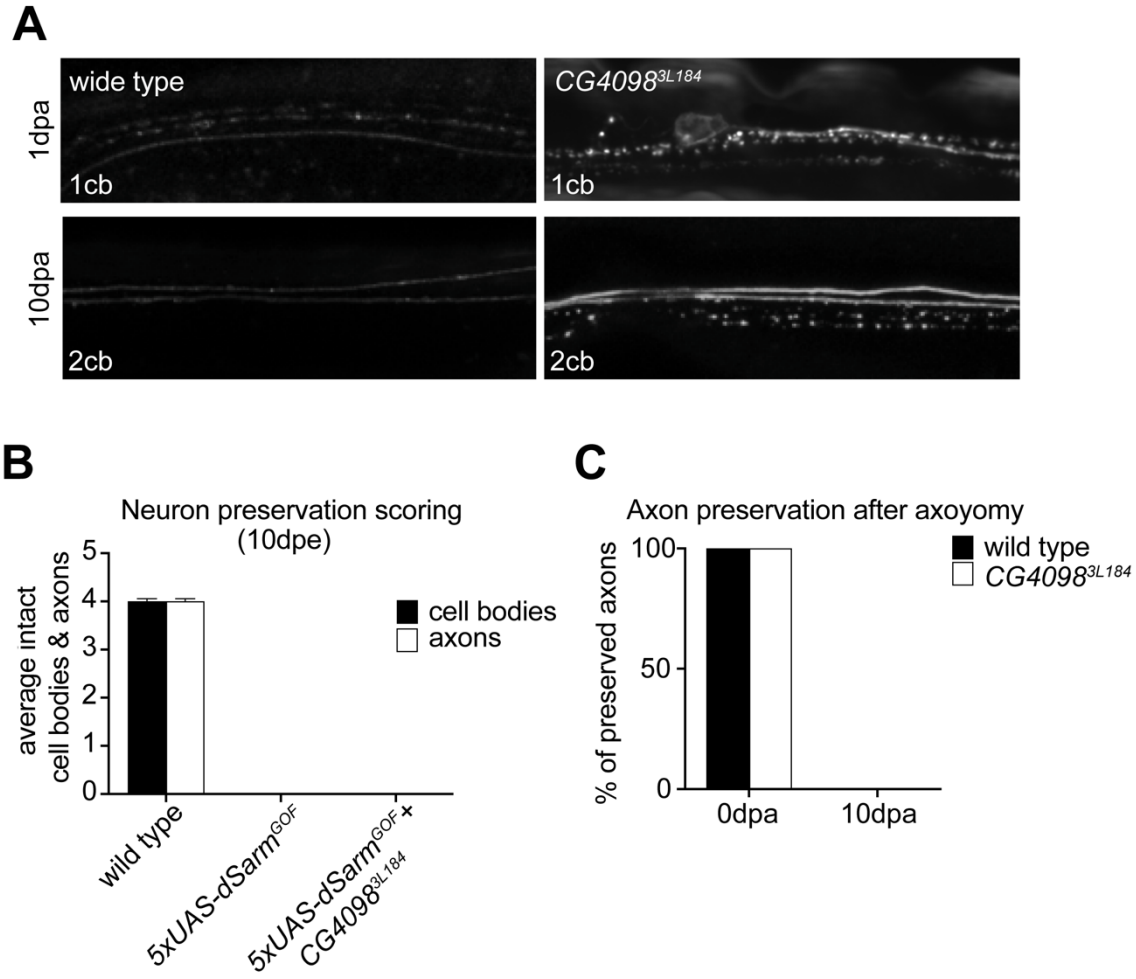

Appendix figure 1.5:

(A) Representative images of axon degeneration at 10 days post axotomy. (cb, cell body; dpa, days post axotomy).

(B) Quantification of neuron preservation when overexpressing $dSarm^{GOF}$. The average number of intact cell bodies or axons were counted in each wing vein. 25 animals were scored. (dpe, days post eclosion).

(C) Quantification of axon preservation after axotomy. The percentage of preserved axons were count on each wing. 25 animals were scored.

APPENDIX II: Understanding the role of Gain-of-Function Sarm1/dSarm in non-neuronal cells.

Appendix II: Results

We found that deletion of the auto-inhibitory ARM domain of dSarm (termed gain-of-function dSarm, dSarm^{GOF}) can actively trigger cell body and axon degeneration in *Drosophila* sensory neurons in the wings, as well as other neurons, with or without the presence of wild-type dSarm. To gain insight into the mechanism of Sarm1^{GOF} activity, we also investigated the functional conservation of mammalian Sarm1 by expressing Sarm1^{GOF} construct under the control of Tetracyclin inducible Expression System (Tet-on 3G) in cultured human embryonic kidney 293T (HEK293T) cells. With the Tet-on 3G inducible system, the expression of Sarm1^{GOF} can be activated by introducing doxycycline (Appendix figure 2.1). We found that significant cell death in HEK293T cells after inducing the expression of Sarm1^{GOF} for 24 hours (Appendix figure 2.2A), and that cell death could be partially suppressed with Wld^{s} overexpression (Appendix figure 2.2B). Sarm1^{GOF} induced cell death was not blocked by the apoptotic cell death caspase 3 inhibitor, z-VAD-fmk, necroptosis inhibitor, Necrostatin-1, or the combined treatment of z-VAD-fmk and Necrostatin-1 (Appendix figure 2.3). These data suggesting that Sarm1^{GOF} induced cell death is not a type of apoptosis or necroptosis, which is somewhat consistent with data from a previous study (Gerdts et al., 2013).

The mechanism through which Sarm1 executes axon destruction remains unclear. As discussed above, one proposed mechanism is that axotomy promotes Sarm1 to activate axon destruction by depleting NAD^+ (Gerdts et al., 2015). Exogenous application of NAD^+ showed axon protection in cultured mouse DRG axons after transection (Araki et al., 2004). However, the importance of NAD^+ in the context of axon degeneration is still not fully resolved.

I found that induction of $Sarm1^{GOF}$ expression in HEK293T cells for 4 hours significantly decreased the amount of NAD^+, and that this was immediately followed by the onset of cell death (Appendix figure 2.4). Suppressing NAD^+ consumption by treatment with the Tankyrase and PARP1 inhibitor, XAV939, (Thorsell et al., 2017) significantly increased NAD^+ levels even in the presence of $Sarm1^{GOF}$, however it did not suppress the cell death (Appendix figure 2.5). In previous work, increasing cellular NAD^+ levels in cultured mouse dorsal root ganglion neurons by knocking out CD38 and Poly [ADP-ribose] polymerase 1 (PARP1), the two major NAD^+ consuming enzymes, also did not protect severed axons against destruction (Sasaki et al., 2009). Although local administration of Nmnat1 by lentivirus inhibited axon degeneration (Sasaki and Milbrandt, 2010), the overall cellular NAD^+ level did not increase (Sasaki et al., 2009). Together

these results appear to uncouple a strict correlation of NAD^+ levels with cell survival and maintenance of axon integrity. Is seems plausible that additional signaling mechanisms downstream of Sarm1, separate from NAD^+ depletion, help promote axon degeneration after axotomy.

NMNAT also acts as a molecular chaperone, independent of its NAD^+ biosynthetic activity, to control the protein quality by refolding the misfolded proteins (Zhai et al., 2008) and maintaining proteostasis. To test the possibility that Sarm1 activation increases endogenous protein aggregation, we examined the localization of endogenous p62/SQSTM1 in HEK293T cells. p62/SQSTM1, an adaptor for the selective recognition of autophagic targets, binds to ubiquitin tagged proteins and promotes their clearance by the ubiquitin-proteasome system or autophagy. Accumulation of p62 positive protein inclusions was previously reported in autophagy loss-of-function mutants, indicating that p62 can be used a biomarker of endogenous protein aggregation (Komatsu et al., 2007). I found that inducing the expression of $Sarm1^{GOF}$ significantly increases the p62 positive puncta 1 hour after $Sarm1^{GOF}$ expression (Appendix figure 2.6), which is earlier than the cell death (4- to 5- hour post induction) and precedes NAD^+ depletion, indicating that increases of cellular protein aggregates may be another early event downstream of Sarm1 activation. While the

accumulation of p62 is often associated with perturbation of proteasome activity, we did not observe changes of proteasome activity, nor the large molecular weight protein aggregates in response to Sarm1^{GOF} expression (data not shown). How p62 accumulation integrates in Sarm1^{GOF} signaling therefore remains unclear.

Given Sarm1^{GOF} induction induces explosive neuronal death and HEK293T cell death, which obscures us from deep analyses of signaling events in these contexts, additional model systems to explore Sarm^{GOF} signaling are required. Interestingly, when overexpressing dSarm^{GOF} in *Drosophila* salivary glands, we found the gland cells exhibited dramatic alterations in their actin cytoskeletal structure (Appendix figure 2.7A). The transgene expression came on at early 3rd instar larval stage when under the control of *sgs3-Gal4*. We noticed that the glands developed abnormal actin structures as early as in the wandering 3rd instar larval stage (wL3, the stage about 6 hours later of early 3rd larval stage), which worsened by head eversion stage (HE, or ~12APF) (Appendix figure 2.7A). Overall salivary gland structure was grossly preserved (Appendix figure 2.7B), although the size of glands with dSarm^{GOF} are smaller at wandering L3 stage when compared to wild type. Importantly, we found that despite the fact that these glands survived, NAD^+ levels are fully depleted in the presence of

dSarm^{GOF}. This indicates that dSarm^{GOF} is capable of driving down NAD^+ to undetectable levels in salivary glands without inducing cell destruction (Appendix figure 2.8). These features make the salivary glands a useful system to study dSarm^{GOF} biochemistry and signaling *in vivo*.

We investigated the localization of dSarm and dSarm^{GOF} in salivary gland cells. The expression of GFP-tagged dSarm (*UAS-dSarm-GFP*) driven by salivary gland specific Gal4 (*sgs3-Gal4*) shows that while dSarm-GFP is diffusely localized, dSarm^{GOF} (*UAS- dSarm^{GOF}-GFP*) exhibits a more punctate localization in the cytosol of gland cells (Appendix figure 2.9). To understand cell biological changes in the glands with dSarm^{GOF}, we also stained the p62 homolog, Ref(2)P, found dSarm^{GOF} expression induces an increase of Ref(2)P puncta, and western blots revealed that total Ref(2)P protein levels increased in dSarm^{GOF} backgrounds compared to wild-type glands (Appendix figure 2.10). Similar to the changes in actin structure, Ref(2)P increase also started from wL3 stage, and became more apparent at HE. Ref(2)P, is an adaptor protein associates with ubiquitinated proteins. Consistent with a UPS-associated role, we also found increased levels of ubiquitinated proteins with staining in salivary glands by staining with anti-ubiquitin antibodies (data not shown). These data argue that in salivary glands, as in HEK293T cells, dSarm^{GOF} promotes ubiquitination.

BTB/BACK domain proteins like Axed often associate with the Cullin E3 ubiquitin ligase complex, which is required for UPS dependent degradation (Stogios and Prive, 2004). However, our group failed to find data supporting a role of the Cullin E3 complex in axon degeneration (Neukomm et al., 2017). To begin to explore potential roles for increased ubiquitination in dSarm^{GOF} glands, I first examined the relative localizations of dSarm^{GOF}, Axed, and ubiquitinated proteins in salivary glands after dSarm activation. Interestingly, I found strong colocalization of dSarm^{GOF}-myc, Axed-GFP, and ubiquitin throughout glands (Appendix figure 2.11). These data highlight a potentially interesting role for dSarm in directing ubiquitination, directly or indirectly, in salivary glands, and raise the possibility that Axed may function with dSarm to promote dSarm-mediated ubiquitination. Whether this is also required for axon death signaling remains an open question.

Appendix II: Material and Method

HEK293T cell culture

HEK293T cells were cultured in DMEM with 10% FBS and 1% penicillin/streptomycin solution. Cells were maintained in a standard humidified tissue culture incubator in 37˚C with 5% CO_2.

cDNA, lentiviral vector construction and packaging

The Tet-on 3G plasmid with full-length Sarm1 or Sarm1^{GOF} fragments were constructed by previous postdoc Jack Wong. Lentiviruses were packaged in HEK cells as described previously (Kutner et al., 2009).

Lentiviral transduction and stable cell line generation

1 million HEK293T cells were plated in 6-well cell culture plate and cultured for 24 hours, followed by the addition of 1ml of lentiviral supernatant. 24 hours after virus addition, media were removed and replaced with fresh culture media with blasticidin. After 48 hours the remaining cells were sub-cultured with fresh media with antibiotics and used for experiments.

Transient Transfection

HEK293T cells were cultured in either 10-cm dishes or 6-well cell culture plate, with 80% confluency. Transient transfection was done by TransIT-293. The plasmids used for transfection are listed in Key Resource Table.

Cell survival assay

1 million HEK293T cells were plated in 6-well cell culture plate for 24 hours. Chemicals including z-VAD-fmk, Necrostatin-1, XAV939, and Tiq-A were individually dissolved in DMSO. The concentrations are indicated in figures. Chemicals were applied at time points indicated in figures, and the cells were harvested together at the terminal time point. For the survival assay, media were removed after incubation with indicated compounds, and cells were washed with 1X PBS. The CellTiter-Glo luminescent cell viability assay (Promega #G7570) was used for cell viability measurements. The luminescence was measured in SpectraMax-M2 microplate reader.

NAD^+ extraction and HPLC metabolite measurment

Culture conditions and compound exposures were performed as described in the cell survival assays. Cells were harvested after treatment,

and rinsed with 1X PBS. The salivary gland tissues were dissected and collected in PBST on ice. NAD^+ metabolites were extracted with a 1M solution of perchloric acid ($HClO_4$), and tubes were placed on ice for 10 minutes, followed by neutralization with 3M K_2CO_3, and incubation on ice for another 10 minutes (Yoshino and Imai, 2013). The mixture was centrifuged and the supernatant was collected for HPLC metabolite measurements. HPLC measurement protocols followed a previous study from the Goodman group (Cambronne et al., 2016).

Immunostaining of HEK293T cells and salivary glands

For salivary glands, the glands were dissected in cold PBST, and fixed in 4% formaldehyde for 20 minutes. Fixed glands were washed with PBST for 15 minutes, and blocked in 5% BSA for 1 hour. After blocking, the glands were washed again with PBST for 1 hour, followed by primary antibodies overnight incubation at 4 ˚C. And then glands were incubated with secondary antibodies overnight at 4 ˚C after 1 hour of PBST wash. The antibodies used are listed in Key Resource Table. Glands were mounted on slides with a drop of Vectashield antifade mounting medium (Vector laboratories #H-1000-10) for imaging.

For HEK293T cells, the 60% confluent cells were plated on chamber slides. After chemical treatment, the cells were washed with 1xPBS, and fixed with 4% paraformaldehyde for 10 minutes. The cells were then washed with PBST, and blocked with BSA for 1 hour. Primary antibodies were incubated for 1hour on ice followed by secondary antibodies incubation for another hour on ice. Cells were then washed and stained with DAPI in vectashield antifade mounting medium, and imaged.

p62 punctae quantification

The images of HEK293T cells with p62 staining were obtained by confocal microscopy with 63x magnification objectives. The number of p62 punctae were counted by ZEN software, and the average p62 punctae per cell (total number p62 punctae/total number of cells per image) in 5 images was calculated.

Appendix II: Figures

Appendix figure 2.1: Tet-on 3G system to control Sarm1^{GOF} expression.

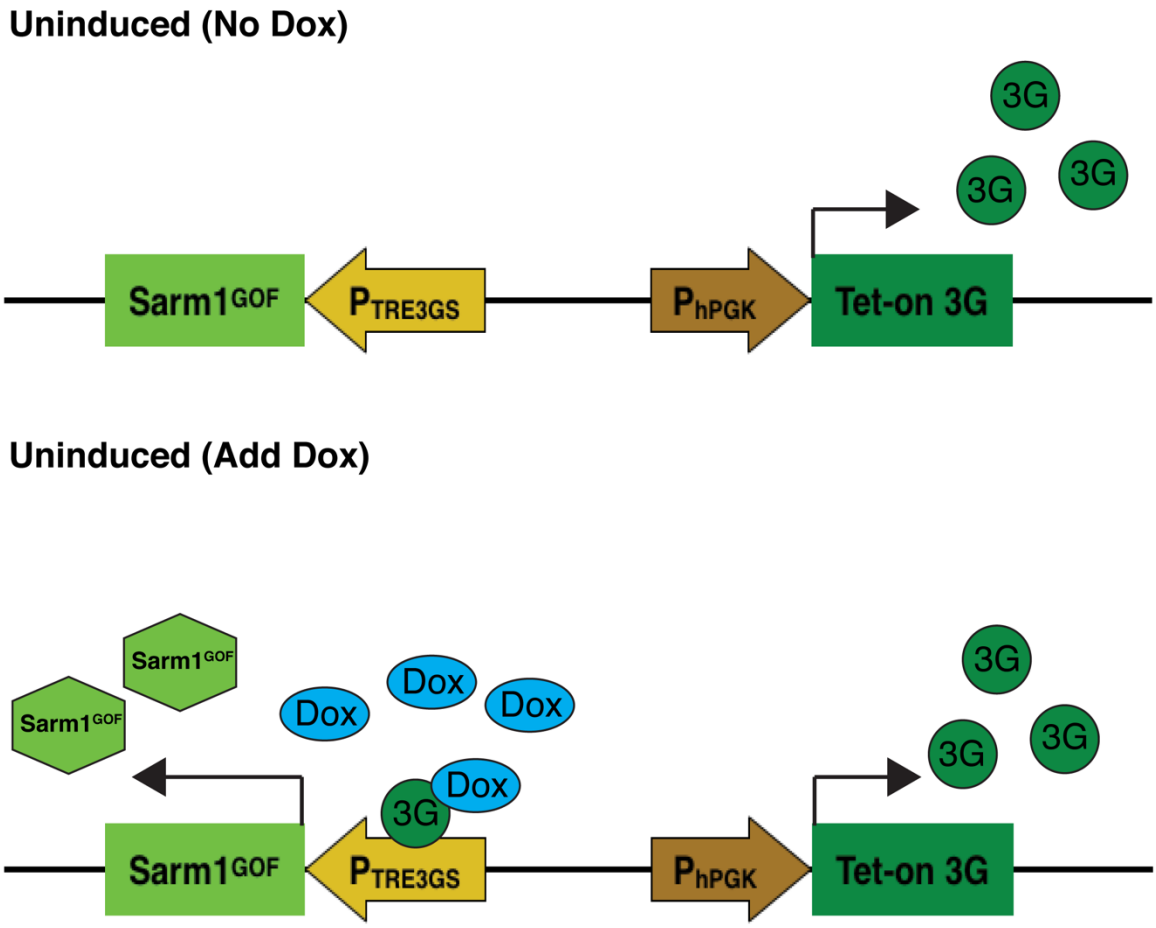

Appendix figure 2.1:

Schematic shows the Tet-on 3G system to control the expression of Sarm1^{GOF}. The 3G protein binds to TRE3GS promoter only in the presence of doxycycline (Dox).

Appendix figure 2.2: Sarm1^{GOF} expression killed HEK293T cells, which could be partially suppressed by Wld^{s}.

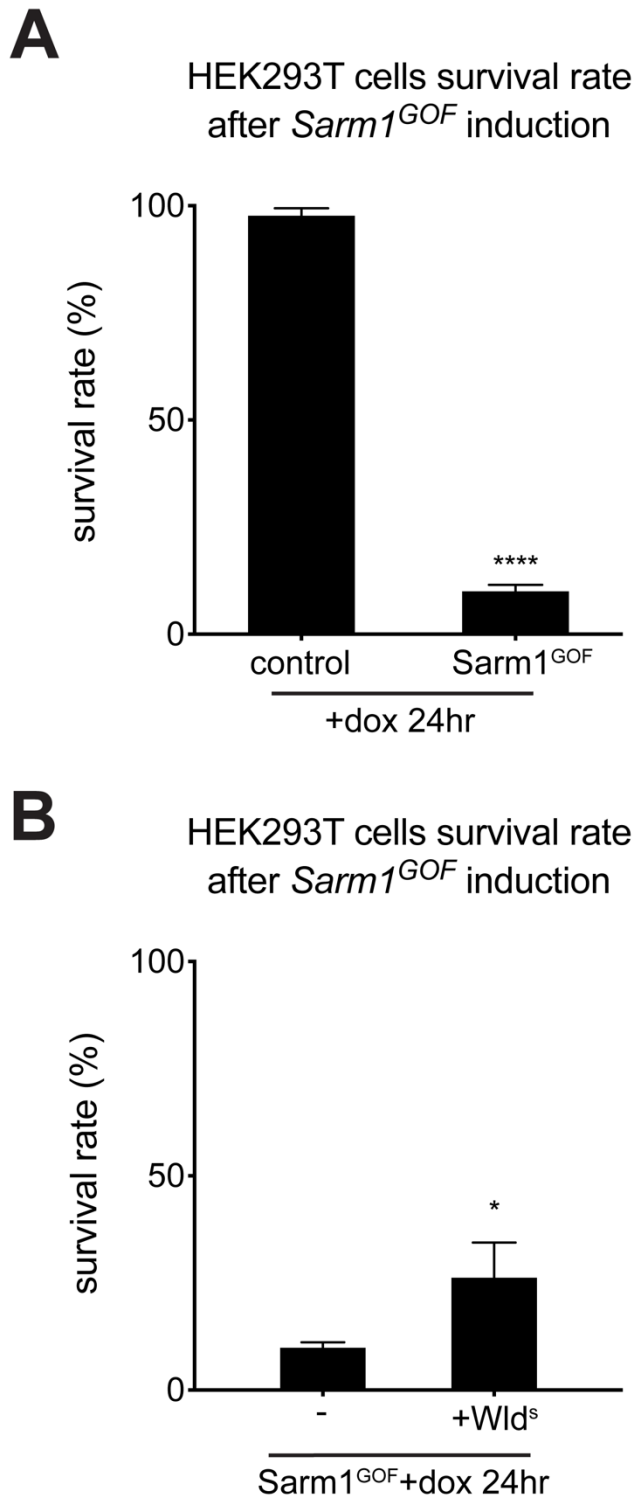

Appendix figure 2.2:

(A) The survival rate of HEK293T cells with or without Sarm1^{GOF} expression driven by doxycycline (dox) is measured by CellTitre-Glo cell survival assay. Percent survival is calculated as luminescence of -dox group/ luminescence of +dox group. Unpaired two-tailed t-test. (****$p < 0.0001$, n = 3 replicates, Error bar = SEM).

(B) The survival rate of Sarm1^{GOF} HEK293T cells with or without Wld^{s} expression. Unpaired two-tailed t-test. (*$p < 0.05$, n = 3 replicates, Error bar = SEM).

Appendix figure 2.3: Neither apoptosis nor necroptosis inhibitors suppressed Sarm1^{GOF} induced cell death in HEK293T cells.

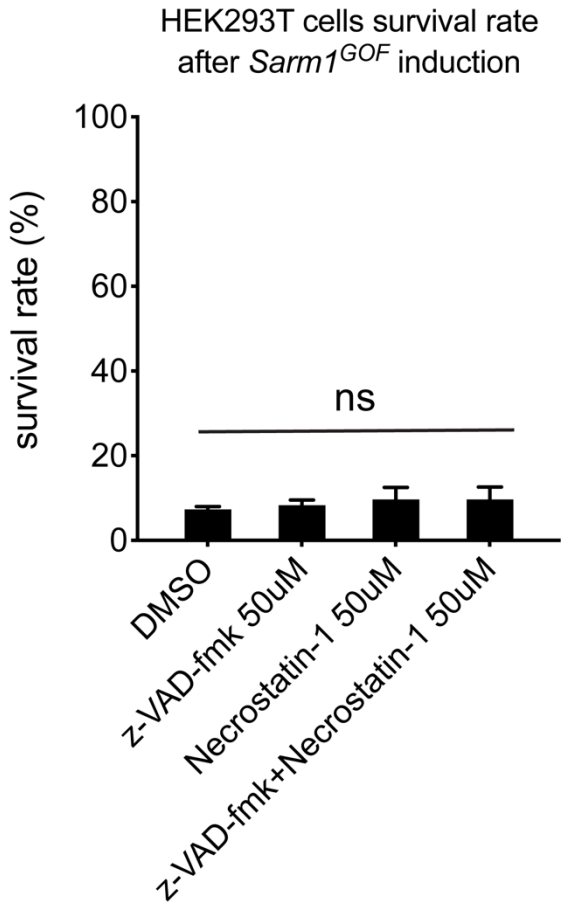

Appendix figure 2.3:

(A) The survival rate of Sarm1^{GOF} HEK293T cells with or without drug treatment is measured by CellTitre-Glo cell survival assay. Cells were treated with doxycycline for 24 hours to drive Sarm1^{GOF} expression before survival assays. Ordinary one-way ANOVA with Dunnett multiple comparisons test. (ns = not significant, n = 3 replicates, Error bar = SEM).

Appendix figure 2.4: Sarm1^{GOF} expression caused NAD$^+$ depletion prior to the initiation of cell death.

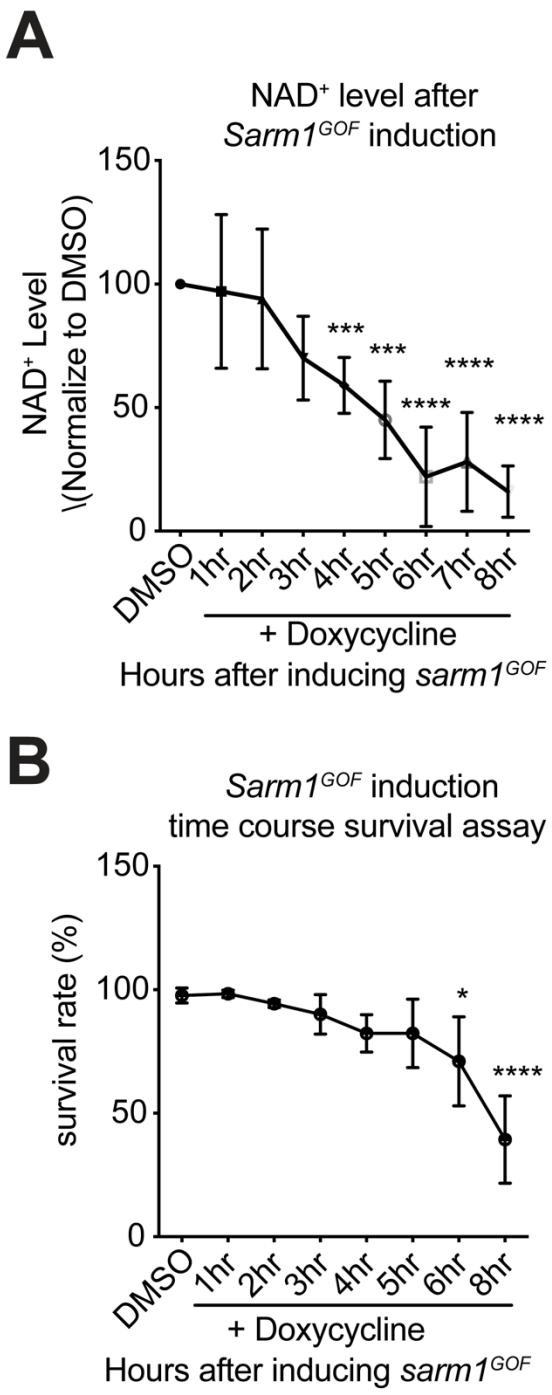

Appendix figure 2.4:

(A) The time course measurement of NAD^+ levels from HEK293T cells after $Sarm1^{GOF}$ expression. Ordinary one-way ANOVA with Dunnett multiple comparisons test. (ns = not significant, ***p < 0.001, ****p < 0.0001, n = 3 replicates, Error bar = SEM).

(B) Time course of survival in $Sarm1^{GOF}$ expressing HEK293T cells. Ordinary one-way ANOVA with Dunnett multiple comparisons test. (ns = not significant, *p < 0.05, ****p < 0.0001, n = 3 replicates, Error bar = SEM).

Appendix figure 2.5: The tankyrase inhibitor, XAV939, increased NAD^+ levesl, but failed to delay cell death of $Sarm1^{GOF}$ cells.

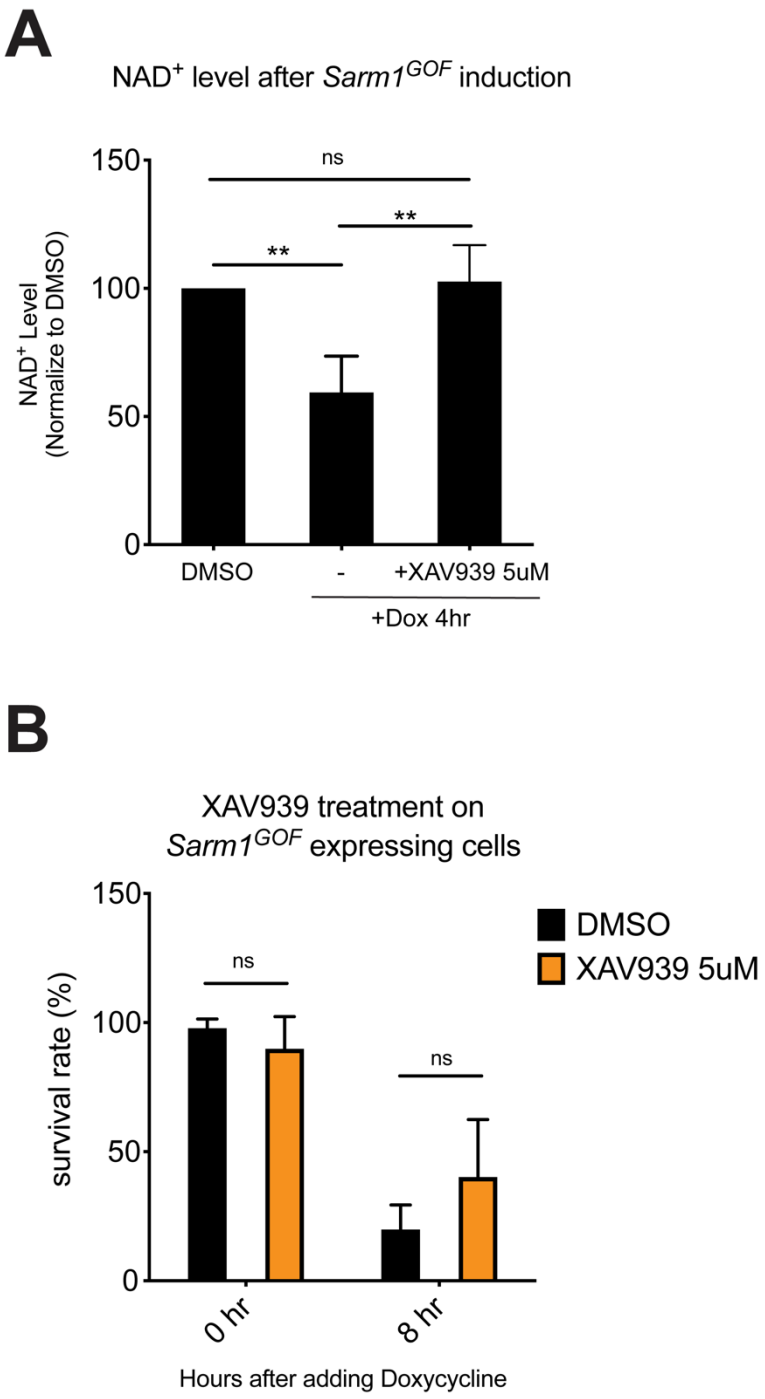

Appendix figure 2.5:

(A) The measurement of NAD^+ level from HEK293T cells after $Sarm1^{GOF}$ expression, with or without the addition of XAV939. Ordinary one-way ANOVA with Tukey's multiple comparisons test. (ns = not significant, *p < 0.05, **p < 0.01, n = 3 replicates, Error bar = SEM).

(B) Survival assay of $Sarm1^{GOF}$ expressing HEK293T cells with or without the addition of XAV939. Two-way ANOVA with Sidak's multiple comparisons test. (ns = not significant, n = 3 replicates, Error bar = SEM).

Appendix figure 2.6: Sarm1^{GOF} increased p62 puncta in HEK293T cells.

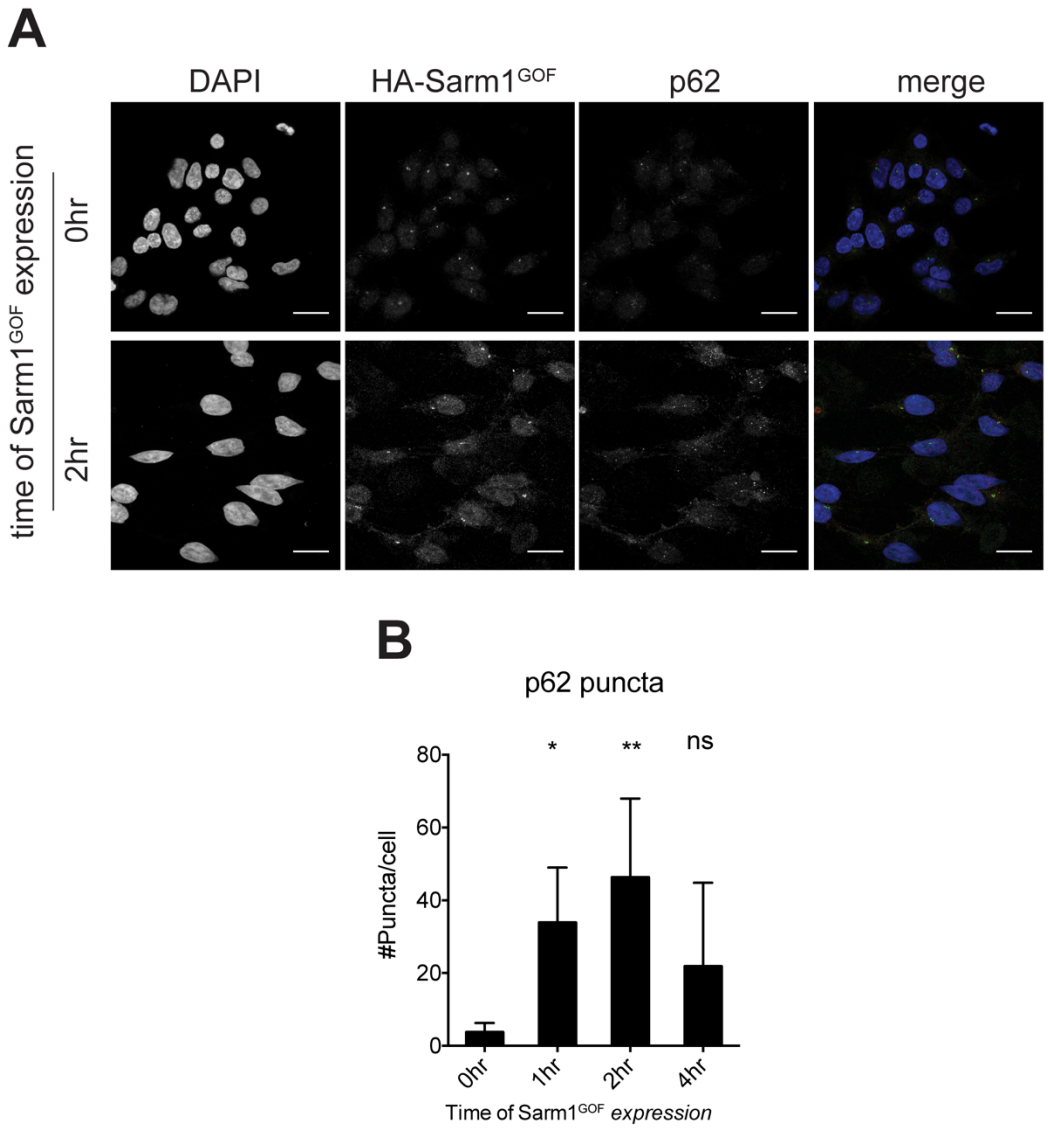

Appendix figure 2.6:

(A) 63x magnification of representative images of HEK293T cells with anti-p62 antibody and DAPI staining. Error bar = 10μm.

(B) Time course quantification of the number of p62 punctae after $Sarm1^{GOF}$ expression. The average p62 punctae number per cells (total number p62 punctae/total number of cells per image) of 5 images were calculated. Ordinary one-way ANOVA with Dunnett multiple comparisons test. (*$p < 0.05$, **$p < 0.01$, ns = not significant, n = 5 images, Error bar = SEM).

Appendix figure 2.7: dSarm^{GOF} induced abnormal actin cytoskeleton structure in Drosophila salivary glands, but tissue structure was preserved.

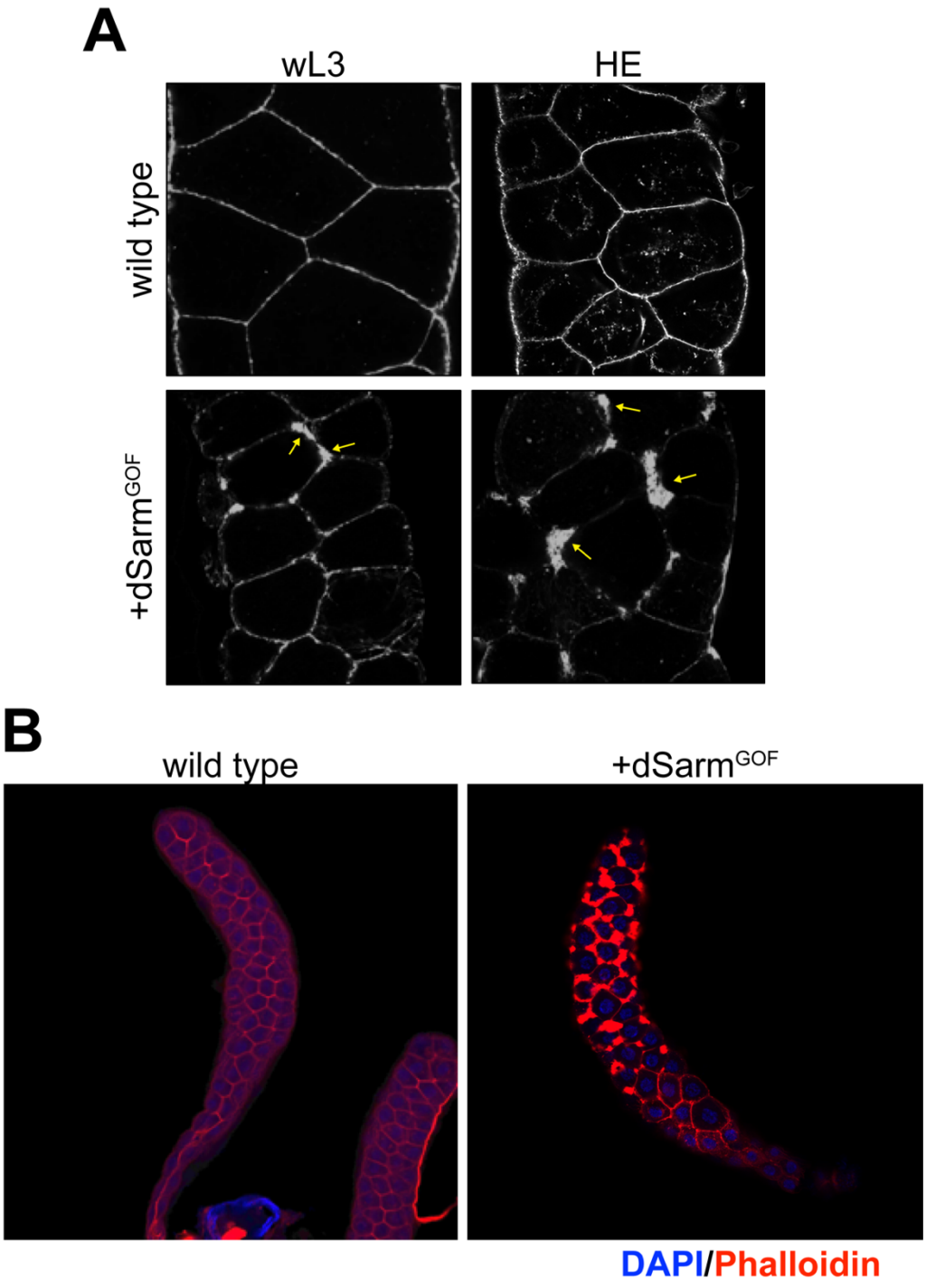

Appendix figure 2.7:

(A) 63x magnification of representative images of salivary glands with phalloidin staining to show abnormal actin cytoskeleton structure. wL3: wandering 3rd instar larval stage; HE: head eversion stage. $dSarm^{GOF}$ expression is driven by *Sgs3-Gal4*, the salivary gland specific driver. Animals with *Sgs-Gal4* alone serves as the wild-type control. The abnormal actin structure is indicated by yellow arrows.

(B) 10x magnification of representative images of salivary glands with phalloidin (red) and DAPI (blue) staining to show abnormal actin cytoskeleton structure at HE. $dSarm^{GOF}$ expression is driven by *sgs3-Gal4*, the salivary gland specific driver. Animals with *sgs-Gal4* alone serve as the wild-type control. Both genotypes of animals showed similar size of salivary glands.

Appendix figure 2.8: dSarm^{GOF} reduced NAD^{+} level in Drosophila salivary glands.

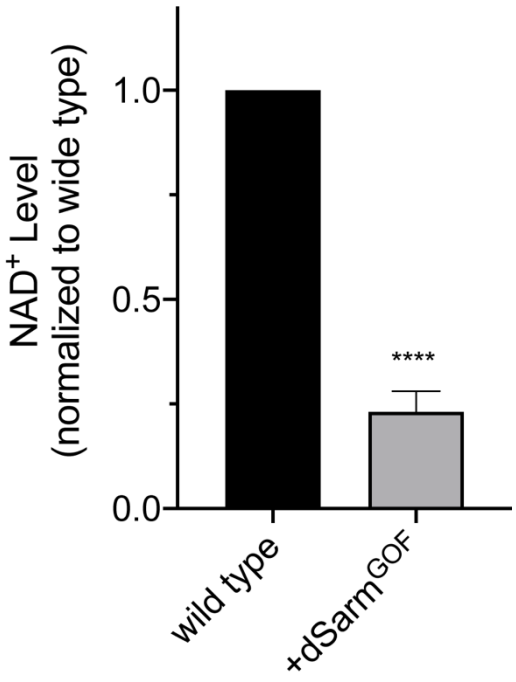

Appendix figure 2.8:

The measurement of NAD^{+} level from wL3 salivary glands with or without dSarm^{GOF} expression. Unpaired two-tailed t-test. (****$p < 0.0001$, n = 3 replicates, Error bar = SEM).

Appendix figure 2.9: dSarm^{GOF} and dSarm exhibited distinct localizations in salivary glands.

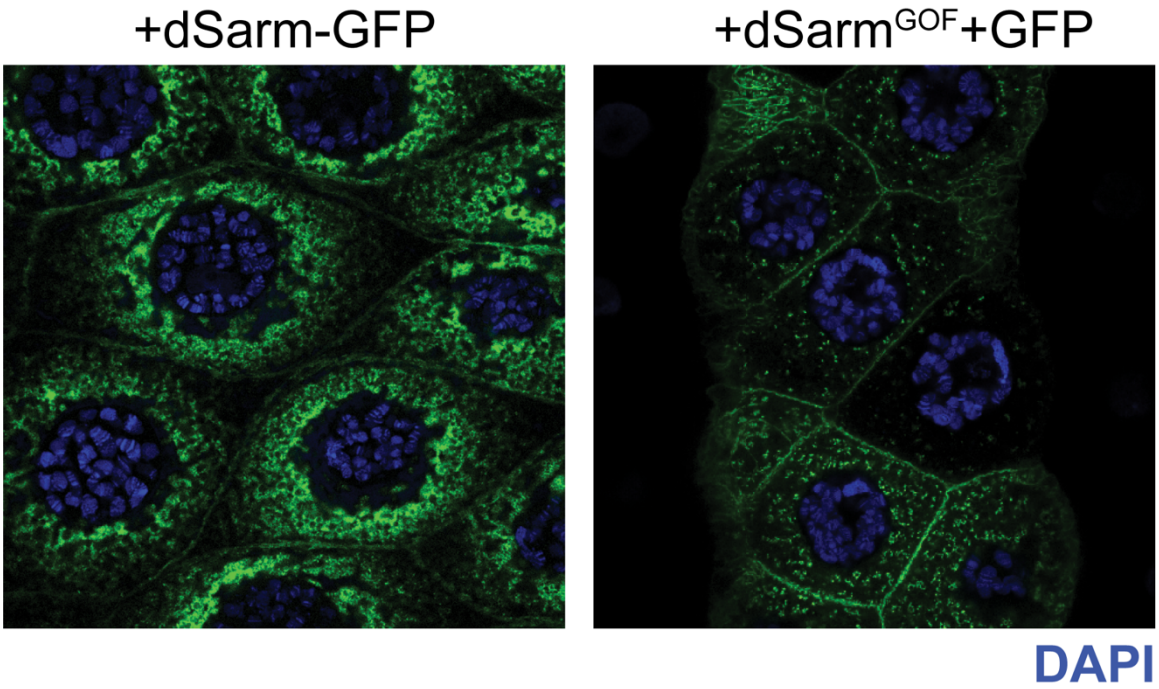

Appendix figure 2.9:

63x magnification of representative images of wL3 salivary glands with the expression of dSarm-GFP or dSarm^{GOF}-GFP, with DAPI staining.

Appendix figure 2.10: dSarm^{GOF} increased Ref(2)P level in Drosophila salivary glands.

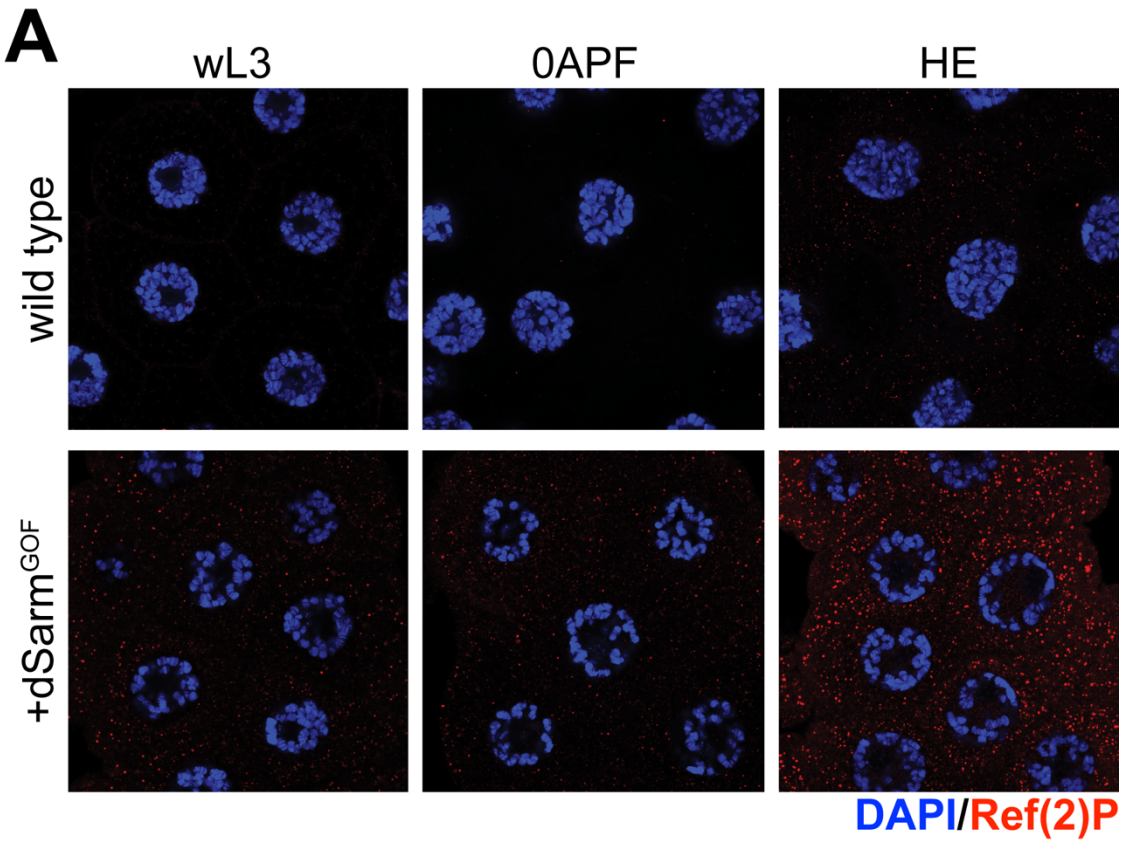

Appendix figure 2.10:

(A) 63x magnification of representative images of salivary glands with Ref(2)P and DAPI staining at wL3, 0APF (0 hour after puparium formation), and HE, to show increased level of Ref(2)P punctae. dSarm^{GOF} expression is driven by *Sgs3-Gal4*, the salivary gland specific driver. Animals with *Sgs-Gal4* alone serve as the wild-type control.

(B) Western blot image of anti-Ref(2)P level. Salivary tissue lysates were obtained from different stages: 0APF and HE. The band of Ref(2)P appears at ~100kD.

Appendix figure 2.11: Axed, dSarm^{GOF} and ubiquitin showed strong colocalization in Drosophila salivary glands.

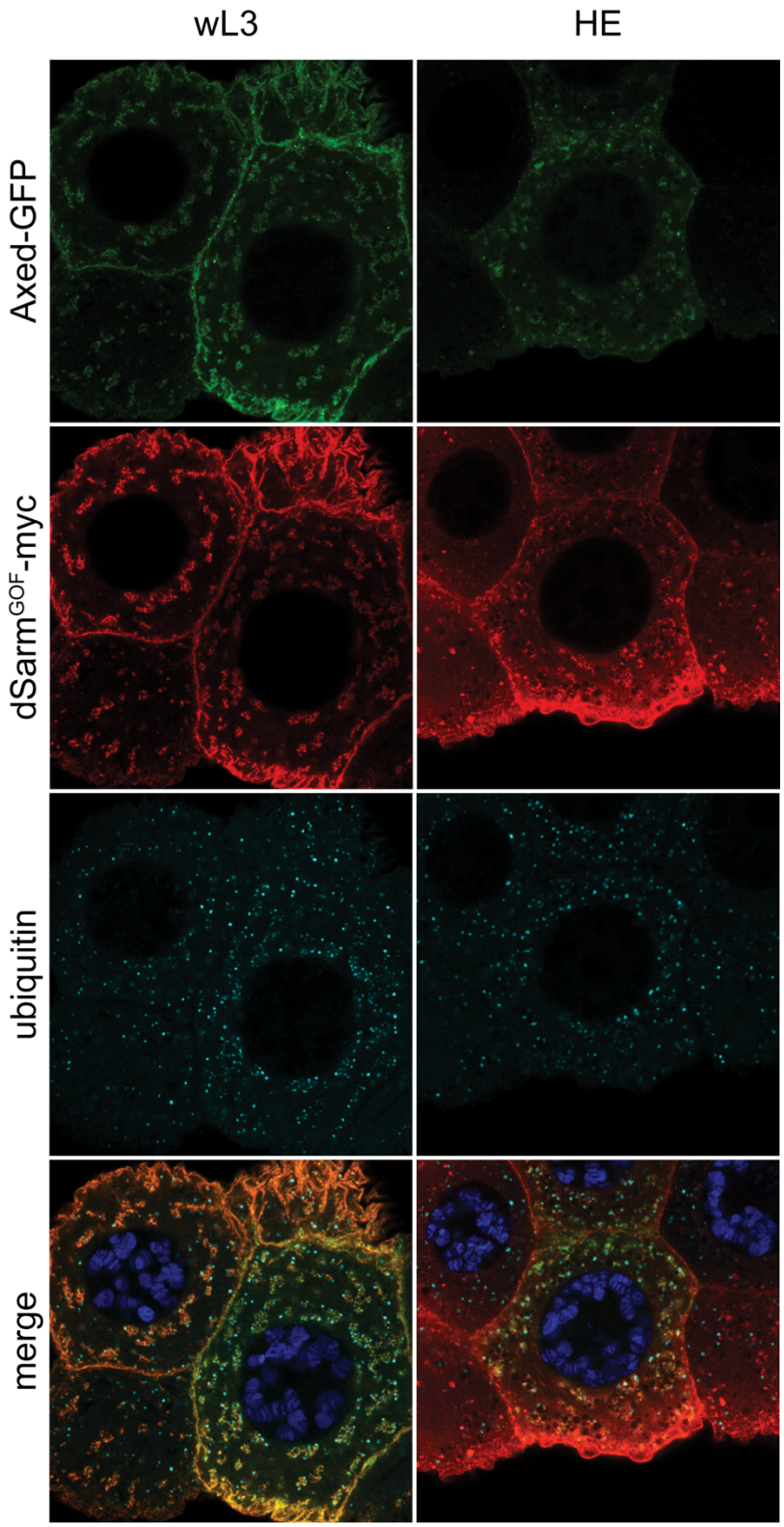

Appendix Figure 2.11:

(A) 63x magnification of representative images of salivary glands with GFP, myc, ubiquitin (FK2) and DAPI staining at wL3 and HE stages, to show the colocalizations of Axed-GFP, dSarm^{GOF}-myc, and ubiquitin.

KEY RESOURCE TABLE

Chemicals, antibiotics, and Recombinant Proteins		
Halocarbon Oil 27	Sigma	Cat #H8773
D-Glucose	Sigma	Cat #G7021
Dulbecco's Modified Eagle Medium (DMEM)	Thermo Fisher	Cat #11965084
Fetal Bovine Serum (FBS)	Thermo Fisher	Cat #10-082-139
Penicillin-Streptomycin	Thermo Fisher	Cat #15070063
CellTiter-Glo luminescent cell viability assay	Promega	Cat #G7570
TranIT-293	Mirus	Cat #MIR2706
Vectashield	Vector laboratories	Cat #H-1000-10
Formaldehyde	Sigma	Cat #252549
K_2CO_3	Sigma	Cat #367877
$MgCl_2$	Sigma	Cat #M8266
$HClO_4$	Sigma	Cat #244252
NaMN	Sigma	Cat #N7764
ε-NAD	Sigma	Cat #2630

β-NMN	Sigma	Cat #N3501
NAM	Sigma	Cat #N3376
ATP	Sigma	Cat #A26209
Nmnat1 protein	Novus Biological	Cat #NBP2-23285
Nmnat2 protein	Novus Biological	Cat #5865-NT-010
Bovine Serum Albumin (BSA)	Thermo Fisher	Cat #BP9700100
Blasticidin S HCl	Thermo Fisher	Cat #A1113903
Hygromycin B	Thermo Fisher	Cat #10687010
Necrostatin-1	Sigma	Cat #N9037
z-VAD-fmk	Sigma	Cat #V116
Doxycycline		
Ethyl methanesulfonate (EMS)	Sigma	Cat #M0880
Rhodamine Phalloidin	Thermo Fisher	Cat #R415
Antibody list		
anti-Raf(2)P	Abcam	Cat #ab178440
anti-ubiquitin (FK2)	Enzo	Cat #BML-PW8810-0100

anti-myc (9E10)	Developmental Studies Hybridoma Bank (DSHB)	
anti-GFP	Abcam	Cat #ab13970
Experimental Models: D. melanogaster genotype		
10xUAS-ivs-mCD8-gfp	Bloomington *Drosophila* Stock Center (BDSC)	RRID:BDSC_32189
elav-Gal4	BDSC	RRID:BDSC_458
FRT19A	BDSC	RRID:BDSC_1709
5xUAS-wld^{S}	Freeman lab	N/A
5xUAS-dNmnat	BDSC	RRID:BDSC_39699
5xUAS-wld$^{S\text{-}dead}$	Freeman lab	N/A
5xUAS-dNmnat^{WR}	BDSC	RRID:BDSC_39700

hep^{r75}	BDSC	RRID:BDSC_6761
OK371-Gal4	BDSC	RRID:BDSC_26160
FRT40A	BDSC	RRID:BDSC_8212
FRTG13 (FRT42B)	BDSC	RRID:BDSC_1956
ase-FLP^{2e}	(Neukomm et al., 2014), Freeman lab	N/A
FRT2A (FRT79D-F)	BDSC	RRID:BDSC_1997
FRT82B	BDSC	RRID:BDSC_2035
$slpr^{BS06}$	BDSC	RRID:BDSC_58807
lic^{G0252}	BDSC	RRID:BDSC_11880

ask1^{MI02915}	BDSC	RRID:BDSC_36163
mkk4^{e01458}	BDSC	RRID:BDSC_17956
dnmnat$^{D4790-1}$	BDSC	RRID:BDSC_39698
Nmnat:GFP:Nmnat^{WT}	BDSC	RRID:BDSC_80087
hiw$^{\Delta N}$	BDSC	RRID:BDSC_51637
drpr$^{\Delta 5}$	(MacDonald et al., 2006)	
nSyb-Gal4	BDSC	RRID:BDSC_39698
ase-FLP^{3b}	(Neukomm et al., 2014), Freeman lab	N/A
5xUAS-drpr^{RNAi}	(MacDonald et al., 2006)	

5xUAS-mcherry-atg8a	BDSC	RRID:BDSC_37750
5xUAS-gfp-lamp	BDSC	RRID:BDSC_42714
5xUAS-syt-gfp	BDSC	RRID:BDSC_6925
5xUAS-syt-gfp	BDSC	RRID:BDSC_6926
PBac[brp(FRT.Stop)V5-2A-LexA-VP16]VK00033	BDSC	RRID:BDSC_56747
13xLexAop-ivs-myr-gfp	BDSC	RRID:BDSC_56747
13xLexAop2-rab3-mcherry	BDSC	RRID:BDSC_52252
13xLexAop-rCD2-rfp[10]		
nSyb-LexA	BDSC	RRID:BDSC_52247
20xUAS-ivs-gcamp6s	BDSC	RRID:BDSC_42746

tub-Gal4	BDSC	RRID:BDSC_5138
nan-Gal4	BDSC	RRID:BDSC_24903
5xUAS-dsarm RNAi	BDSC	RRID:BDSC_63525
$hsFLP^{D5.fco}$		
$dsarm^{896}$	(Osterloh et al., 2012)	
$dsarm^{4790}$	(Osterloh et al., 2012)	
$axed^{0011}$	(Neukomm et al., 2017)	
$axed^{MI13270}$ (transposon insertion)	BDSC	RRID:BDSC_58041
cac^{k}	BDSC	RRID:BDSC_57064
cac^{F}	BDSC	RRID:BDSC_67175

5xUAS-NMNd	This thesis	N/A
5xUAS-mcherry-T2A-NMNd	This thesis	N/A
UAD-Jra^{Jbz} (Jra^{DN})	BDSC	RRID:BDSC 7217
repo-Gal4		
shark RNAi	VDRC	105706
dced-6 RNAi	VDRC	108101
bsk RNAi	VDRC	104569
raptor RNAi	VDRC	13112
5xUAS-draper II	(Logan et al., 2012)	
mmp-1 RNAi	(Uhlirova and Bohmann, 2006)	
Sgs3-Gal4	BDSC	RRID:BDSC 6870
5xUAS-Axed-GFP	(Neukomm et al., 2017)	
dNmnat RNAi	VDRC	32255

5xUAS-dSarm^{GOF}-myc	(Neukomm et al., 2017)	
5xUAS-dSarm^{GOF}-GFP	(Neukomm et al., 2017)	
Oligonucleotides		
Primer for pattB-5xUAS-mCherry-T2A-NMNd forward: AAACCCCTCGAGCAAAACATGACAGATAGCGAGCTGATGCAGC	This thesis	N/A
Primer for pattB-5xUAS-NMNd forward: AAAAACCTCGAGCAAAACATGGTGAGCAAGGGCGAGG	This thesis	N/A
Primer for both NMNd recombinant DNA reverse: CCCCCATCTAGATCAAGTGTTCTGGAGGAACTGTTGC	This thesis	N/A

Primer for attB-5xUAS-CG4098 forward: CCCCAACTCGAGCA AACATGACGAGTTTCGAGT TTGCACTGC	This paper	N/A
Primer for attB-5xUAS-CG4098 reverse: CCCCAATCTAGACTACCAG TGTGCATTTCGTCGGATGA C	This thesis	N/A
Recombinant DNA		
pattB-5xUAS-NMNd	This thesis	N/A
pattB-5xUAS-mCherry-T2A-NMNd	This thesis	N/A
pattB-5xUAS-CG4098	This thesis	N/A
pLVX-TetOne-Blast - Sarm1WT	Built by Jack Wong	N/A
pLVX-TetOne-Blast -Sarm1^{GOF}	Built by Jack Wong	N/A

pHAGE-H Wld^{s}	Built by Jack Wong	N/A
Software and Algorithms		
Prism8	GraphPad	
FIJI	imageJ	
Other: Tools		
MicroPoint Scissors (5-mm cutting edge)	EMS	Cat #72933-04
Tweezers (high precision, ultra fine)	EMS	Cat #78520-5
Chamber slides	Sigma	Cat #C7182
96-well plate	Thermo Fisher	Cat #237108

REFERENCES

1. Adalbert, R., Gillingwater, T.H., Haley, J.E., Bridge, K., Beirowski, B., Berek, L., Wagner, D., Grumme, D., Thomson, D., Celik, A.*, et al.* (2005). A rat model of slow Wallerian degeneration (WldS) with improved preservation of neuromuscular synapses. Eur J Neurosci *21*, 271-277.
2. Araki, T., Sasaki, Y., and Milbrandt, J. (2004). Increased nuclear NAD biosynthesis and SIRT1 activation prevent axonal degeneration. Science *305*, 1010-1013.
3. Avery, M.A., Rooney, T.M., Pandya, J.D., Wishart, T.M., Gillingwater, T.H., Geddes, J.W., Sullivan, P.G., and Freeman, M.R. (2012). WldS prevents axon degeneration through increased mitochondrial flux and enhanced mitochondrial Ca2+ buffering. Curr Biol *22*, 596-600.
4. Avery, M.A., Sheehan, A.E., Kerr, K.S., Wang, J., and Freeman, M.R. (2009). Wld S requires Nmnat1 enzymatic activity and N16-VCP interactions to suppress Wallerian degeneration. J Cell Biol *184*, 501-513.
5. Awasaki, T., Tatsumi, R., Takahashi, K., Arai, K., Nakanishi, Y., Ueda, R., and Ito, K. (2006). Essential role of the apoptotic cell

engulfment genes draper and ced-6 in programmed axon pruning during Drosophila metamorphosis. Neuron *50*, 855-867.

6. Barrio, J.R., Secrist, J.A., 3rd, and Leonard, N.J. (1972). A fluorescent analog of nicotinamide adenine dinucleotide. Proc Natl Acad Sci U S A *69*, 2039-2042.
7. Bell, R.D., Winkler, E.A., Singh, I., Sagare, A.P., Deane, R., Wu, Z., Holtzman, D.M., Betsholtz, C., Armulik, A., Sallstrom, J.*, et al.* (2012). Apolipoprotein E controls cerebrovascular integrity via cyclophilin A. Nature *485*, 512-516.
8. Berger, F., Lau, C., Dahlmann, M., and Ziegler, M. (2005). Subcellular compartmentation and differential catalytic properties of the three human nicotinamide mononucleotide adenylyltransferase isoforms. J Biol Chem *280*, 36334-36341.
9. Billger, M., Wallin, M., and Karlsson, J.O. (1988). Proteolysis of tubulin and microtubule-associated proteins 1 and 2 by calpain I and II. Difference in sensitivity of assembled and disassembled microtubules. Cell Calcium *9*, 33-44.
10. Boulanger, J.J., and Messier, C. (2014). From precursors to myelinating oligodendrocytes: contribution of intrinsic and extrinsic

factors to white matter plasticity in the adult brain. Neuroscience *269*, 343-366.

11. Brace, E.J., and DiAntonio, A. (2017). Models of axon regeneration in Drosophila. Exp Neurol *287*, 310-317.
12. Buckmaster, E.A., Perry, V.H., and Brown, M.C. (1995). The rate of Wallerian degeneration in cultured neurons from wild type and C57BL/WldS mice depends on time in culture and may be extended in the presence of elevated K+ levels. Eur J Neurosci *7*, 1596-1602.
13. Burke, R.E., and O'Malley, K. (2013). Axon degeneration in Parkinson's disease. Exp Neurol *246*, 72-83.
14. Burne, J.F., Staple, J.K., and Raff, M.C. (1996). Glial cells are increased proportionally in transgenic optic nerves with increased numbers of axons. J Neurosci *16*, 2064-2073.
15. Cambronne, X.A., Stewart, M.L., Kim, D., Jones-Brunette, A.M., Morgan, R.K., Farrens, D.L., Cohen, M.S., and Goodman, R.H. (2016). Biosensor reveals multiple sources for mitochondrial NAD(+). Science *352*, 1474-1477.
16. Candelario-Jalil, E., Thompson, J., Taheri, S., Grossetete, M., Adair, J.C., Edmonds, E., Prestopnik, J., Wills, J., and Rosenberg, G.A. (2011). Matrix metalloproteinases are associated with increased

blood-brain barrier opening in vascular cognitive impairment. Stroke *42*, 1345-1350.

17. Canning, P., Cooper, C.D., Krojer, T., Murray, J.W., Pike, A.C., Chaikuad, A., Keates, T., Thangaratnarajah, C., Hojzan, V., Ayinampudi, V.*, et al.* (2013). Structural basis for Cul3 protein assembly with the BTB-Kelch family of E3 ubiquitin ligases. J Biol Chem *288*, 7803-7814.
18. Chen, X.H., Johnson, V.E., Uryu, K., Trojanowski, J.Q., and Smith, D.H. (2009). A lack of amyloid beta plaques despite persistent accumulation of amyloid beta in axons of long-term survivors of traumatic brain injury. Brain Pathol *19*, 214-223.
19. Chen, Y., Akin, O., Nern, A., Tsui, C.Y., Pecot, M.Y., and Zipursky, S.L. (2014). Cell-type-specific labeling of synapses in vivo through synaptic tagging with recombination. Neuron *81*, 280-293.
20. Chuang, C.F., and Bargmann, C.I. (2005). A Toll-interleukin 1 repeat protein at the synapse specifies asymmetric odorant receptor expression via ASK1 MAPKKK signaling. Genes Dev *19*, 270-281.
21. Coleman, M. (2005). Axon degeneration mechanisms: commonality amid diversity. Nat Rev Neurosci *6*, 889-898.

22. Collins, C.A., Wairkar, Y.P., Johnson, S.L., and DiAntonio, A. (2006). Highwire restrains synaptic growth by attenuating a MAP kinase signal. Neuron *51*, 57-69.

23. Conforti, L., Fang, G., Beirowski, B., Wang, M.S., Sorci, L., Asress, S., Adalbert, R., Silva, A., Bridge, K., Huang, X.P.*, et al.* (2007). NAD(+) and axon degeneration revisited: Nmnat1 cannot substitute for Wld(S) to delay Wallerian degeneration. Cell Death Differ *14*, 116-127.

24. Conforti, L., Wilbrey, A., Morreale, G., Janeckova, L., Beirowski, B., Adalbert, R., Mazzola, F., Di Stefano, M., Hartley, R., Babetto, E.*, et al.* (2009). Wld S protein requires Nmnat activity and a short N-terminal sequence to protect axons in mice. J Cell Biol *184*, 491-500.

25. Cunningham, R.L., and Monk, K.R. (2018). Transmission Electron Microscopy for Zebrafish Larvae and Adult Lateral Line Nerve. Methods Mol Biol *1739*, 385-400.

26. Daeron, M., Jaeger, S., Du Pasquier, L., and Vivier, E. (2008). Immunoreceptor tyrosine-based inhibition motifs: a quest in the past and future. Immunol Rev *224*, 11-43.

27. De Vos, K.J., Grierson, A.J., Ackerley, S., and Miller, C.C. (2008). Role of axonal transport in neurodegenerative diseases. Annu Rev Neurosci *31*, 151-173.

28. Deckwerth, T.L., and Johnson, E.M., Jr. (1994). Neurites can remain viable after destruction of the neuronal soma by programmed cell death (apoptosis). Dev Biol *165*, 63-72.

29. Di Stefano, M., Nascimento-Ferreira, I., Orsomando, G., Mori, V., Gilley, J., Brown, R., Janeckova, L., Vargas, M.E., Worrell, L.A., Loreto, A.*, et al.* (2014). A rise in NAD precursor nicotinamide mononucleotide (NMN) after injury promotes axon degeneration. Cell Death Differ *22*, 731-742.

30. Doherty, J., Logan, M.A., Tasdemir, O.E., and Freeman, M.R. (2009). Ensheathing glia function as phagocytes in the adult Drosophila brain. J Neurosci *29*, 4768-4781.

31. Doherty, J., Sheehan, A.E., Bradshaw, R., Fox, A.N., Lu, T.Y., and Freeman, M.R. (2014). PI3K signaling and Stat92E converge to modulate glial responsiveness to axonal injury. PLoS Biol *12*, e1001985.

32. Esparza, J., Kruse, M., Lee, J., Michaud, M., and Madri, J.A. (2004). MMP-2 null mice exhibit an early onset and severe experimental

autoimmune encephalomyelitis due to an increase in MMP-9 expression and activity. FASEB J *18*, 1682-1691.

33. Essuman, K., Summers, D.W., Sasaki, Y., Mao, X., DiAntonio, A., and Milbrandt, J. (2017). The SARM1 Toll/Interleukin-1 Receptor Domain Possesses Intrinsic NAD(+) Cleavage Activity that Promotes Pathological Axonal Degeneration. Neuron *93*, 1334-1343 e1335.
34. Fang, Y., and Bonini, N.M. (2012). Axon degeneration and regeneration: insights from Drosophila models of nerve injury. Annu Rev Cell Dev Biol *28*, 575-597.
35. Fang, Y., Soares, L., Teng, X., Geary, M., and Bonini, N.M. (2012). A novel Drosophila model of nerve injury reveals an essential role of Nmnat in maintaining axonal integrity. Curr Biol *22*, 590-595.
36. Farley, J.E., Burdett, T.C., Barria, R., Neukomm, L.J., Kenna, K.P., Landers, J.E., and Freeman, M.R. (2018). Transcription factor Pebbled/RREB1 regulates injury-induced axon degeneration. Proc Natl Acad Sci U S A *115*, 1358-1363.
37. Finn, J.T., Weil, M., Archer, F., Siman, R., Srinivasan, A., and Raff, M.C. (2000). Evidence that Wallerian degeneration and localized axon degeneration induced by local neurotrophin deprivation do not involve caspases. J Neurosci *20*, 1333-1341.

38. Freeman, M.R., Delrow, J., Kim, J., Johnson, E., and Doe, C.Q. (2003). Unwrapping glial biology: Gcm target genes regulating glial development, diversification, and function. Neuron *38*, 567-580.

39. Freeman, M.R., and Doherty, J. (2006). Glial cell biology in Drosophila and vertebrates. Trends Neurosci *29*, 82-90.

40. Fujioka, H., Dairyo, Y., Yasunaga, K., and Emoto, K. (2012). Neural functions of matrix metalloproteinases: plasticity, neurogenesis, and disease. Biochem Res Int *2012*, 789083.

41. Gaudet, A.D., and Fonken, L.K. (2018). Glial Cells Shape Pathology and Repair After Spinal Cord Injury. Neurotherapeutics *15*, 554-577.

42. Geisler, S., Huang, S.X., Strickland, A., Doan, R.A., Summers, D.W., Mao, X., Park, J., DiAntonio, A., and Milbrandt, J. (2019). Gene therapy targeting SARM1 blocks pathological axon degeneration in mice. J Exp Med *216*, 294-303.

43. George, E.B., Glass, J.D., and Griffin, J.W. (1995). Axotomy-induced axonal degeneration is mediated by calcium influx through ion-specific channels. J Neurosci *15*, 6445-6452.

44. Gerdts, J., Brace, E.J., Sasaki, Y., DiAntonio, A., and Milbrandt, J. (2015). SARM1 activation triggers axon degeneration locally via NAD(+) destruction. Science *348*, 453-457.

45. Gerdts, J., Summers, D.W., Milbrandt, J., and DiAntonio, A. (2016). Axon Self-Destruction: New Links among SARM1, MAPKs, and NAD+ Metabolism. Neuron *89*, 449-460.

46. Gerdts, J., Summers, D.W., Sasaki, Y., DiAntonio, A., and Milbrandt, J. (2013). Sarm1-mediated axon degeneration requires both SAM and TIR interactions. J Neurosci *33*, 13569-13580.

47. Gilley, J., Adalbert, R., Yu, G., and Coleman, M.P. (2013). Rescue of peripheral and CNS axon defects in mice lacking NMNAT2. J Neurosci *33*, 13410-13424.

48. Gilley, J., and Coleman, M.P. (2010). Endogenous Nmnat2 is an essential survival factor for maintenance of healthy axons. PLoS Biol *8*, e1000300.

49. Gilley, J., Orsomando, G., Nascimento-Ferreira, I., and Coleman, M.P. (2015). Absence of SARM1 rescues development and survival of NMNAT2-deficient axons. Cell Rep *10*, 1974-1981.

50. Gilley, J., Ribchester, R.R., and Coleman, M.P. (2017). Sarm1 Deletion, but Not Wld(S), Confers Lifelong Rescue in a Mouse Model of Severe Axonopathy. Cell Rep *21*, 10-16.

51. Glass, J.D., Schryer, B.L., and Griffin, J.W. (1994). Calcium-mediated degeneration of the axonal cytoskeleton in the Ola mouse. J Neurochem *62*, 2472-2475.

52. Greenhalgh, A.D., David, S., and Bennett, F.C. (2020). Immune cell regulation of glia during CNS injury and disease. Nat Rev Neurosci *21*, 139-152.

53. Greer, J.E., Povlishock, J.T., and Jacobs, K.M. (2012). Electrophysiological abnormalities in both axotomized and nonaxotomized pyramidal neurons following mild traumatic brain injury. J Neurosci *32*, 6682-6687.

54. Guest, J.D., Hiester, E.D., and Bunge, R.P. (2005). Demyelination and Schwann cell responses adjacent to injury epicenter cavities following chronic human spinal cord injury. Exp Neurol *192*, 384-393.

55. Heiner, I., Radukina, N., Eisfeld, J., Kuhn, F., and Luckhoff, A. (2005). Regulation of TRPM2 channels in neutrophil granulocytes by ADP-ribose: a promising pharmacological target. Naunyn Schmiedebergs Arch Pharmacol *371*, 325-333.

56. Henninger, N., Bouley, J., Sikoglu, E.M., An, J., Moore, C.M., King, J.A., Bowser, R., Freeman, M.R., and Brown, R.H., Jr. (2016). Attenuated traumatic axonal injury and improved functional outcome

after traumatic brain injury in mice lacking Sarm1. Brain *139*, 1094-1105.

57. Herculano-Houzel, S. (2014). The glia/neuron ratio: how it varies uniformly across brain structures and species and what that means for brain physiology and evolution. Glia *62*, 1377-1391.

58. Hill, C.S., Coleman, M.P., and Menon, D.K. (2016). Traumatic Axonal Injury: Mechanisms and Translational Opportunities. Trends Neurosci *39*, 311-324.

59. Horsefield, S., Burdett, H., Zhang, X., Manik, M.K., Shi, Y., Chen, J., Qi, T., Gilley, J., Lai, J.S., Rank, M.X.*, et al.* (2019). NAD(+) cleavage activity by animal and plant TIR domains in cell death pathways. Science *365*, 793-799.

60. Howe, C.L., LaFrance-Corey, R.G., Mirchia, K., Sauer, B.M., McGovern, R.M., Reid, J.M., and Buenz, E.J. (2016). Neuroprotection mediated by inhibition of calpain during acute viral encephalitis. Sci Rep *6*, 28699.

61. Hwang, S.Y., Jung, J.S., Kim, T.H., Lim, S.J., Oh, E.S., Kim, J.Y., Ji, K.A., Joe, E.H., Cho, K.H., and Han, I.O. (2006). Ionizing radiation induces astrocyte gliosis through microglia activation. Neurobiol Dis *21*, 457-467.

62. Ising, C., and Heneka, M.T. (2018). Functional and structural damage of neurons by innate immune mechanisms during neurodegeneration. Cell Death Dis *9*, 120.

63. Johnson, V.E., Stewart, W., and Smith, D.H. (2013). Axonal pathology in traumatic brain injury. Exp Neurol *246*, 35-43.

64. Kasahara, M., Menon, D.K., Salmond, C.H., Outtrim, J.G., Taylor Tavares, J.V., Carpenter, T.A., Pickard, J.D., Sahakian, B.J., and Stamatakis, E.A. (2010). Altered functional connectivity in the motor network after traumatic brain injury. Neurology *75*, 168-176.

65. Kay, J.N., Chu, M.W., and Sanes, J.R. (2012). MEGF10 and MEGF11 mediate homotypic interactions required for mosaic spacing of retinal neurons. Nature *483*, 465-469.

66. Kim, K.W., Tang, N.H., Piggott, C.A., Andrusiak, M.G., Park, S., Zhu, M., Kurup, N., Cherra, S.J., 3rd, Wu, Z., Chisholm, A.D.*, et al.* (2018). Expanded genetic screening in Caenorhabditis elegans identifies new regulators and an inhibitory role for NAD(+) in axon regeneration. Elife *7*.

67. Kim, Y., Zhou, P., Qian, L., Chuang, J.Z., Lee, J., Li, C., Iadecola, C., Nathan, C., and Ding, A. (2007). MyD88-5 links mitochondria,

microtubules, and JNK3 in neurons and regulates neuronal survival. J Exp Med *204*, 2063-2074.

68. Kitay, B.M., McCormack, R., Wang, Y., Tsoulfas, P., and Zhai, R.G. (2013). Mislocalization of neuronal mitochondria reveals regulation of Wallerian degeneration and NMNAT/WLD(S)-mediated axon protection independent of axonal mitochondria. Hum Mol Genet *22*, 1601-1614.

69. Kneynsberg, A., Combs, B., Christensen, K., Morfini, G., and Kanaan, N.M. (2017). Axonal Degeneration in Tauopathies: Disease Relevance and Underlying Mechanisms. Front Neurosci *11*, 572.

70. Knoferle, J., Koch, J.C., Ostendorf, T., Michel, U., Planchamp, V., Vutova, P., Tonges, L., Stadelmann, C., Bruck, W., Bahr, M.*, et al.* (2010). Mechanisms of acute axonal degeneration in the optic nerve in vivo. Proc Natl Acad Sci U S A *107*, 6064-6069.

71. Komatsu, M., Waguri, S., Koike, M., Sou, Y.S., Ueno, T., Hara, T., Mizushima, N., Iwata, J., Ezaki, J., Murata, S.*, et al.* (2007). Homeostatic levels of p62 control cytoplasmic inclusion body formation in autophagy-deficient mice. Cell *131*, 1149-1163.

72. Kondiles, B.R., and Horner, P.J. (2018). Myelin plasticity, neural activity, and traumatic neural injury. Dev Neurobiol *78*, 108-122.

73. Kuhn, F.J., Heiner, I., and Luckhoff, A. (2005). TRPM2: a calcium influx pathway regulated by oxidative stress and the novel second messenger ADP-ribose. Pflugers Arch *451*, 212-219.

74. Kuhn, F.J., and Luckhoff, A. (2004). Sites of the NUDT9-H domain critical for ADP-ribose activation of the cation channel TRPM2. J Biol Chem *279*, 46431-46437.

75. Kutner, R.H., Zhang, X.Y., and Reiser, J. (2009). Production, concentration and titration of pseudotyped HIV-1-based lentiviral vectors. Nat Protoc *4*, 495-505.

76. Kyrkanides, S., Olschowka, J.A., Williams, J.P., Hansen, J.T., and O'Banion, M.K. (1999). TNF alpha and IL-1beta mediate intercellular adhesion molecule-1 induction via microglia-astrocyte interaction in CNS radiation injury. J Neuroimmunol *95*, 95-106.

77. Lee, T., and Luo, L. (1999). Mosaic analysis with a repressible cell marker for studies of gene function in neuronal morphogenesis. Neuron *22*, 451-461.

78. Li, J., Zhang, W., Guo, Z., Wu, S., Jan, L.Y., and Jan, Y.N. (2016). A Defensive Kicking Behavior in Response to Mechanical Stimuli Mediated by Drosophila Wing Margin Bristles. J Neurosci *36*, 11275-11282.

79. Li, Q., and Barres, B.A. (2018). Microglia and macrophages in brain homeostasis and disease. Nat Rev Immunol *18*, 225-242.

80. Li-Kroeger, D., Kanca, O., Lee, P.T., Cowan, S., Lee, M.T., Jaiswal, M., Salazar, J.L., He, Y., Zuo, Z., and Bellen, H.J. (2018). An expanded toolkit for gene tagging based on MiMIC and scarless CRISPR tagging in Drosophila. Elife *7*.

81. Liddelow, S.A., Guttenplan, K.A., Clarke, L.E., Bennett, F.C., Bohlen, C.J., Schirmer, L., Bennett, M.L., Munch, A.E., Chung, W.S., Peterson, T.C*., et al.* (2017). Neurotoxic reactive astrocytes are induced by activated microglia. Nature *541*, 481-487.

82. Lin, S., Gasmi, L., Xie, Y., Ying, K., Gu, S., Wang, Z., Jin, H., Chao, Y., Wu, C., Zhou, Z*., et al.* (2002). Cloning, expression and characterisation of a human Nudix hydrolase specific for adenosine 5'-diphosphoribose (ADP-ribose). Biochim Biophys Acta *1594*, 127-135.

83. Logan, M.A., Hackett, R., Doherty, J., Sheehan, A., Speese, S.D., and Freeman, M.R. (2012). Negative regulation of glial engulfment activity by Draper terminates glial responses to axon injury. Nat Neurosci *15*, 722-730.

84. Loreto, A., Di Stefano, M., Gering, M., and Conforti, L. (2014). Wallerian Degeneration Is Executed by an NMN-SARM1-Dependent Late Ca(2+) Influx but Only Modestly Influenced by Mitochondria. Cell Rep *13*, 2539-2552.

85. Loreto, A., Di Stefano, M., Gering, M., and Conforti, L. (2015). Wallerian Degeneration Is Executed by an NMN-SARM1-Dependent Late Ca(2+) Influx but Only Modestly Influenced by Mitochondria. Cell Rep *13*, 2539-2552.

86. Lu, T.Y., MacDonald, J.M., Neukomm, L.J., Sheehan, A.E., Bradshaw, R., Logan, M.A., and Freeman, M.R. (2017). Axon degeneration induces glial responses through Draper-TRAF4-JNK signalling. Nat Commun *8*, 14355.

87. Lunn, E.R., Perry, V.H., Brown, M.C., Rosen, H., and Gordon, S. (1989). Absence of Wallerian Degeneration does not Hinder Regeneration in Peripheral Nerve. Eur J Neurosci *1*, 27-33.

88. MacDonald, J.M., Beach, M.G., Porpiglia, E., Sheehan, A.E., Watts, R.J., and Freeman, M.R. (2006). The Drosophila cell corpse engulfment receptor Draper mediates glial clearance of severed axons. Neuron *50*, 869-881.

89. Marion, C.M., McDaniel, D.P., and Armstrong, R.C. (2019). Sarm1 deletion reduces axon damage, demyelination, and white matter atrophy after experimental traumatic brain injury. Exp Neurol *321*, 113040.

90. Martin, S.M., O'Brien, G.S., Portera-Cailliau, C., and Sagasti, A. (2010). Wallerian degeneration of zebrafish trigeminal axons in the skin is required for regeneration and developmental pruning. Development *137*, 3985-3994.

91. Mayer, P.R., Huang, N., Dewey, C.M., Dries, D.R., Zhang, H., and Yu, G. (2010). Expression, localization, and biochemical characterization of nicotinamide mononucleotide adenylyltransferase 2. J Biol Chem *285*, 40387-40396.

92. McLennan, A.G. (2006). The Nudix hydrolase superfamily. Cell Mol Life Sci *63*, 123-143.

93. McPhee, C.K., Logan, M.A., Freeman, M.R., and Baehrecke, E.H. (2010). Activation of autophagy during cell death requires the engulfment receptor Draper. Nature *465*, 1093-1096.

94. Milde, S., Gilley, J., and Coleman, M.P. (2013a). Axonal trafficking of NMNAT2 and its roles in axon growth and survival in vivo. Bioarchitecture *3*, 133-140.

95. Milde, S., Gilley, J., and Coleman, M.P. (2013b). Subcellular localization determines the stability and axon protective capacity of axon survival factor Nmnat2. PLoS Biol *11*, e1001539.

96. Millecamps, S., and Julien, J.P. (2013). Axonal transport deficits and neurodegenerative diseases. Nat Rev Neurosci *14*, 161-176.

97. Nern, A., Pfeiffer, B.D., Svoboda, K., and Rubin, G.M. (2011). Multiple new site-specific recombinases for use in manipulating animal genomes. Proc Natl Acad Sci U S A *108*, 14198-14203.

98. Neukomm, L.J., Burdett, T.C., Gonzalez, M.A., Zuchner, S., and Freeman, M.R. (2014). Rapid in vivo forward genetic approach for identifying axon death genes in Drosophila. Proc Natl Acad Sci U S A *111*, 9965-9970.

99. Neukomm, L.J., Burdett, T.C., Seeds, A.M., Hampel, S., Coutinho-Budd, J.C., Farley, J.E., Wong, J., Karadeniz, Y.B., Osterloh, J.M., Sheehan, A.E.*, et al.* (2017). Axon Death Pathways Converge on Axundead to Promote Functional and Structural Axon Disassembly. Neuron *95*, 78-91 e75.

100. Newman, T.A., Woolley, S.T., Hughes, P.M., Sibson, N.R., Anthony, D.C., and Perry, V.H. (2001). T-cell- and macrophage-

mediated axon damage in the absence of a CNS-specific immune response: involvement of metalloproteinases. Brain *124*, 2203-2214.

101. Noble, L.J., Donovan, F., Igarashi, T., Goussev, S., and Werb, Z. (2002). Matrix metalloproteinases limit functional recovery after spinal cord injury by modulation of early vascular events. J Neurosci *22*, 7526-7535.

102. Orem, B.C., Pelisch, N., Williams, J., Nally, J.M., and Stirling, D.P. (2017). Intracellular calcium release through IP3R or RyR contributes to secondary axonal degeneration. Neurobiol Dis *106*, 235-243.

103. Osterloh, J.M., Yang, J., Rooney, T.M., Fox, A.N., Adalbert, R., Powell, E.H., Sheehan, A.E., Avery, M.A., Hackett, R., Logan, M.A.*, et al.* (2012). dSarm/Sarm1 is required for activation of an injury-induced axon death pathway. Science *337*, 481-484.

104. Page-McCaw, A. (2008). Remodeling the model organism: matrix metalloproteinase functions in invertebrates. Semin Cell Dev Biol *19*, 14-23.

105. Perraud, A.L., Schmitz, C., and Scharenberg, A.M. (2003). TRPM2 Ca2+ permeable cation channels: from gene to biological function. Cell Calcium *33*, 519-531.

106. Pinheiro da Silva, F., Aloulou, M., Benhamou, M., and Monteiro, R.C. (2008). Inhibitory ITAMs: a matter of life and death. Trends Immunol *29*, 366-373.

107. Purice, M.D., Ray, A., Munzel, E.J., Pope, B.J., Park, D.J., Speese, S.D., and Logan, M.A. (2017). A novel Drosophila injury model reveals severed axons are cleared through a Draper/MMP-1 signaling cascade. Elife *6*.

108. Raad, H., Ferveur, J.F., Ledger, N., Capovilla, M., and Robichon, A. (2016). Functional Gustatory Role of Chemoreceptors in Drosophila Wings. Cell Rep *15*, 1442-1454.

109. Raff, M.C., Whitmore, A.V., and Finn, J.T. (2002). Axonal self-destruction and neurodegeneration. Science *296*, 868-871.

110. Raffaelli, N., Sorci, L., Amici, A., Emanuelli, M., Mazzola, F., and Magni, G. (2002). Identification of a novel human nicotinamide mononucleotide adenylyltransferase. Biochem Biophys Res Commun *297*, 835-840.

111. Rafty, L.A., Schmidt, M.T., Perraud, A.L., Scharenberg, A.M., and Denu, J.M. (2002). Analysis of O-acetyl-ADP-ribose as a target for Nudix ADP-ribose hydrolases. J Biol Chem *277*, 47114-47122.

112. Sasaki, Y., and Milbrandt, J. (2010). Axonal degeneration is blocked by nicotinamide mononucleotide adenylyltransferase (Nmnat) protein transduction into transected axons. J Biol Chem *285*, 41211-41215.

113. Sasaki, Y., Nakagawa, T., Mao, X., DiAntonio, A., and Milbrandt, J. (2016). NMNAT1 inhibits axon degeneration via blockade of SARM1-mediated NAD(+) depletion. Elife *5*.

114. Sasaki, Y., Vohra, B.P., Lund, F.E., and Milbrandt, J. (2009). Nicotinamide mononucleotide adenylyl transferase-mediated axonal protection requires enzymatic activity but not increased levels of neuronal nicotinamide adenine dinucleotide. J Neurosci *29*, 5525-5535.

115. Schafer, D.P., Lehrman, E.K., Kautzman, A.G., Koyama, R., Mardinly, A.R., Yamasaki, R., Ransohoff, R.M., Greenberg, M.E., Barres, B.A., and Stevens, B. (2012). Microglia sculpt postnatal neural circuits in an activity and complement-dependent manner. Neuron *74*, 691-705.

116. Smith, L.A., Peixoto, A.A., Kramer, E.M., Villella, A., and Hall, J.C. (1998). Courtship and visual defects of cacophony mutants

reveal functional complexity of a calcium-channel alpha1 subunit in Drosophila. Genetics *149*, 1407-1426.

117. Stevens, B., Allen, N.J., Vazquez, L.E., Howell, G.R., Christopherson, K.S., Nouri, N., Micheva, K.D., Mehalow, A.K., Huberman, A.D., Stafford, B.*, et al.* (2007). The classical complement cascade mediates CNS synapse elimination. Cell *131*, 1164-1178.

118. Stogios, P.J., and Prive, G.G. (2004). The BACK domain in BTB-kelch proteins. Trends Biochem Sci *29*, 634-637.

119. Sundaramoorthy, V., Green, D., Locke, K., O'Brien, C.M., Dearnley, M., and Bingham, J. (2020). Novel role of SARM1 mediated axonal degeneration in the pathogenesis of rabies. PLoS Pathog *16*, e1008343.

120. Thorsell, A.G., Ekblad, T., Karlberg, T., Low, M., Pinto, A.F., Tresaugues, L., Moche, M., Cohen, M.S., and Schuler, H. (2017). Structural Basis for Potency and Promiscuity in Poly(ADP-ribose) Polymerase (PARP) and Tankyrase Inhibitors. J Med Chem *60*, 1262-1271.

121. Tian, X., Gala, U., Zhang, Y., Shang, W., Nagarkar Jaiswal, S., di Ronza, A., Jaiswal, M., Yamamoto, S., Sandoval, H., Duraine, L.*, et al.* (2015). A voltage-gated calcium channel regulates lysosomal

fusion with endosomes and autophagosomes and is required for neuronal homeostasis. PLoS Biol *13*, e1002103.

122. Trinkle-Mulcahy, L. (2019). Recent advances in proximity-based labeling methods for interactome mapping. F1000Res *8*.

123. Turkiew, E., Falconer, D., Reed, N., and Hoke, A. (2017). Deletion of Sarm1 gene is neuroprotective in two models of peripheral neuropathy. J Peripher Nerv Syst *22*, 162-171.

124. Uhlirova, M., and Bohmann, D. (2006). JNK- and Fos-regulated Mmp1 expression cooperates with Ras to induce invasive tumors in Drosophila. EMBO J *25*, 5294-5304.

125. Underhill, D.M., and Goodridge, H.S. (2007). The many faces of ITAMs. Trends Immunol *28*, 66-73.

126. Valakh, V., Frey, E., Babetto, E., Walker, L.J., and DiAntonio, A. (2015). Cytoskeletal disruption activates the DLK/JNK pathway, which promotes axonal regeneration and mimics a preconditioning injury. Neurobiol Dis *77*, 13-25.

127. Walker, L.J., Summers, D.W., Sasaki, Y., Brace, E.J., Milbrandt, J., and DiAntonio, A. (2017). MAPK signaling promotes axonal degeneration by speeding the turnover of the axonal maintenance factor NMNAT2. Elife *6*.

128. Waller, A. (1850). Experiments on the Section of the Glossopharyngeal and Hypoglossal Nerves of the Frog, and Observations of the Alterations Produced Thereby in the Structure of Their Primitive Fibres. Philosophical Transactions of the Royal Society of London *140*, 423-429.

129. Wang, J., Zhai, Q., Chen, Y., Lin, E., Gu, W., McBurney, M.W., and He, Z. (2005). A local mechanism mediates NAD-dependent protection of axon degeneration. J Cell Biol *170*, 349-355.

130. Wang, Q., Zhang, S., Liu, T., Wang, H., Liu, K., Wang, Q., and Zeng, W. (2018). Sarm1/Myd88-5 Regulates Neuronal Intrinsic Immune Response to Traumatic Axonal Injuries. Cell Rep *23*, 716-724.

131. Wanner, I.B., Anderson, M.A., Song, B., Levine, J., Fernandez, A., Gray-Thompson, Z., Ao, Y., and Sofroniew, M.V. (2013). Glial scar borders are formed by newly proliferated, elongated astrocytes that interact to corral inflammatory and fibrotic cells via STAT3-dependent mechanisms after spinal cord injury. J Neurosci *33*, 12870-12886.

132. Weaver, A., Goncalves da Silva, A., Nuttall, R.K., Edwards, D.R., Shapiro, S.D., Rivest, S., and Yong, V.W. (2005). An elevated

matrix metalloproteinase (MMP) in an animal model of multiple sclerosis is protective by affecting Th1/Th2 polarization. FASEB J *19*, 1668-1670.

133. Werner, E., Ziegler, M., Lerner, F., Schweiger, M., and Heinemann, U. (2002). Crystal structure of human nicotinamide mononucleotide adenylyltransferase in complex with NMN. FEBS Lett *516*, 239-244.

134. White, M.A., Lin, Z., Kim, E., Henstridge, C.M., Pena Altamira, E., Hunt, C.K., Burchill, E., Callaghan, I., Loreto, A., Brown-Wright, H.*, et al.* (2019). Sarm1 deletion suppresses TDP-43-linked motor neuron degeneration and cortical spine loss. Acta Neuropathol Commun *7*, 166.

135. Wu, G., Ringkamp, M., Hartke, T.V., Murinson, B.B., Campbell, J.N., Griffin, J.W., and Meyer, R.A. (2001). Early onset of spontaneous activity in uninjured C-fiber nociceptors after injury to neighboring nerve fibers. J Neurosci *21*, RC140.

136. Wu, H.H., Bellmunt, E., Scheib, J.L., Venegas, V., Burkert, C., Reichardt, L.F., Zhou, Z., Farinas, I., and Carter, B.D. (2009). Glial precursors clear sensory neuron corpses during development via Jedi-1, an engulfment receptor. Nat Neurosci *12*, 1534-1541.

137. Xiong, X., Hao, Y., Sun, K., Li, J., Li, X., Mishra, B., Soppina, P., Wu, C., Hume, R.I., and Collins, C.A. (2012). The Highwire ubiquitin ligase promotes axonal degeneration by tuning levels of Nmnat protein. PLoS Biol *10*, e1001440.

138. Yang, J., Wu, Z., Renier, N., Simon, D.J., Uryu, K., Park, D.S., Greer, P.A., Tournier, C., Davis, R.J., and Tessier-Lavigne, M. (2015). Pathological axonal death through a MAPK cascade that triggers a local energy deficit. Cell *160*, 161-176.

139. Yoshino, J., and Imai, S. (2013). Accurate measurement of nicotinamide adenine dinucleotide (NAD(+)) with high-performance liquid chromatography. Methods Mol Biol *1077*, 203-215.

140. Zhai, R.G., Cao, Y., Hiesinger, P.R., Zhou, Y., Mehta, S.Q., Schulze, K.L., Verstreken, P., and Bellen, H.J. (2006). Drosophila NMNAT maintains neural integrity independent of its NAD synthesis activity. PLoS Biol *4*, e416.

141. Zhai, R.G., Zhang, F., Hiesinger, P.R., Cao, Y., Haueter, C.M., and Bellen, H.J. (2008). NAD synthase NMNAT acts as a chaperone to protect against neurodegeneration. Nature *452*, 887-891.

142. Zhang, X., Kurnasov, O.V., Karthikeyan, S., Grishin, N.V., Osterman, A.L., and Zhang, H. (2003). Structural characterization of a

human cytosolic NMN/NaMN adenylyltransferase and implication in human NAD biosynthesis. J Biol Chem *278*, 13503-13511.

143. Zhao, Z.Y., Xie, X.J., Li, W.H., Liu, J., Chen, Z., Zhang, B., Li, T., Li, S.L., Lu, J.G., Zhang, L.*, et al.* (2019). A Cell-Permeant Mimetic of NMN Activates SARM1 to Produce Cyclic ADP-Ribose and Induce Non-apoptotic Cell Death. iScience *15*, 452-466.

144. Zhou, T., Kurnasov, O., Tomchick, D.R., Binns, D.D., Grishin, N.V., Marquez, V.E., Osterman, A.L., and Zhang, H. (2002). Structure of human nicotinamide/nicotinic acid mononucleotide adenylyltransferase. Basis for the dual substrate specificity and activation of the oncolytic agent tiazofurin. J Biol Chem *277*, 13148-13154.

145. Zhuang, M., Calabrese, M.F., Liu, J., Waddell, M.B., Nourse, A., Hammel, M., Miller, D.J., Walden, H., Duda, D.M., Seyedin, S.N.*, et al.* (2009). Structures of SPOP-substrate complexes: insights into molecular architectures of BTB-Cul3 ubiquitin ligases. Mol Cell *36*, 39-50.

146. Ziegenfuss, J.S., Biswas, R., Avery, M.A., Hong, K., Sheehan, A.E., Yeung, Y.G., Stanley, E.R., and Freeman, M.R. (2008). Draper-

dependent glial phagocytic activity is mediated by Src and Syk family kinase signalling. Nature *453*, 935-939.